VALIDATION AND EXTENSION OF MODAL/MOM IN SHIELDING EFFECTIVENESS STUDIES OF METALLIC ENCLOSURES WITH APERTURES

By
Vignesh Rajamani
Bachelor of Engineering (ECE)
University of Madras, India
2002

Submitted to the Faculty of the
Graduate college of the
Oklahoma State University
in partial fulfillments of
the requirements
for the degree of
MASTER OF SCIENCE
December 2004

VALIDATION AND EXTENSION OF MODAL / MOM IN SHIELDING EFFECTIVENESS STUDIES OF METALLIC ENCLOSURES WITH APERTURES

Thesis Approved:

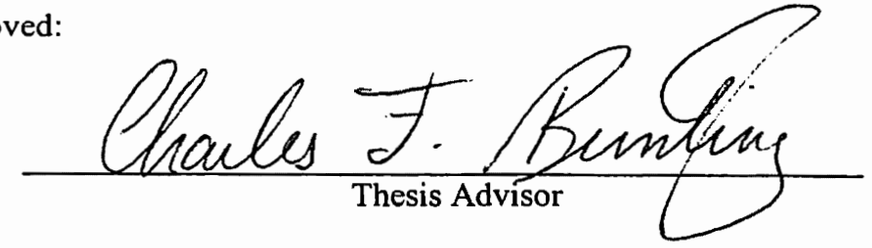

Thesis Advisor

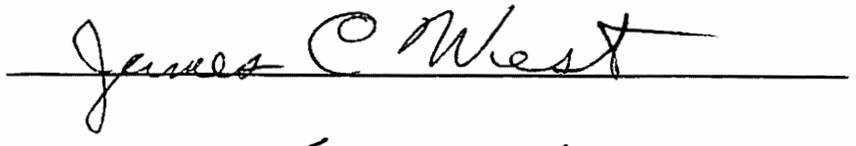

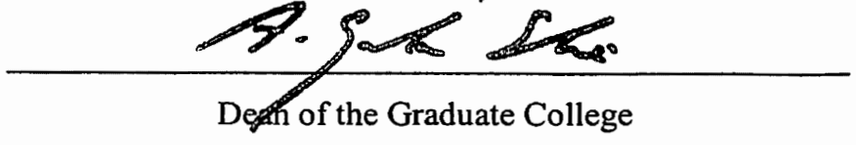

Dean of the Graduate College

ACKNOWLEDGEMENTS

Many people have been a part of my graduate education, as friends, teachers, and colleagues. Dr. Charles F. Bunting, first and foremost, has been all of these. The best advisor and teacher I could have wished for, he is actively involved in the work of all his students, and clearly always has their best interest in mind. Thank you for pushing me. On the personal side, he did not hesitate to invite his students to become an extended part of his family.

I have been indebted in the preparation of this thesis to Dr. James C. West whose patience and kindness, as well as his academic experience, has been invaluable to me. My special thanks are to Dr. Jong – Moon Chung for accepting my request to be on my thesis committee.

I shall always be grateful to Dr. M. D. Deshpande (NASA Langley) for the long telephonic discussions we had together and the knowledge I gained from him. This work would not have been possible without the support and encouragement of Dr. C. J. Reddy (EMSS USA), who helped me all through the thesis with his expertise in FEKO and being there for clearing all my doubts. Special thanks to Zulfiqar Ali Khan who always impressed me with his problem solving ability for making me understand Modal / MoM.

And I would like to thank Mr. Craig R. Birtcher (Arizona State University) who provided me with the experimental data that I regard as so important. I would like to thank Mr. Truong X. Nguyen (NASA Langley) for providing me a copy of NASA report (By ASU).

I would like to thank several of my friends for helping with the preparation of this thesis especially my lab mates who were patient when I listened to my loud rock music. Their honest yet considerate criticisms of this work have helped much in improving its quality. I cannot end without thanking my girl friend Subha, the constant support and encouragement from her which was always there when I needed it.

Lastly, and most importantly, I wish to thank my parents, Rajamani and Bhama. They bore me, raised me, supported me, taught me, and loved me. To them I dedicate this thesis.

TABLE OF CONTENTS

LIST OF FIGURES

Chapter 1

1.0 INTRODUCTION

Apertures of various sizes and shapes on a metallic enclosure are used for input and output connections, control panels, visual-access windows, etc. Since these apertures may behave as efficient antennas at same electromagnetic (EM) frequencies, they also become sources of electromagnetic interference (EMI) problems for both EM emission and susceptibility. If the electronic components that are located inside these enclosures are not shielded properly, improper operation of equipment may result and in some cases may lead to permanent damage of equipment. With significant development in technology, flights are equipped with lot of electronics for different operations. When conceiving electric or electronic systems, it is necessary to take into account the constraints of electromagnetic compatibility in order to define the most appropriate configurations, less sensitive to perturbations. Decreasing the electromagnetic radiation from the electronic equipment is important from the EMI view point. An understanding of shielding effectiveness which is defined as "The relative capability of a shield to eliminate undesirable electric and magnetic fields and plane waves" may help in locating components appropriately to reduce the EM emissions or improve the immunity of electronic components inside the metallic enclosure. The primary interest that motivates this work is shielding avionics within aircraft structures.

Shielding effectiveness can be calculated using numerical and analytical methods. Numerical methods such as the Finite Difference Time Domain (FDTD) method, and the hybrid Finite element method/ Method of Moments can model complex structures inside enclosures but often require large computing time and memory. For electrically large apertures and enclosures these methods though more accurate, become difficult for designers to use to investigate effects of EM shielding on the design parameters. Analytical formulations that are used to find the shielding effectiveness are based on different assumptions whose validity becomes questionable at higher frequencies. Bethe [4] presented a small-hole theory, based on a quasi-static analysis for the problem of field penetration through electrically small apertures. According to Bethe's analysis, the field distribution in an aperture is essentially that which would exist if the aperture were immersed in static electric and magnetic fields.

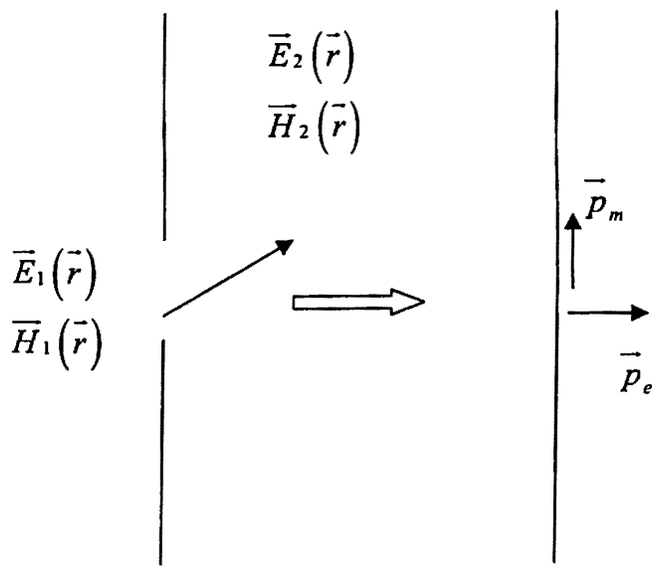

Figure 1.1 An illustration of Bethe's small hole theory.

Bethe's theory shows that if a field exists on one side of a conducting plane wall of zero

thickness and an electrically small aperture is then cut in the wall, the field in the second region is the same as that from an electric dipole normal to the wall and a magnetic dipole tangential to the wall, both at the center of the aperture with the aperture closed. (Ref: Figure 1.1). Therefore, the field in the vicinity of the aperture may be represented by the superposition of the original internal field at the location of the aperture (before the aperture was cut in the wall) and the fields of an electric and magnetic dipole located at the center of the aperture. The relationship between the dipole moments of these dipoles to the original electric and magnetic fields is described by the polarizabilities that are functions of the size and shape of the holes. Bethe's method of solution is applicable to small elliptical apertures as well as to circular apertures, but not to rectangular or more complicated geometrical figures. The estimated fields are valid at distances that are large in terms of the maximum linear dimension of the aperture. However, at closer distances, Bethe's theory breaks down. Bethe's analysis is limited to the frequencies below the first resonance frequency of the aperture. Frequency of operation is suppose to be small that the fields are essentially constant at the apertures.

In this thesis, a method that is suitable for large but regularly shaped enclosures and apertures that was developed at NASA Langley Research Center, a general hybrid modal / moment method technique, called Modal / MoM (Modal / Moment method) (MNI – Modal / MoM with normal incidence), will be discussed and the validity of the code will be verified using a commercial moment method code called FEKO. MNI discussed here has certain advantages over other techniques. Some of the important features of the code are

1. It is computationally efficient in calculating the fields at any point inside the enclosure, excited due to a normally incident plane wave impinging upon the shielding enclosure over a wide range of frequencies.
2. The fields that are calculated using this technique are accurate.
3. It can calculate the shielding effectiveness with respect to the probe that is located inside the cavity

Khan modified MNI to enable plane waves at oblique incidence [10]. MOI (Modal MoM with oblique incidence) will be validated for the shielding effectiveness at oblique angle of incidence. The range over which the results using MOI can be trusted is discussed by comparing the computed data with the measured results from Arizona State University [48]. Emphasis is laid on computing the input impedance of a probe (wire antenna) that is located inside the enclosure. This is done to find out the points where the probe can be placed so that maximum energy can be coupled to the probe. In some cases coupling maximum power to the probe is necessary and in some cases the probe must be placed at a point where it does not couple energy at all (Example: Probes that are run over the fuel tank must be shielded properly else it will lead to sparking and damage). An investigation of the input impedance of the probe is discussed along with the current distribution on the wire and the fields induced because of the current. The goal of this investigation is to study the differences in input impedance of the probe with respect to different locations inside the enclosure and to determine the location where the probe has to be placed for the probe to couple maximum energy or to shield the probe from other sources.

Organization of Thesis

This Thesis is organized into five chapters.

Chapter 2 discusses the theoretical and numerical models that have been used in studying the shielding effectiveness. Chapter 3 contains the formulation of MNI followed by the formulation used in the development of MOI. This is followed by the classical method of moments approach of solving for the current on a wire radiator in free space and determining the current distribution. Finally the expressions that are used in MNI for solving for the current on the probe located inside the cavity and solving for the input impedance of the probe are explained. Chapter 4 presents the SE results for various scenarios regarding number of apertures, size of apertures for a range of frequencies and SE results for different size of apertures for various angles of incidence. These results are presented in comparison to FEKO results for the same cases hence validating MNI and MOI whose results were questionable when the aperture size is made really big (Same as the size of the wall of the enclosure) and SE results for oblique angle of incidence. An investigation on the input impedance of the wire antenna that is located inside the box is also discussed in the final section. These results are presented to investigate the position of the probe inside the cavity where it can couple maximum energy or no energy. From this the reader gets a sense of where to place the probe inside the enclosure for his application and for that particular frequency sweep. In Chapter 5, the conclusion of this thesis will be presented along with recommendations for future work.

Chapter 2

2.0 SE ESTIMATION TECHNIQUES

Shielding Effectiveness (SE) is one of the major aspects of any EMC (Electromagnetic Compatibility) design process. When electronic equipment intended to handle certain input levels, whether logic signals or continuous analog signals, picks up undesired inputs, an upset may occur. The upsets are like erroneous reading, fluctuating needle etc. In aircraft, for example, instruments are closely packaged due to limited space. The RADAR display performance can be visibly distorted by nearby tachometers which may radiate a rotating magnetic field. The radar display is subject to some position shift each time the aircraft changes direction or altitude relative to the earth's field. A magnetic (i.e. permeable) shield enclosure minimizes these effects as well as supporting and positioning the tube [55]. Therefore the ability to accurately estimate the SE of an enclosure can be valuable. A wide range of techniques are available for the calculation of SE, varying from analytical analysis, the numerical simulation and finally experimental measurement.

In characterizing the shielding performance of the structure there exists two approaches. One approach includes irradiating the box under test and sampling the field levels inside as seen in Figure 2.1 (a). Another approach attempts to more directly assess the potential impact of an EM threat via an exploration of the possible fields coupled to a particular

probe orientation by exciting the probe with a voltage gap as can be seen in Figure 2.1 (b).

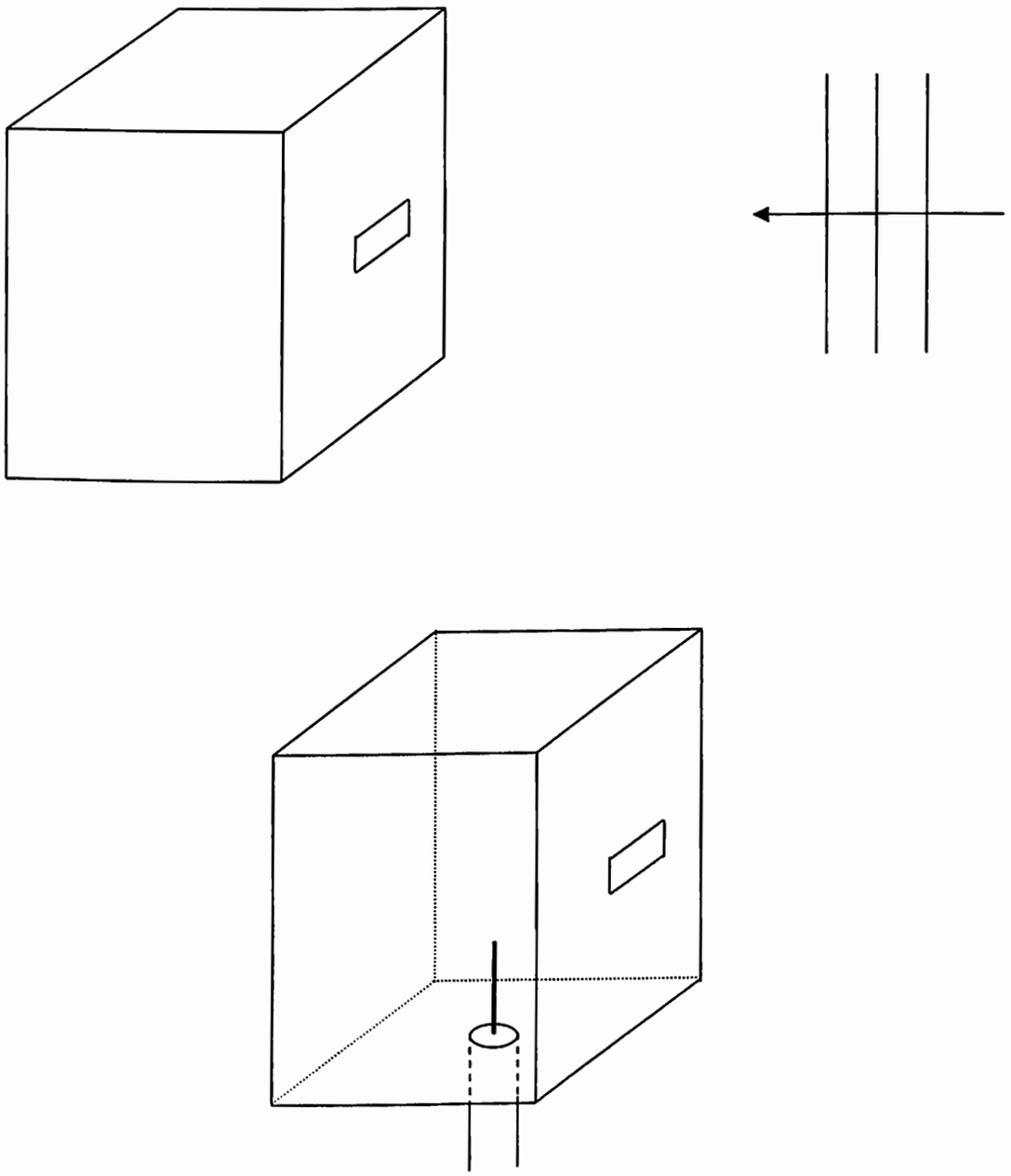

Figure 2.1 (a) Plane wave excitation - External excitation (b) Excitation on the probe using voltage gap - Internal excitation.

Both analytical and numerical solutions have their own advantages and disadvantages. An analytical solution will be the fastest method giving accurate results but some of the assumptions that are used limit their application for certain frequencies. Among these conditions are restriction on the size and geometry of the apertures and it is always not possible to obtain rigorous solution. Varying one of the parameters may invalidate the solution and invites reinvestigation of the problem.

Numerical solutions can be either in the time domain or frequency domain and involve simple algorithms and can support arbitrary shapes and enclosure contents. Numerical solutions also require high computational power and may occupy large memory to give reasonable accuracy. The results are compared with a set of measured results and the measured results cannot be always reliable. Accurate measurements are not always possible due to the limitations of screened rooms and anechoic chambers and perturbation caused by the measurement probe. This perturbation caused by the probe itself is a potential source of error. The laboratory measurements for one case might not be the same as the other one and in the real world the problem is continuously changing. The results obtained from measurements are good when designed for a particular case and can point out the potential source of error but when we look at the bigger picture (Trying to find the fields at every point inside the enclosure), a complete design of SE is not possible with measurements only.

Bombart [31] and Kaden [34] showed that the field penetrating a small aperture may be much larger than field attenuated due to skin depth. Their assumption of the field

penetrating through a small aperture into a long cylindrical shell immersed in a uniform axial magnetic field has been verified in their results showing a good agreement between the theoretical and experimental values. The limitation in Bombart where he considers only the impressed magnetic field was later relaxed by Taylor [50] considering a general impressed field on a small elliptical shaped aperture in a parallel plate shield. It was concluded that the field penetrating a small aperture in an arbitrarily formed electromagnetic shield is approximately that of static-crossed electric and magnetic dipoles, except for frequencies near the resonance of the interior cavity. For a low Q cavity, this restriction vanishes and the magnetic dipole moment of the equivalent source distribution lies in the plane of the aperture and the corresponding electric dipole moment is perpendicular to the aperture. A Taylor expansion is also applicable to apertures that are smaller than the operating wavelength.

Mendez [40, 41] presented an analysis for EM radiation from rectangular enclosures with an aperture excited by center fed thin dipole and a square loop. Two problems have been addressed in his approach, a cavity with a small aperture in the wall and a larger aperture-both for the frequencies below the lowest enclosure resonance thus allowing the cavity to be considered a perfect conductor. The fields inside the enclosure due to internal sources are determined assuming no apertures present. Then for the apertures, Bethe's theory (Ref: Figure 1.1) is used replacing the apertures equivalent electric and magnetic dipoles taking the polarizabilities of each aperture. The radiated field is the field radiated by the dipoles in the semi-infinite metal backed region and imposing suitable boundary conditions. The validity of this is only for small apertures and rectangular geometries and

limited to the frequencies below the lowest enclosure resonance. The cavity wall losses are neglected comparing them with the energy leaking from the apertures. For the open cavity and a longitudinal dipole that produces TM modes only, it is assumed that the apertures produces a complete reflection of the transverse field components hence doubling the transverse magnetic fields and canceling the transverse electric field. With a transverse loop TE modes are present so the transverse electric fields are doubled canceling the transverse magnetic field. Fields at the open end are then given in terms of fields that would exist at the same place in a semi infinite waveguide, modified according to the reflection assumptions made. The radiated fields due to the structure are found using equivalence principle.

Method of moments was employed by Audone [2] and Cerri [21] to calculate the shielding effectiveness of a rectangular enclosure with single aperture. The internal field due to an internal current source is calculated using internal dyadic Green's function assuming no apertures. The aperture is then introduced assuming equivalence principle introducing equivalent magnetic current radiating internally and externally. The external fields can be found using external dyadic Green's function for internal Green's function in the E field expression or if the field is calculated along the central axis of the enclosure wall with the aperture, it is possible to assume that magnetic currents are located in an infinite metal plate. By means of this approach, one can use free space Green's function which takes into account the presence of the metallic sheet. Integral equations are developed by matching the tangential internal fields both due to the internal current source and the unknown equivalent magnetic current source to the external fields radiated

by the equivalent magnetic current at the aperture. The unknown magnetic current is solved using the integral equation. Ref: Figure 2.2

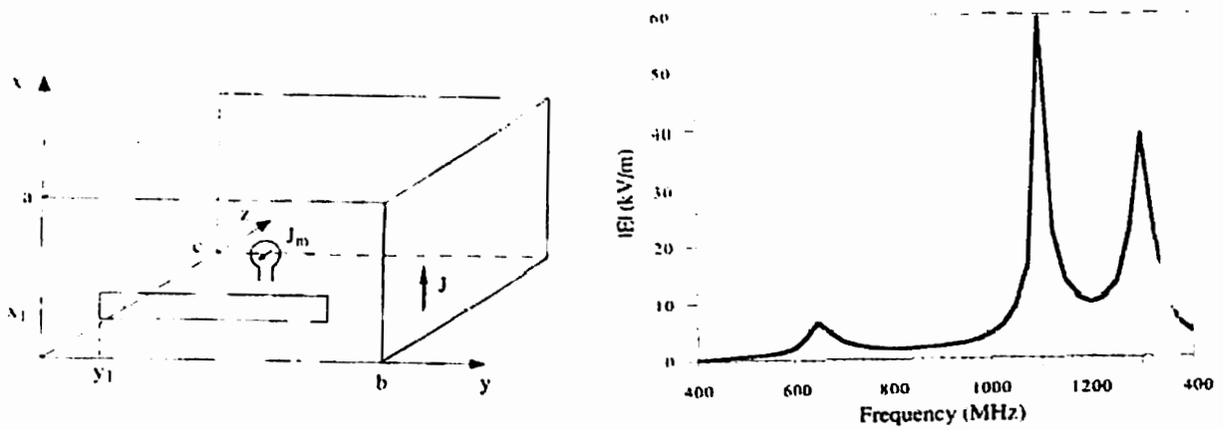

Figure 2.2 (a) Cavity with rectangular aperture excited using a loop inside the cavity (b) E field amplitude at the center of the aperture for the electric dipole excitation. Ref: [21]

A transmission line model was validated by De Smedt [51] uses a single aperture in the center of the front wall of the rectangular enclosure. The rectangular box is represented as a short circuited length of rectangular waveguide with a single mode of operation. The transition between free space and waveguide is represented by considering the aperture as a length of coplanar strip transmission line. The voltage and current at a given point give the electric and magnetic shielding at that point, respectively. This is a simple approach compared to FEM and FDTD and can be applied for frequencies above and below the cutoff of the dominant mode. This approach has certain limitations such as thin apertures, single mode, negligible coupling between the apertures and does not consider the incidence angle or polarization of the impinging EM field. The fields can be calculated at points in front of the aperture. Ref: Figure 2.3.

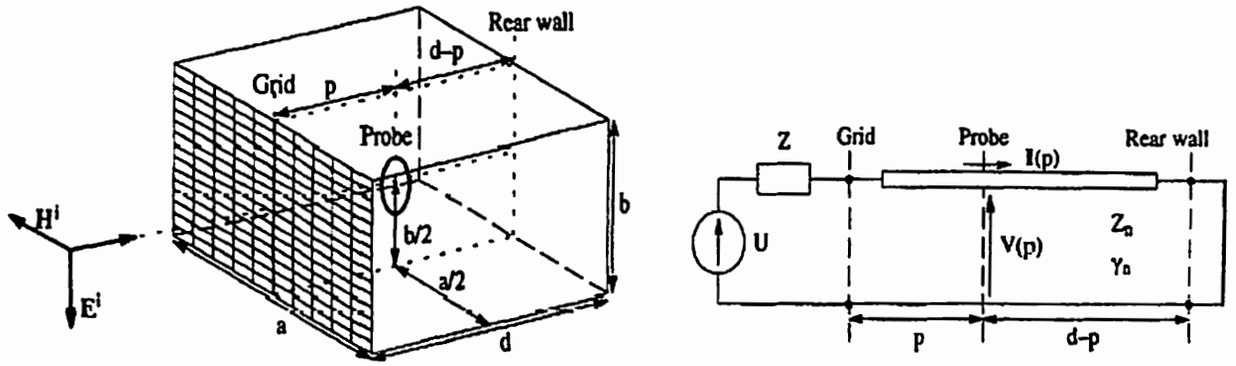

Figure 2.3 (a) Rectangular enclosure with a grid wall. (b) Equivalent circuit. Ref: [51]

Another model based on circuital approach has been proposed to predict the field distribution on rectangular apertures backed by rectangular cavities [43]. The aperture is modeled as a length of rectangular strip ended by a short and the metallic box backing the aperture is modeled as load impedance that is calculated by regarding the box as a length of rectangular waveguide ended on one side by a short and by considering only the fundamental propagation of TE_{10} mode. The thevenin equivalent of this structure is evaluated and connected to the load given by the backing cavity. In order to evaluate the electromagnetic field on the aperture, the final value of the field is calculated by considering the divider between the impedance of the metallic cabinet. This model has a limitation of only permitting single aperture. Ref: Figure 2.4.

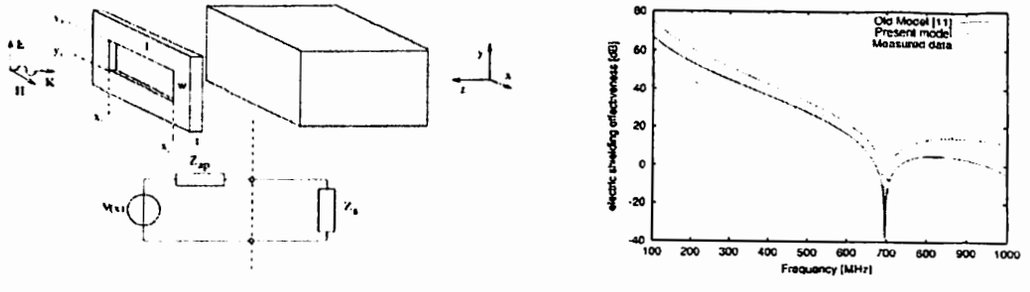

Figure 2.4 (a) Circuit model of the problem. (b) SE in the center of the enclosure. Ref: [43]

A power balance technique was introduced by Hill [18] to calculate the SE of the enclosures with electrically large and small apertures. It is assumed that under steady state conditions, the power transmitted to the enclosure through the apertures is equal to the sum of the power leakage from the apertures, the power dissipated in the cavity walls, the absorption of the power in some objects inside the cavity and the power absorbed by any receiving antenna inside the cavity. This approach yields a simple expression for the average field strength through out the cavity. The limitation of this method is that it does not yield fine detail of the interior fields like any other numerical method but has the advantage of being applicable in CW and RF pulse fields and not requiring all the geometrical details of the enclosures, the apertures and the loads. This theory is similar to the one developed for reverberation chamber where the average power density is assumed to be uniform throughout the chamber. Ref: Figure 2.5

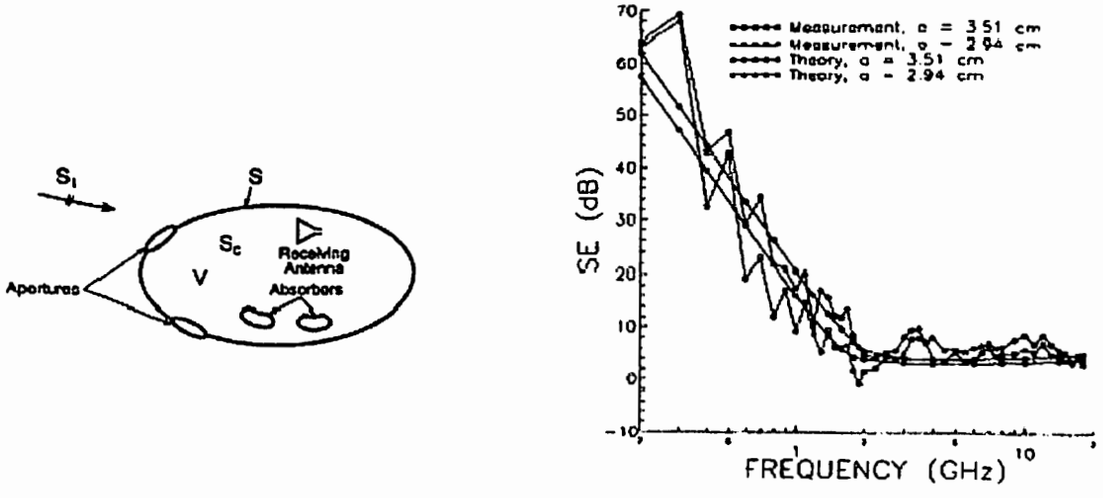

Figure 2.5 (a) Aperture excitation of a cavity containing absorbers and a receiving antenna. (b) Calculated and measured SE for the NSWC rectangular cavity with a circular aperture. Ref: [18]

Many other numerical techniques have been used for solving these kinds of problems yielding good accuracy. The Finite element method (FEM) [49] [20] [48] finite difference time domain (FDTD) [22] [33] [44] [16] [46] [48] [23] method of moments

[52] [37] [53] transmission line method (TLM) [1] [35] [42] and hybrid methods 15] have all been used and are verified to yield results with good accuracy. The general limitations of all these approaches are the size of the enclosure, size of the apertures and the computation overhead with increase in frequency. When the aperture size is small and the frequency of interest is a high frequency then to attain a reasonable accuracy, a small step size must be chosen. This results in an enormous number of cells for the cavity space and thus requires large memory and computation time.

The numerical method using TLM was compared with the analytical model similar to Cerri [21] and with the approximate solution of Robinson [38] [39]. The comparison showed that all the results showed good agreement with the measured results. The major disadvantages with the analytical methods are that they cannot be applied to arbitrary geometries and cavity contents. Every time there is a change in the geometry of the problem, using analytical methods, the whole problem has to be reinvestigated. The disadvantage of any numerical technique is that complex structures result in large computational overhead. The measured results are also not accurate as there is some error introduced into the system that goes unnoticed during the measuring process like during the measuring process the losses in the cables must be cancelled in order to get the accurate measurement and eliminating the losses is not trivial. So these will contribute to errors during the measuring process.

The main focus of all the analytical models and numerical techniques has been that of determining the field at one point inside the enclosure for a given set of conditions. Most

use a plane wave excitation to expose the apertures and assume the worst case of normal incidence. Practically speaking restricting ourselves to normal incidence case is not true for all cases and this was also shown in some of the results from Khan's work [10]. This led to the study of statistical investigation of shielding effectiveness. This approach [6]-[8] exposes the enclosure and the apertures to a reverberating environment where both external and internal fields are not plane waves but waves from all different directions. The finite element method used in [6]-[8] is used to calculate the coupling between the external and internal fields. Random points are chosen to calculate the electric and magnetic fields and then the shielding effectiveness is calculated based on the maximum values of the fields obtained through this random selection process. The study indicates that the shielding effectiveness values for a single point inside the box have a normal distribution over the frequency range. The statistical investigation requires the field values at a number of random points inside the enclosure and hence requires a fast and efficient computational tool. This cannot be achieved with techniques like finite element method because of computer memory and time restraints.

In this thesis emphases is laid on the application of MNI and MOI and define a limitation on particular cases and the results from running those codes. The aperture is represented as a very thin waveguide structure located on an infinite ground plane and hence the aperture fields can be represented using modal expansions. The aperture being small compared to the wall is then replaced by equivalent magnetic currents using the equivalence principle. The internal fields can be found using cavity Green's functions and external fields can be found using free space Green's functions with the magnetic

currents as the radiating source. The external and internal fields are then matched at the aperture to obtain an integro-differential equation to be solved for unknown magnetic currents using method of moments. MNI allows an arbitrary number of apertures on both sides of the cavity. The excitation source is external and far away from the cavity so that cavity is illuminated by a plane wave.

MNI and MOI are techniques that are limited by the assumptions of relatively small apertures compared to cavity walls, negligible effects of cavity edges because of the location of apertures on an infinite ground plane, and a lossless empty cavity. Also the formulation has been developed only for rectangular apertures and cavities. Nevertheless, MNI and MOI are efficient tools to be employed for the computation of the statistical properties of shielding effectiveness of metallic enclosures. It gives almost closed form accuracy and is fast compared to traditional numerical techniques. Modal MoM was employed by Bunting [9, 11] for studying the bulk properties of cavity volume and aperture size over a range of frequencies using statistical analysis. A significant number of random samples indicate negative SE values implying field intensities higher than the external fields. SE decreases with the increasing aperture size. The validation of Modal / MoM (MNI and MOI) is the main focus of this work. Modal / MoM (MNI and MOI) is suspected to give bad results when the aperture size is assumed to be the size of the wall. As Modal / MoM (MNI and MOI) assumes the plates are infinitely long (Ref: Fig 2.6), the approximations that it provides for the biggest aperture size is believed to be incorrect.

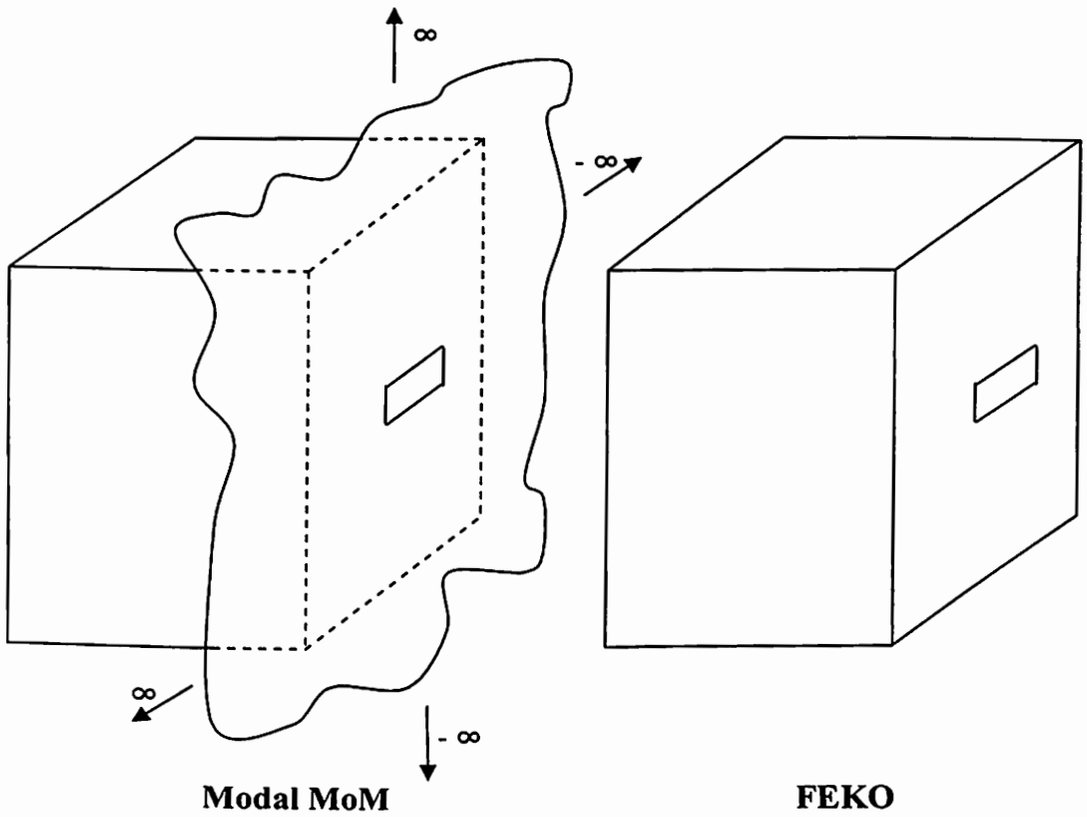

Figure 2.6 Modeling of cavity in Modal MoM and FEKO

FEKO is a full wave, method of moments (MoM) based, computer code for the analysis of electromagnetic problems such as: Shielding, coupling, antenna design, antenna placement analysis, microstrip antennas and circuits, strip lines, dielectric bodies, scattering analysis etc. In order to solve electrically large problems MoM has been hybridized with the asymptotic high frequency techniques, physical optics (PO) and the uniform theory of diffraction (UTD). The true hybridization reduces the computational resource requirements, enabling the analysis of very large problems.

FEKO does not assume an infinite ground plane so the same case is developed in FEKO which assumes RWG (**R**ao - **W**ilton - **G**lisson) basis functions for its approximation hence eliminates the errors that are produced in Modal MoM. Some of the important results here discuss the reliability on Modal MoM for some structures like this.

The multiple angle of incidence case (MOI) which was developed from MNI is used to find the shielding effectiveness of the box when the plane wave source flies by the face of the aperture [10]. As there are no standard results to compare these results, the values that are predicted by MOI must be validated. The multiple angle of incidence case was simulated using FEKO which has a better approximation for this problem than MOI and the results are compared. Some of the special cases are also compared with the measured results from ASU [48]. This comparison puts a bound on the angle of incidence for which MOI can accurately predict the shielding effectiveness.

In the next chapter, a description of MNI and MOI are presented with an emphasis on the determination of input impedance of an infinitely thin wire probe. Also the current distribution on the wire and the shielding effectiveness with respect to the current on the probe is presented.

Chapter 3

3.0 FORMULATION OF PROBLEM

The **MNI** (**M**odal / MoM with **N**ormal **I**ncidence) code is efficient and it is accurate. Fields at any point inside the box can be calculated when a plane wave illuminates the aperture. The aperture is represented as a very thin waveguide structure and hence the aperture field can be represented using modal expansions. Any number of apertures, location, size and orientation can all be defined by the user. This was an improvement of the code developed by Cerri and Audone [2, 21] which can support only one aperture at the wall. MNI also supports an infinitely thin wire inside the enclosure. The input impedance of the wire, the current induced on the wire due to plane wave excitation and also the current induced on the wire due to excitation on the probe using a voltage gap can be calculated. There are also some limitations in MNI such as supporting only TE_{10} mode at the aperture and neglects all the higher order modes. Only the E polarized plane wave at normal incidence is supported. No other polarizations and angle of incidence can be supported by MNI.

As the main focus of this approach is to shield the avionics inside the aircraft, restricting ourselves to only one angle of incidence will not be practical because there may be sources with arbitrary angles of incidence and polarization that will be incident on the windows which acts like radiating antennas. Due to the incident waves from different

angles, the field inside the aircraft will build up and that leads to interaction with the other electronic devices leading to damage. In order to prevent this, the shielding effectiveness at every point inside the enclosure, due to all the different incident waves is needed. In this thesis the field at the center of the enclosure which is usually used for comparison with other standard results is calculated.

Khan [10] modified MNI and relaxed it limitations on the angle of incidence and polarization angles. MNI was not able to support two apertures on the same wall without any apertures on the back wall. **MOI** (**M**odal MoM with **O**blique angle of **I**ncidence) is able to support any number of apertures on the same wall without altering anything in the opposite wall but does not support any apertures in the back wall. The user can define any number of modes at the aperture which was not possible in MNI. Considering only one mode is a weak assumption as there might be effects of modes other than TE_{10} that exist on the aperture that are ignored. When the problem approached with various angles of incidence and polarizations, it is important to include the effects of different modes on the aperture. MOI can calculate shielding effectiveness versus

- Frequency for a given incidence angle and polarization
- Angle of incidence for a given frequency and polarization
- Polarization for a given frequency and incidence angle.

MNI is used for frequency sweep results and MOI was used for sweep in incidence angle. In this chapter a brief introduction to the problem will be presented in the next section followed by the assumptions of MNI and how well MOI varies from MNI will also be discussed. Some of the important derivations for MOI for multiple angles of incidence

and solving for the input impedance of the probe located inside the box using MNI are also included. Some of the things explained here closely follow the NASA report [19] where MNI was presented and Khan's work [10] which served as a motivation for this thesis. The work done here is a way of verifying the results of Khan's work [10]. Though this work is much of validation, detailed derivations from different references have been included for the sake of completeness and for the reader to understand the modifications done. The derivations will serve as a guide for a reader to follow this work.

In this chapter the basic definition of shielding effectiveness and the formulation of MNI and MOI will be presented. The analysis on the current on a wire is also presented with the discussion about the input impedance.

3.1 Definition of SE and basic geometry of the problem to be solved

The shielding effectiveness of an enclosure can be determined from the following expression:

$$E - Shielding\,(dB) = -20.0 \log\left(\frac{\left|\vec{E}_{int}\right|}{\left|\vec{E}_{ext}\right|}\right) \tag{1}$$

Where $\vec{E}_{int}$ is the electric field at a given point inside the enclosure and $\vec{E}_{ext}$ is the field at the same point in absence of the enclosure. Therefore, the problem of estimation of shielding effectiveness is essentially the problem of calculating the cavity fields inside the box while it is excited by a plane wave. The wave being incident on the apertures from free space.

Some of the basic assumptions in Modal MoM are given below.

- The thickness of the walls is zero and can be neglected.
- The apertures are relatively small compared to the area of the wall in which they are located.
- The diffracted fields due to edges of the wall are neglected.
- Due to infinite ground plane, there is no coupling between aperture on the front wall to the aperture on the back wall (usually referred as external coupling)

These assumptions are a result of using the equivalence principle on the apertures where the apertures are replaced by equivalent magnetic currents. These magnetic currents then radiate inside and outside the cavity. Greens functions are used to calculate the fields due to these current sources. Finally we match the tangential fields at the apertures to obtain integro-differential equations with unknown modal amplitudes of the magnetic currents resulting in the matrix equation of the form $[A][x]=[B]$ for those mode amplitudes.

Figure 3.1.1 shows the geometry of a rectangular enclosure with apertures on its front wall.

The dimensions of the cavity are $a \times b \times c$. There are R number of apertures and the dimensions of the r^{th} aperture are $L_r \times W_r$. The orientation of the reference axes is also shown with the origin at the lower right corner of the front wall.

Figure 3.1.2 gives the geometry of the equivalent problem in which the apertures have been replaced by equivalent magnetic currents. These magnetic currents are used as radiation sources to calculate internal and external scattered fields by employing Green's functions.

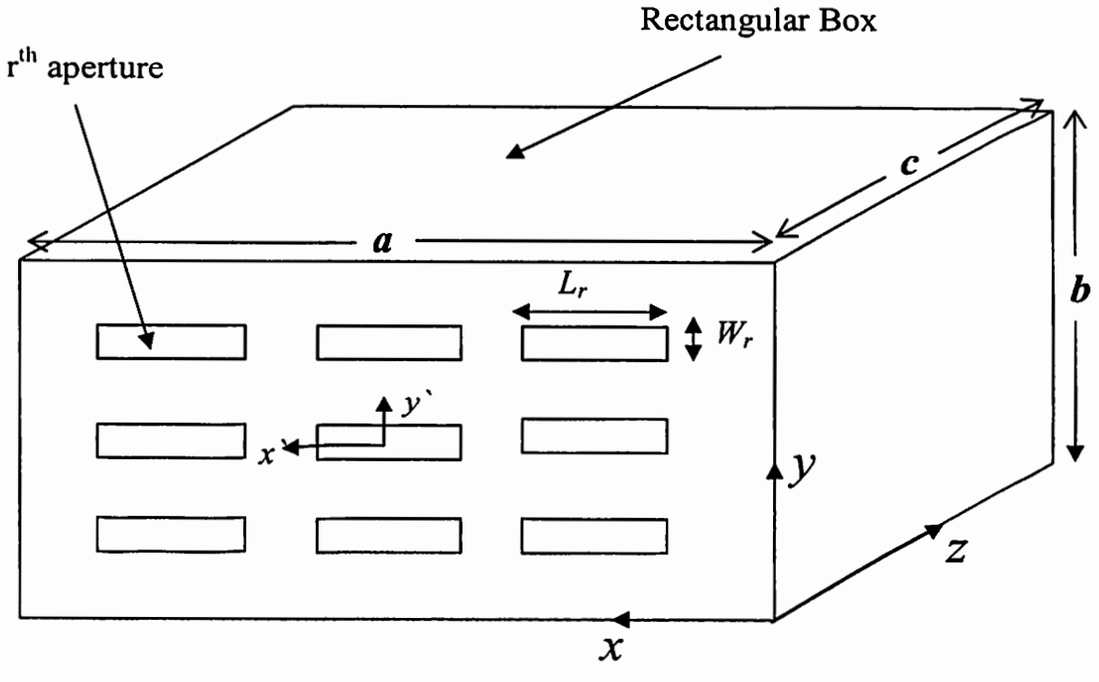

Figure 3.1.1 Geometry of rectangular enclosure with rectangular apertures illuminated by an arbitrary polarized plane wave at oblique incidence. Ref: [54]

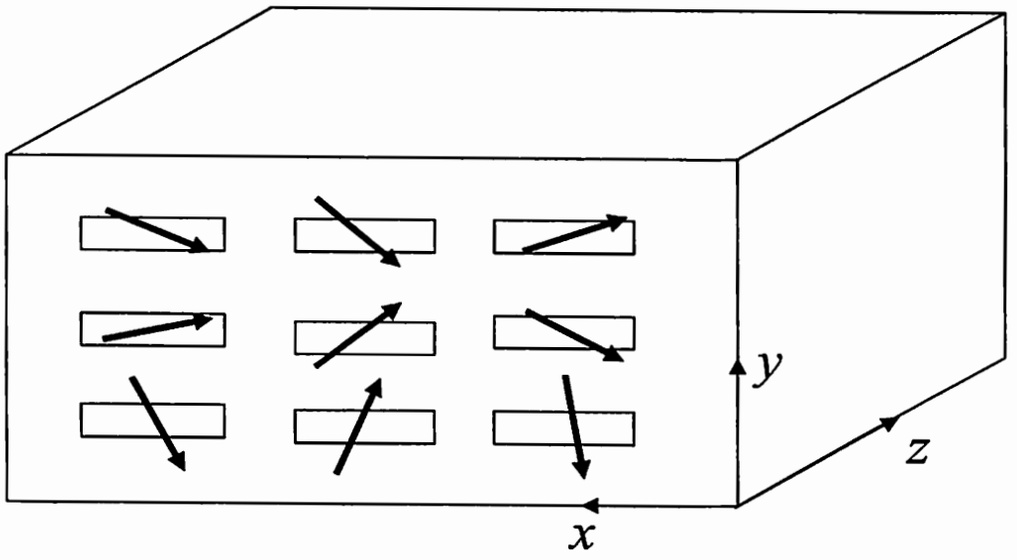

Figure 3.1.2 Geometry of the equivalent problem with apertures replaced by magnetic current sources. Ref: [54]

3.2 Shielding effectiveness development for fields with oblique incidence

In this section the formulation for MNI are presented. This section is subdivided into many subsections where the development of every single component is described individually. The detailed version of the formulations can be found in [19].

3.2.1 Overview of the problem

A plane wave of unity amplitude with arbitrary angles of incidence and polarization is illuminating the cavity with apertures in the front wall. It is given as

$$\overrightarrow{H}_i = \hat{x}H_{xi} + \hat{y}H_{yi} + \hat{z}H_{zi} \tag{2}$$

This induces fields at the apertures of the cavity. We can express the induced aperture fields using the eigen-function expansion corresponding to the waveguide modes supported by the aperture as

$$\vec{E}_{apt} = \sum_{r=1}^{R} \sum_{p} \sum_{q} \left(\hat{x} V_{rpq} \Phi_{rpq} + \hat{y} U_{rpq} \Psi_{rpq} \right) \tag{3}$$

Where V_{rpq} and U_{rpq} are the unknown modal amplitudes of the induced aperture fields, r represents the r^{th} aperture, p and q are the order of aperture waveguide modes and Φ_{rpq} and Ψ_{rpq} are the orthogonal eigen-functions. Using equivalence principles, we replace apertures by equivalent magnetic current sources radiating both inside and outside the cavity. When applying equivalence we assume that the apertures are lying in an infinite ground plane [1, 21]. This assumption is valid if the aperture size is relatively small compared to the cavity walls in which they are located.

$$\vec{M}_{apt} = \sum_{r=1}^{R} \sum_{p} \sum_{q} \left(-\hat{y} V_{rpq} \Phi_{rpq} + \hat{x} U_{rpq} \Psi_{rpq} \right) \tag{4}$$

These equivalent magnetic currents are then taken as the sources responsible for the fields both inside the cavity as well as the scattered fields outside the cavity. Then the problem can be divided in two regions: Region I (the external region) for $z \leq 0$ and Region II (the cavity or internal region) for $0 \leq z \leq c$.

The internal problem (Region II) consists of a rectangular volume enclosed by the cavity and illuminated by various equivalent magnetic current sources. The external problem (Region I) consists of magnetic sources backed by an infinite ground plane and radiating into the free space. We can replace the ground planes using image theory, thus eliminating any electric current equivalent sources.

The external scattered fields in Region I can be determined using free space Green's functions with the equivalent magnetic currents as sources.

$$\overline{H}^{I} = \hat{x}H_x^{I} + \hat{y}H_y^{I} + \hat{z}H_z^{I} \tag{5}$$

The total electromagnetic field outside the enclosure is obtained by superposition of the field due to incident wave and the scattered field due to apertures.

$$\overline{H}_{ext} = \overline{H}_i + \overline{H}^{I} \tag{6}$$

Similarly the cavity fields in Region II can be found using cavity Green's functions.

$$\overline{H}^{II} = \hat{x}H_x^{II} + \hat{y}H_y^{II} + \hat{z}H_z^{II} \tag{7}$$

The boundary conditions require the tangential fields at the apertures to be continuous.

$$\left(H_{xi} + H_x^{I}\right)\Big|_{z=0} = H_x^{II}\Big|_{z=0} \tag{8}$$

$$\left(H_{yi} + H_y^{I}\right)\Big|_{z=0} = H_y^{II}\Big|_{z=0} \tag{9}$$

The resulting equations can be reduced to a matrix equation $[A][x]=[B]$ using Galerkin's method. The matrix equation is then numerically solved for unknown magnetic current amplitudes U_{rpq} and V_{rpq} contained in the vector $[x]$.

3.3 Individual component development

3.3.1 Incident electromagnetic field

The incident time harmonic field can be written as:

$$\vec{H}_i = \left(\hat{\theta}_i H_{\theta_i} + \hat{\phi}_i H_{\phi_i}\right) e^{-j\vec{k}_i.\vec{r}} = \left(\hat{\theta}_i H_i \cos\alpha_0 + \hat{\phi}_i H_i \sin\alpha_0\right) e^{-j\vec{k}_i.\vec{r}} \quad (10)$$

Where,

$\vec{k}_i.\vec{r} = k_0 x \sin\theta_i \cos\phi_i + k_0 y \sin\theta_i \sin\phi_i + k_0 z \cos\theta_i$

k_0 = free space wave number = $\omega\sqrt{\mu_0\varepsilon_0}$

(θ_i, ϕ_i) = Angles of incident plane wave

α_0 = polarization of the incident plane wave

$\theta_i = 0$ is for the normally incident plane wave.

The angle of incidence and polarization have been defined in Figure 3.3.1.1.

We can separate the x, y, z components of the incident plane wave as:

$$H_{xi} = H_i\left(\cos\alpha_0 \cos\theta_i \cos\phi_i - \sin\alpha_0 \sin\phi_i\right) e^{-j\vec{k}_i.\vec{r}} \quad (11)$$

$$H_{yi} = H_i\left(\cos\alpha_0 \cos\theta_i \sin\phi_i + \sin\alpha_0 \cos\phi_i\right) e^{-j\vec{k}_i.\vec{r}} \quad (12)$$

$$H_{zi} = -H_i\left(\cos\alpha_0 \sin\theta_i\right) e^{-j\vec{k}_i.\vec{r}} \quad (13)$$

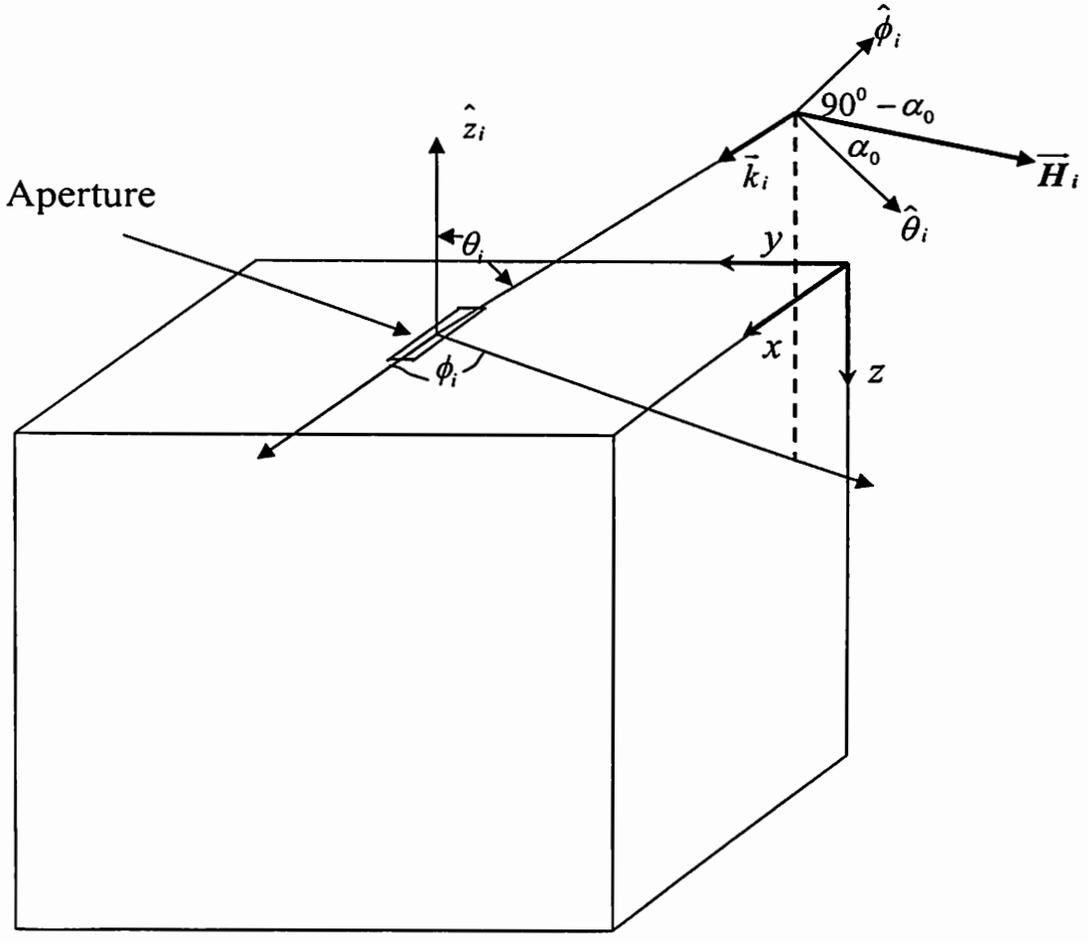

Figure 3.3.1.1 Definition of Angle of Incidence and Polarization. Ref: [54]

3.3.2 Aperture fields and equivalent magnetic currents

The incident plane wave will induce EM fields at the apertures. Since the aperture is just a very thin rectangular waveguide, we can express the aperture fields using modal expansion as follows:

$$\vec{E}_{apt} = \sum_{r=1}^{R} \begin{bmatrix} \hat{y}\sum_{p}\sum_{q} U_{rpq} \sin\left(\frac{p\pi}{L_r}\left(\frac{L_r}{2}+x-x_{cr}\right)\right)\cos\left(\frac{q\pi}{W_r}\left(\frac{W_r}{2}+y-y_{cr}\right)\right) \\ +\hat{x}\sum_{p}\sum_{q} V_{rpq} \cos\left(\frac{p\pi}{L_r}\left(\frac{L_r}{2}+x-x_{cr}\right)\right)\sin\left(\frac{q\pi}{W_r}\left(\frac{W_r}{2}+y-y_{cr}\right)\right) \end{bmatrix} \tag{14}$$

Where,

U_{rpq}, V_{rpq} = unknown modal amplitudes of the pq^{th} mode at r^{th} aperture, nonzero at aperture(in general), zero otherwise

L_r, W_r = Length and width of r^{th} aperture

R = Total number of apertures

(x_{cr}, y_{cr}) = Center of r^{th} aperture

Using the equivalence principle, we can replace the aperture fields in (14) by equivalent magnetic currents as follows:

$$\begin{aligned} \vec{M}_{apt} &= \hat{n} \times \vec{E}_{apt} = -\hat{z} \times \vec{E}_{apt} \\ &= \sum_{r=1}^{R} \begin{bmatrix} \hat{x}\sum_{p}\sum_{q} U_{rpq} \sin\left(\frac{p\pi}{L_r}\left(\frac{L_r}{2}+x-x_{cr}\right)\right)\cos\left(\frac{q\pi}{W_r}\left(\frac{W_r}{2}+y-y_{cr}\right)\right) \\ -\hat{y}\sum_{p}\sum_{q} V_{rpq} \cos\left(\frac{p\pi}{L_r}\left(\frac{L_r}{2}+x-x_{cr}\right)\right)\sin\left(\frac{q\pi}{W_r}\left(\frac{W_r}{2}+y-y_{cr}\right)\right) \end{bmatrix} \\ &= \sum_{r=1}^{R}\left[\hat{x}\sum_{p}\sum_{q} U_{rpq}\Psi_{rpqx} - \hat{y}\sum_{p}\sum_{q} V_{rpq}\Phi_{rpqy}\right] \end{aligned} \tag{15}$$

Where,

$$\Psi_{rpqx} = \sin\left(\frac{p\pi}{L_r}\left(\frac{L_r}{2}+x-x_{cr}\right)\right)\cos\left(\frac{q\pi}{W_r}\left(\frac{W_r}{2}+y-y_{cr}\right)\right) \tag{16}$$

$$\Phi_{rpqy} = \cos\left(\frac{p\pi}{L_r}\left(\frac{L_r}{2}+x-x_{cr}\right)\right)\sin\left(\frac{q\pi}{W_r}\left(\frac{W_r}{2}+y-y_{cr}\right)\right) \tag{17}$$

The advantage of representing the magnetic current over the apertures in terms of the entire domain basis functions, i.e. Ψ_{rpqx} and Φ_{rpqy}, is that only a few unknowns per aperture are needed for convergence. Therefore, MNI requires considerable less computational time as compared to other numerical methods.

3.3.3 External EM fields scattered due to apertures

Consider the r^{th} aperture on $z=0$ plane. The external fields are represented by a superscript 1. The EM field radiated in free space due to $\overrightarrow{M}_r$ can be obtained from the electric vector potential using:

$$\overrightarrow{E}^1\left(\overrightarrow{M}_r\right) = \frac{-1}{\varepsilon_0}\nabla\times\overrightarrow{F}^1 \tag{18}$$

$$\overrightarrow{H}^1\left(\overrightarrow{M}_r\right) = \frac{-j\omega}{k_0^2}\left(k_0^2+\nabla\nabla\bullet\right)\overrightarrow{F}^1 \tag{19}$$

Where the electric vector potential $\overrightarrow{F}^1$ is given by:

$$\overrightarrow{F}^1 = \frac{\varepsilon_0}{4\pi}\iint_{Apt} 2\overrightarrow{M}_r\frac{e^{-jk_0\left|\vec{r}-\vec{r}'\right|}}{\left|\vec{r}-\vec{r}'\right|}ds \tag{20}$$

The factor 2 in above equation comes from the image theory since the magnetic current is parallel to an infinite PEC ground plane. In deriving this equation, it has been assumed

that the $z = 0$ plane is infinite. Expressing $\frac{e^{-jk_0\left|\vec{r}-\vec{r}'\right|}}{\left|\vec{r}-\vec{r}'\right|}$ in terms of plane waves:

$$\frac{e^{-jk_0\left|\vec{r}-\vec{r}'\right|}}{\left|\vec{r}-\vec{r}'\right|} = \frac{1}{2\pi j}\int_{-\infty}^{\infty}\int_{-\infty}^{\infty}\frac{e^{-jk_0\left|\vec{z}-\vec{z}'\right|}}{k_z}e^{jk_x(x-x')+jk_y(y-y')}dk_x dk_y \tag{21}$$

The electric vector potential in (20) can be written in the form

$$\vec{F}' = \frac{\varepsilon_0}{4\pi^2}\int_{-\infty}^{\infty}\int_{-\infty}^{\infty}\left(\frac{e^{-jk_0\left|\vec{z}-\vec{z}'\right|}}{jk_z}\vec{m}_r\right)e^{jk_x x+jk_y y}dk_x dk_y \tag{22}$$

Where,

$$\vec{m}_r = \frac{\varepsilon_0}{4\pi}\iint_{Apt}\vec{M}_r e^{-jk_x x'-jk_y y'}ds \tag{23}$$

$$k_z = \sqrt{k_0^2 - k_x^2 - k_y^2} \quad \text{for } k_0^2 \geq k_x^2 + k_y^2 \tag{24}$$

$$= -j\sqrt{k_x^2 + k_y^2 - k_0^2} \quad \text{for } k_0^2 \leq k_x^2 + k_y^2$$

Substituting equation (22) in equation (18), the scattered electric field $\left\{E_x', E_y' \text{and } E_z'\right\}$ due to the r^{th} aperture can be obtained. Superposition of the scattered electric field due to all apertures on the $z = 0$ plane gives the total electric field scattered by all the apertures. Similarly, using superposition and equation (22) in (19), gives the total scattered magnetic field due to all apertures. In these expressions, ψ_{rpqx} is the Fourier transform of Ψ_{rpqx} and ϕ_{rpqy} is the Fourier transform of Φ_{rpqy} [10].

3.3.4 EM fields inside the enclosure

The equivalent magnetic currents radiate electromagnetic fields into the enclosure. The total EM field at any point inside the enclosure is obtained by the superposition of fields due to each equivalent magnetic current source.

The electromagnetic field inside the enclosure (represented as superscript 11) due to the r^{th} aperture can be obtained from:

$$\vec{E}^{11}\left(\vec{M}_r\right)=\frac{-1}{\varepsilon_0}\nabla\times\vec{F}^{11} \tag{25}$$

$$\vec{H}^{11}\left(\vec{M}_r\right)=\frac{-j\omega}{k_0^2}\left(k_0^2+\nabla\nabla\bullet\right)\vec{F}^{11} \tag{26}$$

The electric vector potential appearing in (25) and (26) satisfies the inhomogeneous wave equation:

$$\nabla^2\vec{F}^{11}+k_0^2\vec{F}^{11}=-\varepsilon_0\vec{M}_r \tag{27}$$

If $\tilde{G}_m\left(x,y,z;x',y',z'\right)$ is the dyadic Green's function for the rectangular enclosure for a unit dyad $\vec{I}\left(x',y',z'\right)=\hat{x}\hat{x}+\hat{y}\hat{y}+\hat{z}\hat{z}$ inside the enclosure, then the electric vector potential $\vec{F}^{11}$ can be written in the form:

$$\vec{F}^{11}=\iiint\limits_{source}\tilde{G}_m\left(x,y,z;x',y',z'\right)\bullet\vec{M}_r\left(x',y',z'\right)dx'dy'dz' \tag{28}$$

Substitution of (28) in (27) yields

$$\nabla^2\tilde{G}_m+k_0^2\tilde{G}_m=-\varepsilon_0\vec{I}\delta\left(x-x'\right)\delta\left(y-y'\right)\delta\left(z-z'\right) \tag{29}$$

Since the apertures are in the xy-plane and $\vec{M}_r$ can have both the x- and y- directions,

$\vec{I}(x',y',z') = \hat{x}\hat{x} + \hat{y}\hat{y}$, hence equations (29) can be written in component forms as:

$$\nabla^2 G_{mxx} + k_0^2 G_{mxx} = -\varepsilon_0 \delta(x-x')\delta(y-y')\delta(z-z') \tag{30}$$

$$\nabla^2 G_{myy} + k_0^2 G_{myy} = -\varepsilon_0 \delta(x-x')\delta(y-y')\delta(z-z') \tag{31}$$

Though the other green's function components like $G_{xy}, G_{yx}, G_{yz}, G_{zy}, G_{xz}, G_{zx}$ exist only G_{xx} and G_{yy} are considered because SE_y component is calculated when calculating shielding effectiveness. Considering the x component of the magnetic current and using the proper boundary conditions, the solution of equation (30) can be written as:

$$G_{xx} = \sum_{m,n}^{\infty} \frac{\varepsilon_0}{k_l} \frac{\varepsilon_{0m}\varepsilon_{0n}}{ab} \sin\left(\frac{m\pi x'}{a}\right) \cos\left(\frac{n\pi y'}{b}\right) \frac{\cos\left(k_l(z-c)\right)}{\sin(k_l c)} \sin\left(\frac{m\pi x}{a}\right) \cos\left(\frac{n\pi y}{b}\right) \delta(z') \tag{32}$$

In expression (32), $\sum_{m,n}^{\infty}(\bullet) = \sum_{m=1}^{\infty}\sum_{n=0}^{\infty}(\bullet)$, and

$$k_l = \sqrt{k_0^2 - \left(\frac{m\pi}{a}\right)^2 - \left(\frac{n\pi}{b}\right)^2} \quad \text{for} \quad k_0^2 \geq \left(\frac{m\pi}{a}\right)^2 + \left(\frac{n\pi}{b}\right)^2 \tag{33}$$

$$= -j\sqrt{\left(\frac{m\pi}{a}\right)^2 + \left(\frac{n\pi}{b}\right)^2 - k_0^2} \quad \text{for} \quad k_0^2 \leq \left(\frac{m\pi}{a}\right)^2 + \left(\frac{n\pi}{b}\right)^2$$

$$\varepsilon_{0n} = \begin{cases} 1, n = 0 \\ 2, n \neq 0 \end{cases}$$

Substituting (32) and into (28) the electric vector potential $\vec{F}^{11x}$ due to the x-component of $\vec{M}_r$ on the plane $z = 0$ is obtained. Detailed expressions can be found in Khan's work [6].

Likewise, considering the y-component of the magnetic current and using the proper

boundary conditions, the solution of equation (31) can be written as:

$$G_{yy} = \sum_{m,n}^{\infty} \frac{-\varepsilon_0}{k_l} \frac{\varepsilon_{0m}\varepsilon_{0n}}{ab} \cos\left(\frac{m\pi x'}{a}\right) \sin\left(\frac{n\pi y'}{b}\right) \frac{\cos\left(k_l(z-c)\right)}{\sin(k_l c)}$$

$$\cos\left(\frac{m\pi x}{a}\right) \sin\left(\frac{n\pi y}{b}\right) \delta(z') \tag{34}$$

for the aperture located in the $z = 0$ plane. Substituting (34) into (28) the electric vector potential $\vec{F}^{11y}$ due to the y-component of $\overrightarrow{M_r}$ for the apertures in the $z = 0$ plane is obtained. Detailed expressions can be found in Khan's work [10].

3.3.5 Application of Boundary conditions at apertures

The total tangential magnetic fields inside the cavity from apertures are written as:

$$H_x^{11} = \left(H_x^{11x} + H_x^{11y}\right) \tag{35}$$

$$H_y^{11} = \left(H_y^{11x} + H_y^{11y}\right) \tag{36}$$

Using continuity of tangential magnetic fields across the apertures in the $z = 0$ plane yields

$$H_{xi}\big|_{z=0} + H_x^1\big|_{z=0} = \left(H_x^{11x} + H_x^{11y}\right)\Big|_{z=0} \tag{37}$$

$$H_{yi}\big|_{z=0} + H_y^1\big|_{z=0} = \left(H_y^{11x} + H_y^{11y}\right)\Big|_{z=0} \tag{38}$$

In deriving equations (37) and (38) it is assumed that the cavity is excited by a plane wave incident from $z = -\infty$. The field expressions derived in the earlier sections will be substituted in (37) solving for the boundary conditions for the x component and in (38) solving for the boundary conditions in the y direction. Detailed expressions can be found in Khan's work [10].

Now selecting $\Psi_{r'p'q'x}$ as a testing function taking Fourier transform and using Galerkin's method reduces the final equations satisfying the boundary conditions.

$$I_{r'p'q'xi} + \sum_{r=1}^{R}\sum_{p,q}\frac{\omega\varepsilon_0 U_{rpq}}{4\pi^2 k_0^2}\int_{-\infty}^{\infty}\int_{-\infty}^{\infty}\psi_{rpqx}\psi^{*}_{rpqx}\frac{\left(k_0^2-k_x^2\right)}{k_I}dk_x dk_y$$

$$\sum_{r=1}^{R}\sum_{p,q}\frac{-\omega\varepsilon_0 V_{rpq}}{4\pi^2 k_0^2}\int_{-\infty}^{\infty}\int_{-\infty}^{\infty}\phi_{rpqy}\psi^{*}_{r'p'q'x}\frac{\left(-k_x k_y\right)}{k_I}dk_x dk_y$$

$$= \frac{-j\omega}{k_0^2}\sum_{r=1}^{R}\sum_{p,q}U_{rpq}\sum_{m,n}^{\infty}\frac{-\varepsilon_0}{k_I}\frac{\varepsilon_{0m}\varepsilon_{0n}}{ab\sin\left(k_I c\right)}\left(k_0^2-\left(\frac{m\pi}{a}\right)^2\right)\cos\left(k_I c\right)S_{rpqmnx}S_{r'p'q'mnx}$$

$$-\frac{j\omega}{k_0^2}\sum_{r=1}^{R}\sum_{p,q}-V_{rpq}\sum_{m,n}^{\infty}\frac{-\varepsilon_0}{k_I}\frac{\varepsilon_{0m}\varepsilon_{0n}}{ab\sin\left(k_I c\right)}\left(-\frac{m\pi}{a}\right)\frac{n\pi}{b}\cos\left(k_I c\right)S_{rpqmny}S_{r'p'q'mnx} \qquad (39)$$

Rearranging the terms in (58) we get,

$$I_{r'p'q'xi} = \sum_{r=1}^{R}\sum_{p,q}\left(U_{rpq}Y^{x1x1}_{rpqr'p'q'} + V_{rpq}Y^{x1y1}_{rpqr'p'q'}\right) \qquad (40)$$

$I_{r'p'q'xi}$ is the coupling of testing function with x component of incident magnetic field.

Where,

$$Y^{x1x1}_{rpqr'p'q'} = \frac{-j\omega}{k_0^2}\sum_{m,n}^{\infty}\frac{-\varepsilon_0}{k_I}\frac{\varepsilon_{0m}\varepsilon_{0n}}{ab\sin\left(k_I c\right)}\left(k_0^2-\left(\frac{m\pi}{a}\right)^2\right)\cos\left(k_I c\right)S_{rpqmnx}S_{r'p'q'mnx}$$

$$-\frac{\omega\varepsilon_0}{4\pi^2 k_0^2}\int_{-\infty}^{\infty}\int_{-\infty}^{\infty}\psi_{rpqx}\psi^{*}_{r'p'q'x}\frac{\left(k_0^2-k_x^2\right)}{k_z}dk_x dk_y \qquad (41)$$

$$Y^{x1y1}_{rpqr'p'q'} = \frac{j\omega}{k_0^2}\sum_{m,n}^{\infty}\frac{-\varepsilon_0}{k_I}\frac{\varepsilon_{0m}\varepsilon_{0n}}{ab\sin\left(k_I c\right)}\left(-\frac{m\pi}{a}\right)\frac{n\pi}{b}\cos\left(k_I c\right)S_{rpqmny}S_{r'p'q'mnx}$$

$$+\frac{\omega\varepsilon_0}{4\pi^2 k_0^2}\int_{-\infty}^{\infty}\int_{-\infty}^{\infty}\phi_{rpqy}\psi^{*}_{r'p'q'x}\frac{\left(-k_x k_y\right)}{k_z}dk_x dk_y \qquad (42)$$

$$I_{r'p'q'xi} = \iint_{r'p'q'} H_{xi}\Psi_{r'p'q'x}dxdy \qquad (43)$$

Now selecting $-\Phi_{r'p'q'y}$ as a testing function and use of Galerkin's method reduces the above equation to:

$$I_{r'p'q'yi} = \sum_{r=1}^{R}\sum_{p,q}\frac{-\omega\varepsilon_0 V_{rpq}}{4\pi^2 k_0^2}\int_{-\infty}^{\infty}\int_{-\infty}^{\infty}\phi_{rpqy}\phi^{*}_{rpqy}\frac{\left(k_0^2-k_y^2\right)}{k_I}dk_x dk_y$$

$$+\sum_{r=1}^{R}\sum_{p,q}\frac{\omega\varepsilon_0 U_{rpq}}{4\pi^2 k_0^2}\int_{-\infty}^{\infty}\int_{-\infty}^{\infty}\psi_{rpqx}\phi^{*}_{r'p'q'y}\frac{\left(-k_x k_y\right)}{k_I}dk_x dk_y$$

$$+\frac{j\omega}{k_0^2}\sum_{r=1}^{R}\sum_{p,q}U_{rpq}\sum_{m,n}^{\infty}\frac{-\varepsilon_0}{k_I}\frac{\varepsilon_{0m}\varepsilon_{0n}}{ab\sin\left(k_I c\right)}\frac{m\pi}{a}\left(-\frac{n\pi}{b}\right)\cos\left(k_I c\right)S_{rpqmnx}S_{r'p'q'mny}$$

$$+\frac{j\omega}{k_0^2}\sum_{r=1}^{R}\sum_{p,q}-V_{rpq}\sum_{m,n}^{\infty}\frac{-\varepsilon_0}{k_I}\frac{\varepsilon_{0m}\varepsilon_{0n}}{ab\sin\left(k_I c\right)}\left(k_0^2-\left(\frac{n\pi}{b}\right)^2\right)\cos\left(k_I c\right)S_{rpqmny}S_{r'p'q'mny} \quad (44)$$

Rearranging the terms in (44) we get,

$$I_{r'p'q'yi} = \sum_{r=1}^{R}\sum_{p,q}\left(U_{rpq}Y^{y1x1}_{rpqr'p'q'} + V_{rpq}Y^{y1y1}_{rpqr'p'q'}\right) \quad (45)$$

$I_{r'p'q'yi}$ is the coupling of testing function with y component of incident magnetic field.

Where,

$$Y^{y1x1}_{rpqr'p'q'} = \frac{\omega\varepsilon_0}{4\pi^2 k_0^2}\int_{-\infty}^{\infty}\int_{-\infty}^{\infty}\psi_{rpqx}\phi^{*}_{r'p'q'y}\frac{\left(-k_x k_y\right)}{k_z}dk_x dk_y$$

$$+\frac{j\omega}{k_0^2}\sum_{m,n}^{\infty}\frac{-\varepsilon_0}{k_I}\frac{\varepsilon_{0m}\varepsilon_{0n}}{ab\sin\left(k_I c\right)}\frac{m\pi}{a}\left(\frac{n\pi}{b}\right)\cos\left(k_I c\right)S_{rpqmnx}S_{r'p'q'mny} \quad (46)$$

$$Y^{x1y1}_{rpqr'p'q'} = \frac{-\omega\varepsilon_0}{4\pi^2 k_0^2}\int_{-\infty}^{\infty}\int_{-\infty}^{\infty}\phi_{rpqy}\phi^{*}_{r'p'q'y}\frac{\left(k_0^2-k_y^2\right)}{k_z}dk_x dk_y$$

$$+\frac{-j\omega}{k_0^2}\sum_{m,n}^{\infty}\frac{-\varepsilon_0}{k_I}\frac{\varepsilon_{0m}\varepsilon_{0n}}{ab\sin\left(k_I c\right)}\left(k_0^2-\left(\frac{n\pi}{b}\right)^2\right)\cos\left(k_I c\right)S_{rpqmny}S_{r'p'q'mny} \quad (47)$$

$$I_{r'p'q'yi} = -\iint_{r'p'q'} H_{yi}\Phi_{r'p'q'y}dxdy \quad (48)$$

3.3.6 Final Matrix equation for MOI

Equations (59) and (65) can be written in matrix form as:

$$\begin{bmatrix} Y^{xlxl}_{rpqr'p'q'} & Y^{xlyl}_{rpqr'p'q'} \\ Y^{ylxl}_{rpqr'p'q'} & Y^{ylyl}_{rpqr'p'q'} \end{bmatrix} \begin{bmatrix} U_{rpq} \\ V_{rpq} \end{bmatrix} = \begin{bmatrix} I_{r'p'q'xi} \\ I_{r'p'q'yi} \end{bmatrix} \tag{49}$$

Where,

$Y^{xlxl}_{rpqr'p'q'}$ - Mutual admittance between x- components of currents on z = 0 plane

$Y^{xlyl}_{rpqr'p'q'}$ - Mutual coupling between x- and y- components of currents on z = 0 plane

$Y^{ylxl}_{rpqr'p'q'}$ - Mutual admittance between y- and x- components of currents on z = 0 plane

$Y^{ylyl}_{rpqr'p'q'}$ - Mutual coupling between x- component of currents on z = 0 plane

U_{rpq} - Complex modal amplitude of pq^{th} mode for aperture on z = 0 plane. (For x- directed aperture field)

V_{rpq} - Complex modal amplitude of pq^{th} mode for aperture on z = 0 plane. (For y- directed aperture field)

The matrix equation (49) is in the required form $[A][x]=[B]$ which can be numerically solved for the unknown amplitudes of equivalent magnetic currents induced on the apertures due to the incident field. From the knowledge of these amplitudes, electromagnetic field inside as well as outside the cavity can be determined.

In the matrix equation, the vector $[x]$ represents the unknown modal amplitudes of the aperture fields. The matrix $[A]$ has been obtained from the geometrical configuration of the problem, i.e. the dimensions of the cavity, the number and location of apertures on the

front wall and the media inside and outside the aperture. The matrix$[A]$, therefore, does not change as long as the geometrical details of the problem at hand are not changed. The matrix$[B]$ depends upon the incident wave and is the independent variable for our matrix equation. MNI considers only the normal incidence *E- polarized* plane wave case and hence uses a special form of the matrix$[B]$. The generalization of the MNI is the modification of the matrix$[B]$ to allow oblique incidence arbitrary polarized plane waves. This requires the derivation of the general forms of the expressions I_{rpqxi} and I_{rpqyi} used in the MNI code which can be found in Khan's work [6].

As indicated above through the derivations, the MNI which is able to support only the normal incidence and single polarization case has been modified to accommodate a variety of incidence angles and polarizations. With this modifications being made to MNI, the new one does not accommodate a wire inside the cavity hence MNI is used for the problem of solving the currents on the probe that exists inside the cavity.

3.4 Shielding effectiveness development for fields with normal incidence: Current induced on the probe

In this section the current induced on a wire radiator is found using method of moments. By determining the current distribution of the wire radiator, the value of the current at the bottom when it is attached to the cavity wall is analyzed. This section is directly related to the problem of finding the induced current on the probe attached to the cavity wall. First the current induced on a wire radiator in free space is derived and from that it is expanded to the wire inside the cavity problem.

Integral equation for a wire radiator

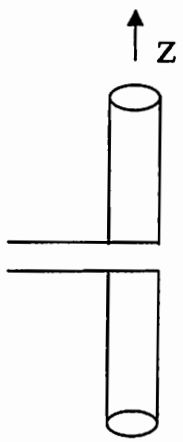

Figure 3.4.1 A wire radiator

Consider a solid wire with infinite conductivity 'σ' with finite radius 'a'. The current density on the wire is given by the formula $J = \sigma E$. 'E' being the electric field induced due to the current. The current distribution on the wire can be represented by Fig 3.4.2 (a) and by taking Pocklington's Integral equation assumption; the current distribution can be redrawn as in Fig 3.4.2 (b)

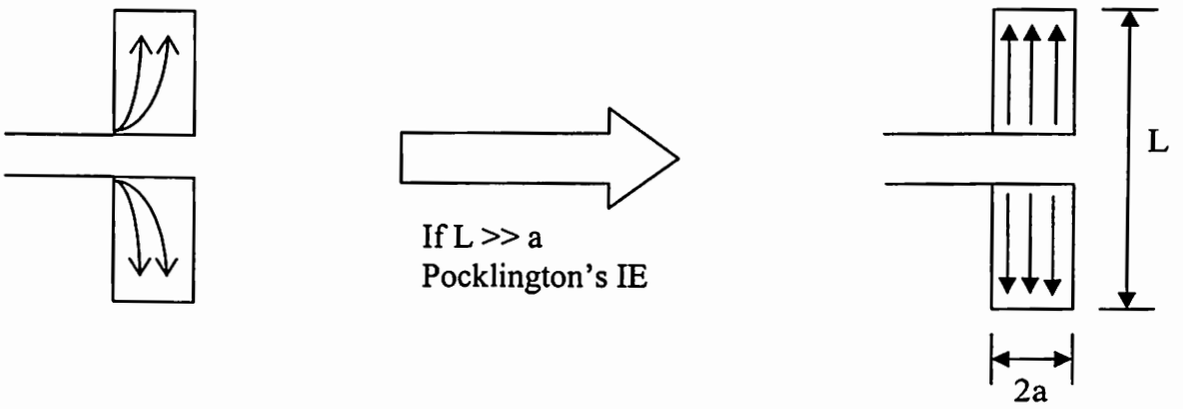

Figure 3.4.2 (a) Current distribution on a wire radiator (b) Current distribution after Pocklington's

Assume a incident wave is impinges on the surface of a conducting wire and this is referred to the incident wave E_z^i. When the wire is an antenna, the incident field is produced by the voltage at the gap in the bottom. Part of the incident field, impinges the wire and induces on its surface a linear current density J_s. The induced current density J_s reradiates and produces a electric field that is referred to as the scattered electric field E_z^s. Therefore at any point in space the total electric field E_{ztot} is the sum of the incident field and the scattered fields.

$$E_{ztot} = E_z^s + E_z^i \tag{50}$$

When the observation point is moved to the surface of the wire ($r = r_s$) and the wire is perfectly conducting, the total tangential electric field vanishes. In cylindrical co ordinates, the electric field radiated by the dipole has a radial component (E_ρ) and a tangential component (E_z). Therefore the tangential electric field on the surface reduces to

$$E_{ztot} = E_z^s + E_z^i = 0$$
$$E_z^s = -E_z^i \tag{51}$$

In general, the scattered electric field generated by the induced current density J_s is given by

$$\begin{aligned}\vec{E}_s &= -j\omega\vec{A} - \frac{j}{\omega\mu\varepsilon}\nabla\left(\nabla\bullet\vec{A}\right) \\ &= -j\frac{1}{\omega\mu\varepsilon}\left[k^2 A + \nabla\left(\nabla\bullet\vec{A}\right)\right]\end{aligned} \tag{52}$$

However, for the observations at the wire surface only the z component of (52) is needed and that can be written as

$$E_z^s = -j\frac{1}{\omega\mu\varepsilon}\left(k^2 A_z + \frac{\partial^2 A_z}{\partial z^2}\right) \tag{53}$$

Neglecting the edge effects, A_z can be written as

$$A_z = \frac{\mu}{4\pi}\iint_s J_z \frac{e^{-jkR}}{R} ds' = \frac{\mu}{4\pi}\int_{-l/2}^{l/2}\int_0^{2\pi} J_z \frac{e^{-jkR}}{R} a d\phi' dz' \tag{54}$$

If the wire is very thin, the current density J_z is not a function of the azimuthal angle ϕ, and we can write it as

$$2\pi a J_z = I_z(z') \Rightarrow J_z = \frac{1}{2\pi a} I_z(z') \tag{55}$$

Where, $I_z(z')$ is assumed to be an equivalent filament line source current located at a radial distance $\rho = a$ from the z axis. Thus A_z reduces to

$$A_z = \frac{\mu}{4\pi}\int_{-l/2}^{l/2}\left[\frac{1}{2\pi a}\int_0^{2\pi} I_z(z')\frac{e^{-jkR}}{R}ad\phi'\right]dz' \tag{56}$$

$$\begin{aligned} R &= \sqrt{(x-x')^2+(y-y')^2+(z-z')^2} \\ &= \sqrt{(\rho 2+a2)-2\rho a\cos(\phi-\phi')+(z-z'^2)} \end{aligned} \tag{57}$$

Where, ρ is the radial distance to the observation point and a is the radius.

The observations are not a function of ϕ because of the symmetry of the scatterer. For simplicity $\phi = 0$ is chosen. For observations on the surface $\rho = a$ of the scatterer, (56) and (57) reduce to

$$\begin{aligned} A_z(\rho=a) &= \mu\int_{-l/2}^{l/2} I_z(z')\left[\frac{1}{2\pi}\int_0^{2\pi}\frac{e^{-jkR}}{R}ad\phi'\right]dz' \\ &= \mu\int_{-l/2}^{l/2} I_z(z')G(z,z')dz' \end{aligned} \tag{58}$$

$$R(\rho=a) = \sqrt{4a^2\sin^2\left(\frac{\phi'}{2}\right)+(z-z')^2} \tag{59}$$

Thus for observations at the surface $\rho = a$ of the scatterer, the z component of the scattered electric field can be expressed as

$$E_z^{\ s} = \frac{1}{j\omega\varepsilon}\int_{-\frac{l}{2}}^{\frac{l}{2}}\left[\left(\frac{\partial^2}{\partial z^2}+k^2\right)G(z,z')\right]I(z')dz' = -E_z^{\ i} \tag{60}$$

(60) is referred to as Pocklington's integral equation and it can be used to determine the equivalent filamentary line source current of the wire and thus the current density on the wire, by knowing the incident field on the surface of the wire.

If we assume the wire to be very thin $(a \ll \lambda)$ such that $G(z,z')$ reduces to

$$G(z,z') = G(R) = \frac{e^{-jkR}}{4\pi R} \tag{61}$$

In (60) $I_z(z')$ represents the equivalent filamentary line source current located on the surface of the wire. This is obtained by knowing the incident field on the surface of the wire. By point matching techniques, this is solved by matching the boundary conditions at discrete points on the surface of the wire. Often it is easier to choose the matching points to be at the center of the wire especially along the axis in which $I_z(z')$ is located. By reciprocity the current can be moved to the center of the wire and matching points are selected on the surface of the wire. Thus the current distribution on the wire conductor can be found.

Thus it can be seen that at the matched point the current must be maximum. When the current is maximum at that point then the field that is generated by that current will also be maximum.

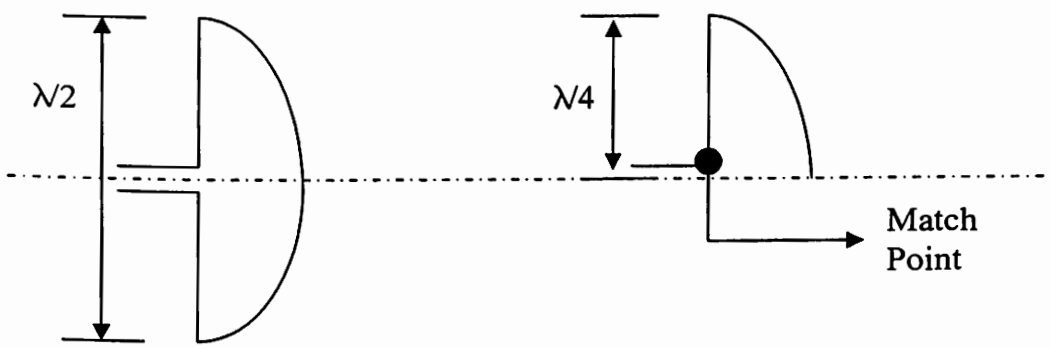

Figure 3.4.3 (a) Current distribution on a half wave dipole (b) Current distribution on a quarter wave monopole

The current distribution of a half wave dipole antenna is shown in Fig 3.4.3 (a). It can be seen that the current is maximum at the center and zero at the ends of the antenna. The current distribution on a λ/4 monopole is shown in Fig 3.4.3 (b). As can be seen the current is maximum at the bottom of the monopole where it is fed and goes to zero at the top edge. Considering the monopole inside the enclosure and being attached to one of the walls of the cavity, at the point where the input impedance of the antenna is matched, the current will be maximum. For our case the monopole is excited at the bottom and attached to the cavity wall at the bottom. So at the frequency where the input impedance of the monopole is matched, a maximum current is expected.

3.5 Development of current on the probe using MNI

This section describes how MNI handles the problem of finding the current on the wire that is located on one of its cavity walls. As explained before, MNI alone supports a wire inside the cavity while MOI does not so the development with MNI is presented here. The scattered electric field $\sum_{r=1}^{R} \vec{E}_{ext}\left(\vec{M}_{rx}\right)$, scattered magnetic field $\sum_{r=1}^{R} \vec{H}_{ext}\left(\vec{M}_{rx}\right)$ due to the equivalent magnetic currents exterior to the cavity and the scattered electric field $\sum_{r=1}^{R} \vec{E}_{int}\left(\vec{M}_{rx}\right)$, scattered magnetic field $\sum_{r=1}^{R} \vec{H}_{int}\left(\vec{M}_{rx}\right)$ due to the equivalent magnetic currents interior to the cavity obtained are used. Using the cavity modal functions, the scattered electric field $\vec{E}_{int}\left(\vec{J}_p\right)$ and the magnetic field $\vec{H}_{int}\left(\vec{J}_p\right)$ due to the current induced on the probe are obtained. Continuity of the tangential magnetic fields across the window apertures yields

$$\left[\vec{H}_{in}(f)+\sum_{r=1}^{R}\vec{H}_{ext}\left(\vec{M}_{rx}\right)\right]\times\hat{n}=\left[\vec{H}_{int}\left(\vec{M}_{rx}\right)+\sum_{r=1}^{R}\vec{H}_{int}\left(\vec{J}_{p}\right)\right]\times\hat{n} \tag{62}$$

$\vec{H}_{in}$ - Incident magnetic field

$\vec{H}_{ext}\left(\vec{M}_{rx}\right)$ - Scattered magnetic field (external)

$\vec{H}_{int}\left(\vec{M}_{rx}\right)$ - Scattered magnetic field (internal)

Where, $\hat{n}$ is the unit normal vector to the aperture. Likewise, forcing the tangential electric field over the wire to zero yields

$$\left[\left[\vec{E}_{int}\left(\vec{M}_{rx}\right)\right]+\vec{E}_{int}\left(\vec{J}_{p}\right)\right]\bullet\hat{l}=0 \tag{63}$$

Where, $\hat{l}$ is the unit vector along the probe. Equations (62) and (63) are the required integral equations to be solved for the aperture voltages and the wire current. The tangential aperture electric fields over the apertures can be expressed as

$$\vec{E}_{apt}=\hat{y}\sum_{r=1}^{R}\sum_{p=1,3,..}^{P}\frac{U_{pr}}{W_{r}}sin\left(\frac{p\pi}{L_{r}}\left(\frac{L_{r}}{2}+x-x_{cr}\right)\right)$$

$$\text{for } x_{cr}-\frac{L_{r}}{2}\le x\le x_{cr}+\frac{L_{r}}{2} \text{ and } y_{cr}-\frac{W_{r}}{2}\le y\le y_{cr}+\frac{W_{r}}{2} \tag{64}$$

Where, U_{pr} is the amplitude of the p^{th} mode on the r^{th} aperture, (L_r, W_r) are the length and width of the r^{th} aperture, (x_{cr}, y_{cr}) are the coordinates of the r^{th} aperture. The equivalent magnetic currents over the aperture can be written as

$$\vec{M}_{rx}=-\hat{n}\times\hat{y}\sum_{p=1,3,..}^{P}\frac{U_{pr}}{W_{r}}\sin\left(\frac{p\pi}{L_{r}}\left(\frac{L_{r}}{2}+x-x_{cr}\right)\right)$$

The current induced on the wire can be written as

$$\vec{J}_p = \hat{y}\frac{I_0}{\pi d_0}\frac{sin\left(k_0\left(L_w - y\right)\right)}{sin\left(K_0 L_w\right)} \tag{65}$$

Where, I_0 is the total current on the wire at the point where it is connected to the wall of the cavity. d_0 is the wire diameter and L_w is the wire length. Selecting the expansion and testing functions for the magnetic currents on the apertures and the electric current on the wire as given in equations (64) and (65) respectively, the integral equations in (62) and (63) are transformed into a matrix equation given by

$$\begin{bmatrix} [Y] & [C] \\ [C]^T & Z_{ww} \end{bmatrix}\begin{bmatrix} [U] \\ I_0 \end{bmatrix} = \begin{bmatrix} [I_{rp}] \\ 0 \end{bmatrix} \tag{66}$$

The admittance matrix $[Y]$ is equation (66) represents mutual coupling between the modes on the apertures, the sub matrix $[C]$ represents the mutual coupling between the aperture modes and the wire current, and Z_{ww} represents the self impedance of the wire. The elements of the admittance matrix are given by

$$Y_{rpr'p'} = -\frac{j\omega}{k_0^{\,2}}\sum_{m,n}^{\infty} -\frac{\varepsilon_0}{k_I}\frac{\varepsilon_{0m}\varepsilon_{0n}}{absin\left(k_I c\right)}\left(k_0^{\,2} - \left(\frac{m\pi}{a}\right)^2\right)cos\left(k_I c\right) I_{rpmnx} I_{r'p'mnx}$$
$$- \frac{\omega\varepsilon_0}{4\pi^2 k_0^{\,2}}\int_{-\infty}^{\infty}\int_{-\infty}^{\infty}\Psi_{rpx}\left(\Psi_{r'p'x}\right)^*\frac{\left(k_0^{\,2} - \left(k_x\right)^2\right)}{k_z}dkxdky \tag{67}$$

if r and r' apertures are on the same side wall, and

$$Y_{rpr'p'} = -\frac{j\omega}{k_0^{\,2}}\sum_{m,n}^{\infty} -\frac{\varepsilon_0}{k_I}\frac{\varepsilon_{0m}\varepsilon_{0n}}{absin\left(k_I c\right)}\left(k_0^{\,2} - \left(\frac{m\pi}{a}\right)^2\right)cos\left(k_I c\right) I_{rpmnx} I_{r'p'mnx} \tag{68}$$

if r and r' apertures are on different walls of the cavity.

The expression for I_{rpmnx} is given by

$$I_{rpmnx} = \frac{-p\pi L_r}{\left((p\pi)^2 - \left(\frac{m\pi L_r}{a}\right)^2\right)}\left[\cos(p\pi)\sin\left(\frac{m\pi}{a}(L_r + x_{cr})\right) + \sin\left(\frac{m\pi}{a}(L_r - x_{cr})\right)\right]$$

$$\frac{\sin\left(\frac{n\pi W_r}{2b}\right)}{\frac{n\pi W_r}{2b}}\cos\left(\frac{n\pi y_{cr}}{b}\right) \tag{69}$$

and $I_{r'p'mnx}$ is the same as equation (69) with r, p replaced by r', p' respectively.

The expression Ψ_{px} is given by

$$\Psi_{rpx} = \frac{L_r W_r}{2j} e^{-jk_x x_{cr} - jk_y y_{cr}}\left[e^{j\frac{p\pi}{2}}\frac{\sin\left(\frac{p\pi}{2} - \frac{k_x L_r}{2}\right)}{\frac{p\pi}{2} - \frac{k_x L_r}{2}} - e^{-j\frac{p\pi}{2}}\frac{\sin\left(\frac{p\pi}{2} + \frac{k_x L_r}{2}\right)}{\frac{p\pi}{2} + \frac{k_x L_r}{2}}\right]$$

$$\frac{\sin\left(\frac{k_y W_r}{2}\right)}{\frac{k_y W_r}{2}} \tag{70}$$

$\left(\Psi_{r'p'x}\right)^*$ is the complex conjugate of $\Psi_{r'p'x}$ where r, p in equation (70) is replaced by r', p' respectively. The elements of the coupling matrix $[C]$ are given by

$$C_{pq} = -\sum_{m,n}^{\infty}\frac{\varepsilon_{0m}\varepsilon_{0n}}{ab}\frac{\sin\left(k_l\left(c - z_p\right)\right)}{\sin\left(k_l c\right)}\sin\left(\frac{m\pi x_p}{a}\right)F_{1n}I_{rpmnx} \tag{71}$$

Where,

$$F_{1n} = \frac{k_0}{\sin\left(k_0 L_w\right)}\left(\cos\left(k_0 L_w\right) - \cos\left(\frac{n\pi L_w}{b}\right)\right) \tag{72}$$

and $\left(x_p, y_p, z_p\right)$ are the coordinates of the point where the wire connects to the walls of the cavity. The self impedance of the wire is given by

$$Z_{ww} = -j\frac{\omega\mu_0}{4(k_0)^2}\sum_{m,n}^{\infty}\frac{\varepsilon_{0m}\varepsilon_{0n}}{abk_I}\left((k_0)^2-\left(\frac{n\pi}{b}\right)^2\right)sin^2\left(\frac{m\pi x_p}{a}\right)F1nF1n\left[\frac{sin\left(\frac{m\pi d_0}{2a}\right)}{\frac{m\pi d_0}{2a}}\right]$$

$$\left\{\frac{sin\left(k_I\left(c-z_p\right)\right)sin\left(k_I\left(c-\frac{d_0}{2}\right)\right)}{sin\left(k_Ic\right)}+\frac{sin\left(k_Iz_p\right)sin\left(k_I\left(c-z_p-\frac{d_0}{2}\right)\right)}{sin\left(k_Ic\right)}\right\}$$

$$-j\frac{\omega\mu_0}{4(k_0)^2}\sum_{m,n}^{\infty}\frac{\varepsilon_{0m}\varepsilon_{0n}}{abk_I}\left((k_0)^2-\left(\frac{n\pi}{b}\right)^2\right)sin^2\left(\frac{m\pi x_p}{a}\right)F1nF1n\left\{\frac{sin\left(k_I\left(c-z_p\right)\right)F_{0z}+sin\left(k_Iz_p\right)F_{cz}}{k_Id_0sin\left(k_Ic\right)}\right\}$$

$$\left[2cos\frac{m\pi}{a}\frac{d_0}{2}\right] \qquad (73)$$

Where,

$$F_{0z} = cos\left(k_I\left(z_p-\frac{d_0}{2}\right)\right)-cos\left(k_Iz_p\right)$$

$$F_{cz} = cos\left(k_I\left(c-z_p-\frac{d_0}{2}\right)\right)-cos\left(k_I\left(c-z_p\right)\right)$$

$$k_I = \sqrt{(k_0)^2-\left(\frac{m\pi}{a}\right)^2-\left(\frac{n\pi}{b}\right)^2} \qquad \text{If } (k_0)^2 \geq \left(\frac{m\pi}{a}\right)^2+\left(\frac{n\pi}{b}\right)^2$$

$$k_I = -j\sqrt{\left(\frac{m\pi}{a}\right)^2+\left(\frac{n\pi}{b}\right)^2-(k_0)^2} \qquad \text{If } \left(\frac{m\pi}{a}\right)^2+\left(\frac{n\pi}{b}\right)^2 \geq (k_0)^2$$

The elements of the column matrix on the right hand side of the equation (66) are calculated from

$$I_{rp} = \int\int_{overr}\vec{H}_{in}(f)\bullet\hat{y}\times\hat{n}\frac{1}{W_r}\sin\left(\frac{p\pi}{L_r}\left(\frac{L_r}{2}+x-x_{cr}\right)\right)dxdy \qquad (74)$$

3.6 Input impedance of the wire using MNI

The input impedance of the wire inside the cavity is determined by assuming the wire is fed at the point (x_p, y_p, z_p) by a delta gap generator. In this transmission mode, the matrix equation takes the form

$$\begin{bmatrix} [Y] & [C] \\ [C]^T & Z_{ww} \end{bmatrix} \begin{bmatrix} [U] \\ I'_0 \end{bmatrix} = \begin{bmatrix} [0] \\ 1 \end{bmatrix} \tag{75}$$

Where, I'_0 is the unknown current on the wire when assumed to be excited by a delta gap source at the connection to the walls of the cavity. From the solution of the matrix equation (75), the input impedance if the wire inside the cavity is determined from

$$Z_{in}(f) = 1/I'_0(f) \tag{76}$$

In this chapter all the analytical expressions that have been used in the development of MNI and MOI has been discussed. As it appears in the derivation, MNI turns out to be a special case of MOI. For calculating the current induced on the probe and to find the input impedance of the probe MNI is used. A dipole is assumed to radiate in free space, the field induced due to a current in the dipole and also the input impedance of the dipole is calculated and the analysis is extended to a monopole inside the cavity following MNI. In the next chapter all the results for validation of Modal MoM and the results for the energy coupling on the probe are discussed.

Chapter 4

4.0 RESULTS

The results have been grouped under two major sections. The first section discusses the validation of MNI and MOI for which results have been doubtful when the size of the aperture is as big as the size of the wall. To validate MNI and MOI the same case is designed using FEKO and the results are compared. The results are also compared with a set of measured results and it shows better agreement with FEKO. The second section discusses about the energy coupling to the wire antenna that is introduced into the metallic enclosure by monitoring the currents and the field that is induced because of the current flow on the wire. There are no standard results to compare this with but for a particular case of a closed cavity and the wire antenna being excited internally, the input reactance is compared with the results from [36].

In general, this chapter includes all the results that validate MNI and MOI for the extreme case of having one wall of the cavity open when a plane wave at normal incidence is the source. These results put a measure on how much MOI can be trusted when the plane wave is incident on the cavity with apertures from different angles and different polarizations. The energy coupling results provides a conclusion on where the probe has to be located to couple maximum energy or not to pick up any energy due to external radiation.

4.1 Single Aperture Case

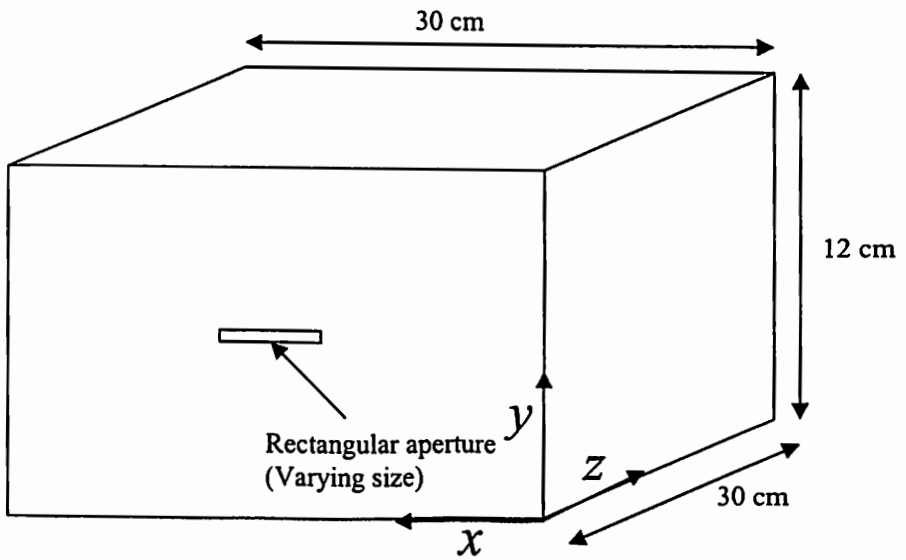

Figure 4.1.1 Geometry of the cavity with a single aperture at the front wall.

The geometrical configuration of the box is shown in the Figure 4.1.1. The aperture is located at the front face of the box. The box is excited with a y polarized plane wave. The plane wave is incident on the box at the front face (at the face where the aperture is present). An illustration of the plane wave excitation can be found in Fig 4.1.2. Using MNI fields at any point inside the box can be calculated, but for simplicity the field at the center of the box is calculated. The aperture size is varied from 10 x 0.5 (in cm) to 30 x 12 (in cm). For the varying size of the aperture, the field at the same point is calculated for a frequency sweep from 100 MHz to 1 GHz. The results for Shielding Effectiveness of the y- directed fields, obtained from Modal MoM are shown in the Figure 4.1.3

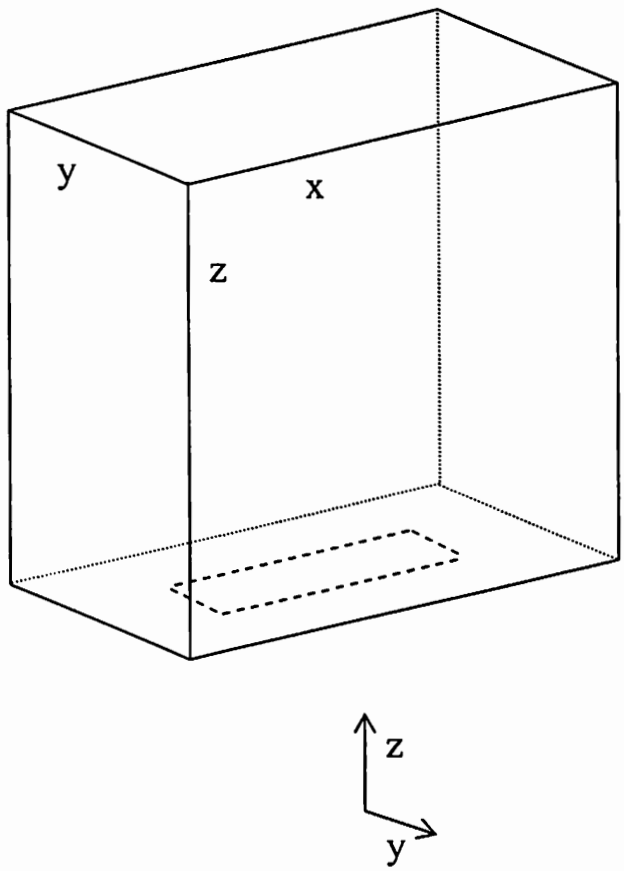

Figure 4.1.3 An illustration of the plane wave excitation.

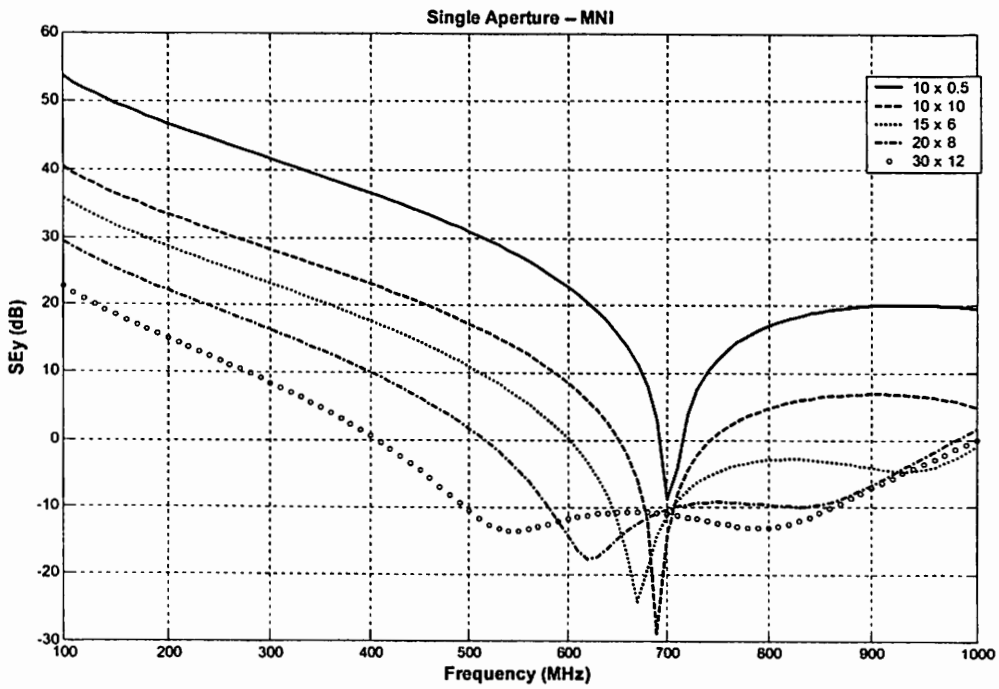

Figure 4.1.3 SEy results from MNI for varying aperture sizes (Single Aperture).

From the results it can be observed that the resonant frequency is around 700 MHz. When the frequency is varied from 100 MHz to 1 GHz, the shielding effectiveness drops to a minimum and then constantly increases there after. As the aperture size is increased, the null shifts towards the lower frequency side. A clear shift towards the low frequency can be seen in the null when the aperture size is comparatively large as in the 20 x 8 and 30 x 12 (in cm) cases. As MNI assumes an infinite ground plane, when the aperture size is made as big as the side of the box, the shielding effectiveness values obtained are not trusted to be right. This is because of the assumption in MNI that the aperture size has to be small compared to the cavity wall in which it is located. In order to validate this, the same scenario with varying aperture size was created in FEKO and the field at the center of the box is calculated. The results obtained from FEKO are shown in Figure 4.1.4.

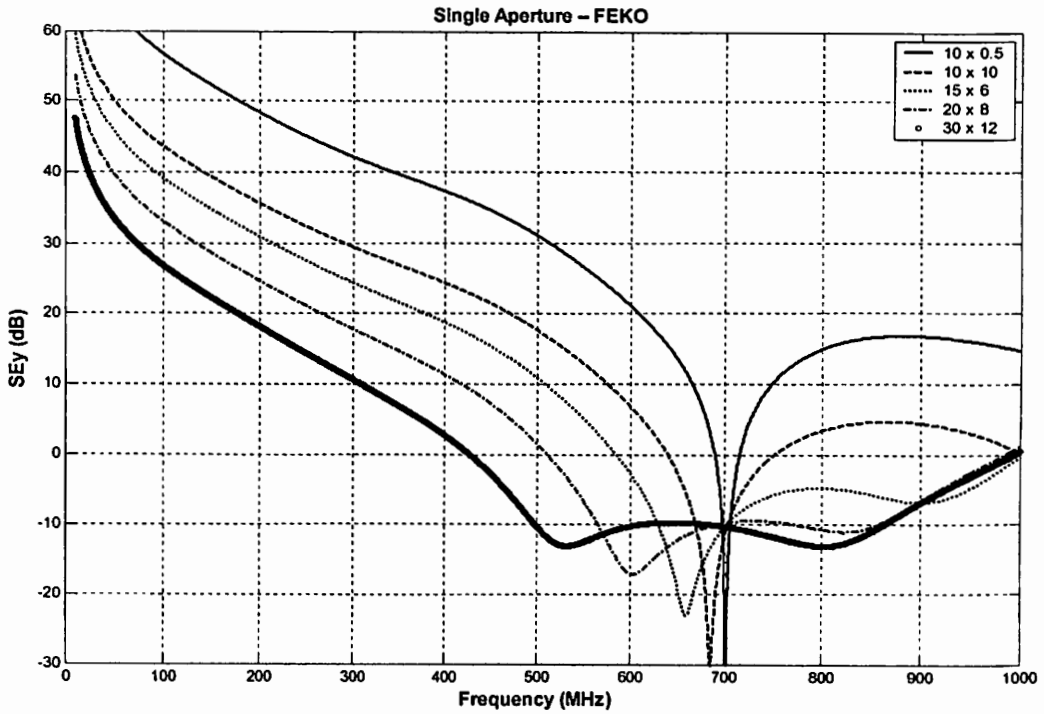

Figure 4.1.4 SEy results from FEKO for varying aperture sizes (Single Aperture).

From the results it can be seen that it follows the same pattern as observed via MNI when the aperture size is increased. The results obtained from MNI and FEKO are compared to validate MNI. This is shown in Figure 4.1.5.

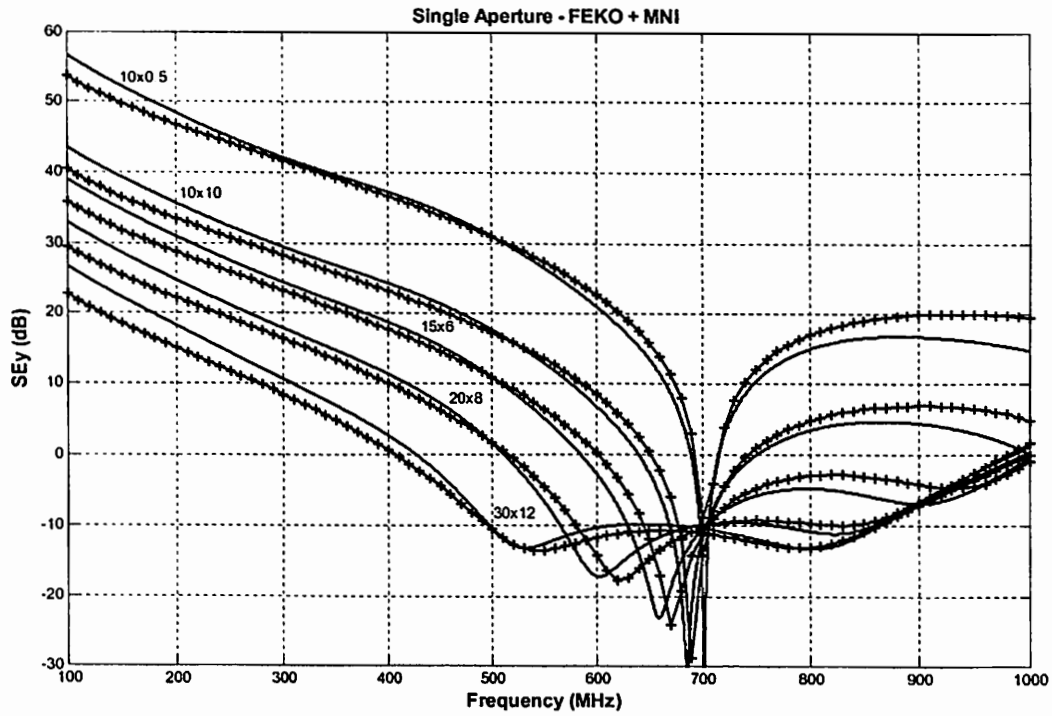

Figure 4.1.5 Comparison of SEy results from MNI and FEKO (Single Aperture).

From the results it can be seen that the SEy values obtained for different aperture size with MNI and FEKO shows good agreement in the range between 400 and 800 MHz. FEKO values agree well with MNI values at the lower frequencies better than the high frequency side. At 1 GHz when the aperture size is small, FEKO values are lower than the MNI values. There is a difference of about 5 dB at 1 GHz. But the pattern of the graph remains the same in MNI and FEKO. In order to solve for the difference between FEKO and MNI for the smallest apertures, the same problem was carried out for different grid size and a convergence study was done. In FEKO the grid size was made smaller

from $\lambda/15$ to $\lambda/25$ and the difference in SEy was about 0.2 dB. The other thing that has to be noted here is that in MNI only the dominant TE_{10} mode is considered at the apertures. Inclusion of higher order modes may decrease the value of SEy and the graphs might be close to each other for the smallest aperture case.

On the high frequency side, the number of variables that has to be solved using FEKO increases and due to certain limitations that many variables cannot be solved which also might be the reason for the low values. One other limitation with FEKO is that for a problem of finding the shielding effectiveness for a range of frequencies, it takes about 3 hours on a Xeon workstation with 4G RAM but MNI takes about 5-10 minutes. Comparing these, MNI is much faster than FEKO but the accuracy remains a question. Further research is required to ensure the accuracy. When the aperture size is increased and made all the way to the size of the box (Equivalent to having the box open at this side) the SEy values obtained from FEKO and MNI agrees well. This is an important aspect to note as the SE values from MNI have always been suspicious for this particular case due to the assumption in MNI of the dominant TE_{10} mode in the aperture. It is surprising to see that MNI still computes the correct values even for this special case. The comparison of MNI and FEKO for this special case is shown in Figure 4.1.6. The number of modes on the aperture was increased and the same computation was done for the smallest aperture (10x0.5) and the largest aperture size (30x12). The results are given in Figures 4.1.7 and 4.1.8. From these graphs it can be seen that inclusion of higher order modes at the aperture does not drastically change SEy. The effect of inclusion of higher order modes is more for the largest aperture case than in the smallest aperture case.

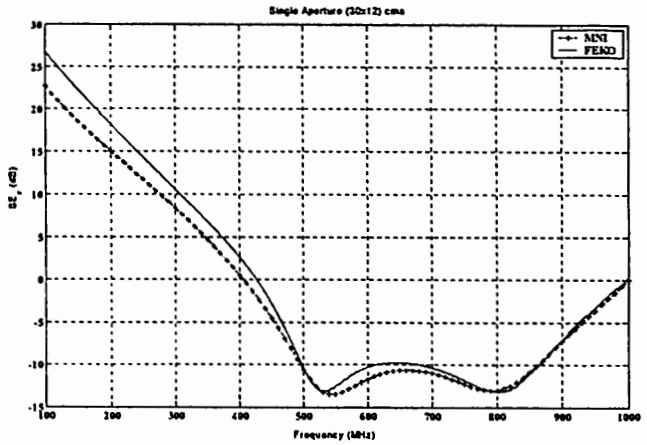

Figure 4.1.6 Comparison of SEy results from MNI and FEKO for aperture size (30 x 12) cms.

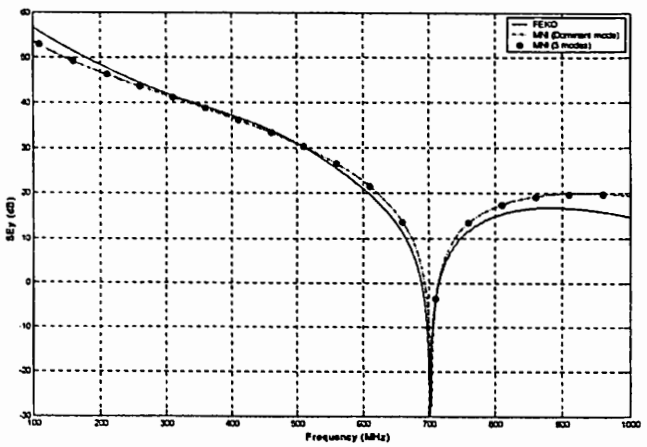

Figure 4.1.7 Comparison of SEy results from MNI (Dominant mode), MNI (5 modes) and FEKO for aperture size (10 x 0.5) cms.

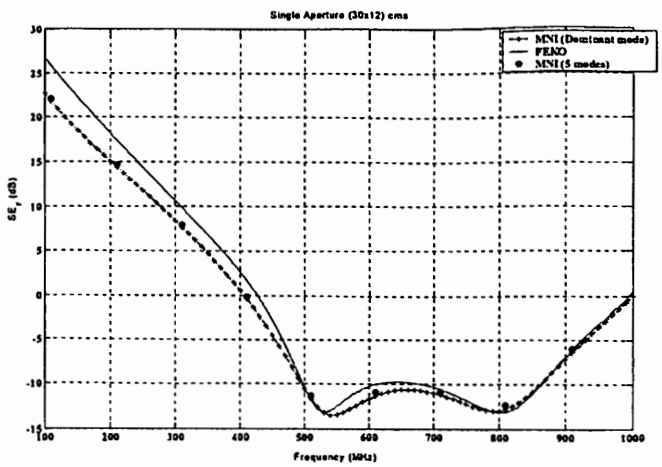

Figure 4.1.8 Comparison of SEy results from MNI (Dominant mode), MNI (5 modes) and FEKO for aperture size (30 x12) cms.

4.1.1 Multiple Incidence Angles:

The MNI that was developed in NASA was not able to support multiple angles of incidence. The code was capable of supporting only normal angle of incidence and zero polarization. The same Modal MoM code was modified by Khan – MOI [10] to support multiple angles of incidence and different polarizations. The results that were published in [54] haven't been compared with any other standard or measured results. So in order to validate the results computed using MOI and to put a bound on the range over which MOI can be trusted, the same has been modeled in FEKO and the results were compared. For some cases, measured results from ASU [48] has been included. MOI was used to compute the SEy values at the center of the box with different aperture sizes and for certain frequencies like 500 MHz, 800 MHz and 1 GHz. The incidence angle was varied from -85 to 85 degrees (171 values) with one degree step. Note:- 0 degree is the normal angle of incidence. The same was developed in FEKO and the results from FEKO were compared with MOI results. The comparison of FEKO and MOI at 500 MHz for different aperture sizes is shown in Figure 4.1.1.1 and 4.1.1.2.

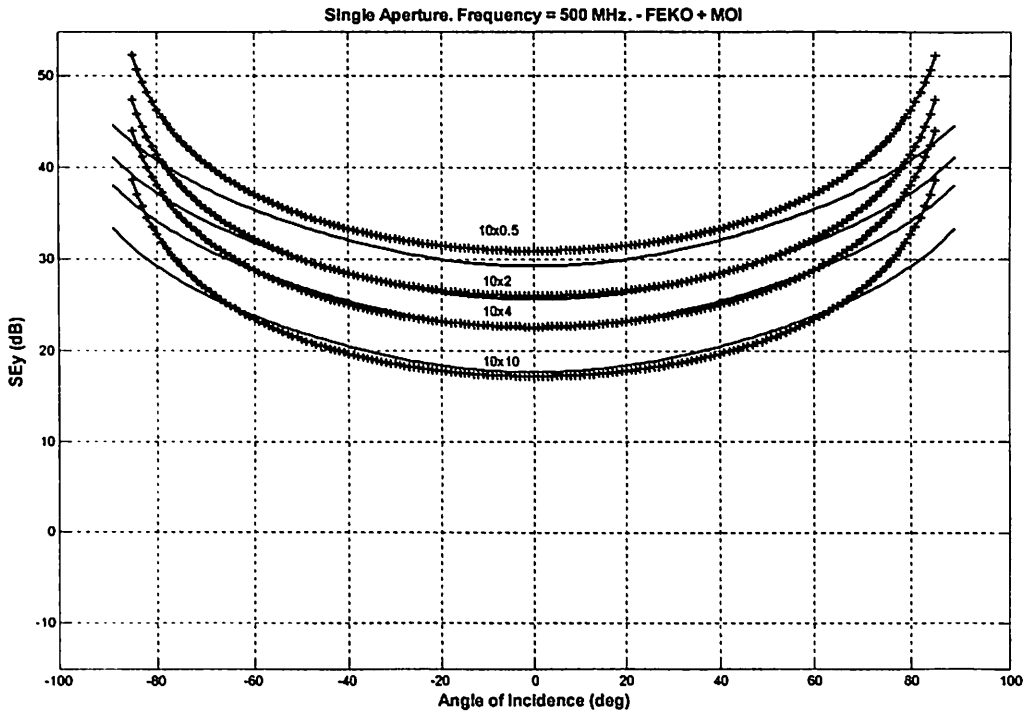

Figure 4.1.1.1 Comparison of SEy results from MOI and FEKO for varying angles of incidence at a frequency of 500 MHz (Single Aperture-Thin).

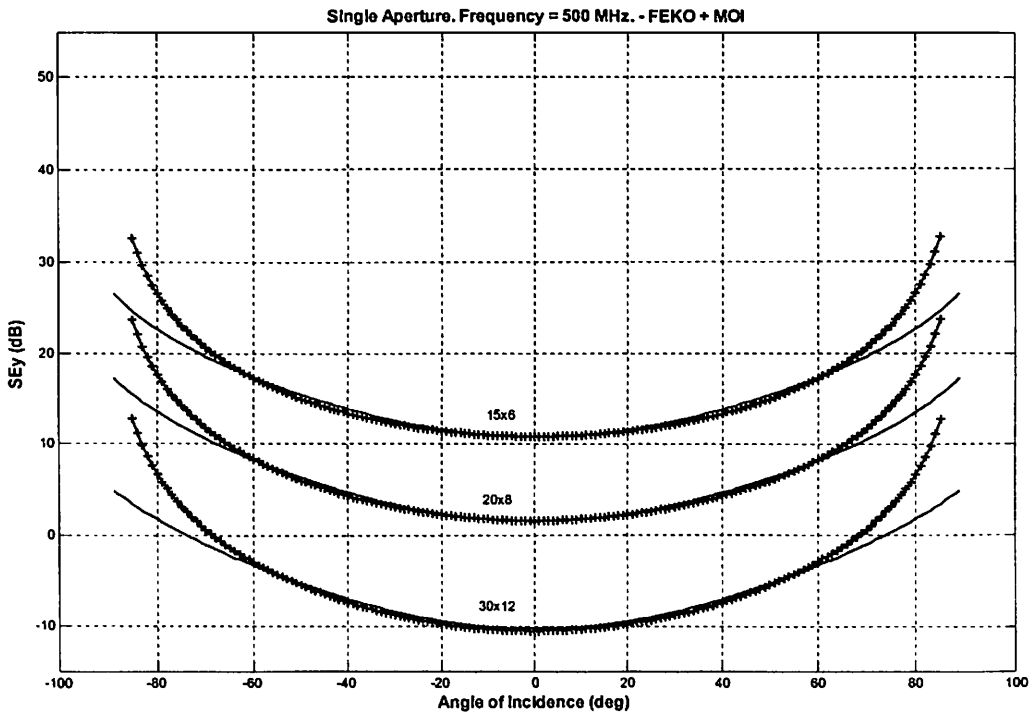

Figure 4.1.1.2 Comparison of SEy results from MOI and FEKO for varying angles of incidence at a frequency of 500 MHz (Single Aperture-Large).

From the graph it is clear that MOI and FEKO values agree well at normal incidence. The graph is also symmetric with respect to zero angle of incidence. When the plane wave is located at -85 and 85 degrees with respect to the center of the aperture then the SEy value that is computed by FEKO is smaller indicating larger field penetration compared to the values computed by MOI. This is an important question to be answered. In order to verify how the SEy values differ with increase in frequency, the results at 800 MHz and 1GHz are also compared. . The comparison of FEKO and MOI at 800 MHz and 1GHz for different aperture sizes is shown in Figures 4.1.1.3, 4.1.1.4, 4.1.1.5 and 4.1.1.6

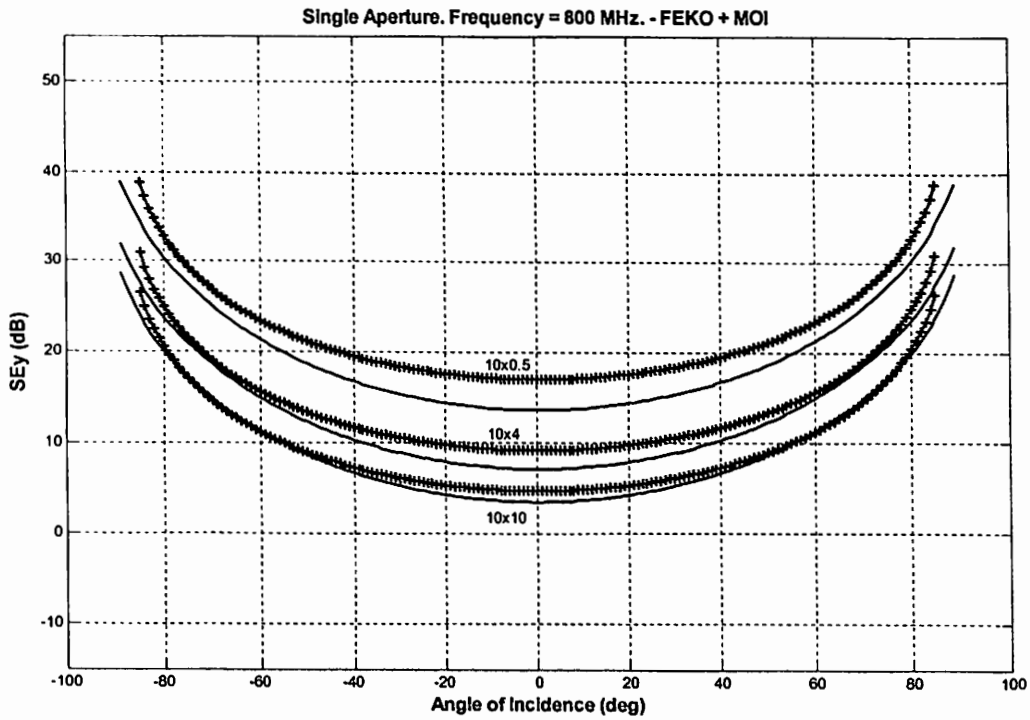

Figure 4.1.1.3 Comparison of SEy values from MOI and FEKO for multiple angles of incidence at a frequency of 800 MHz (Single Aperture-Thin).

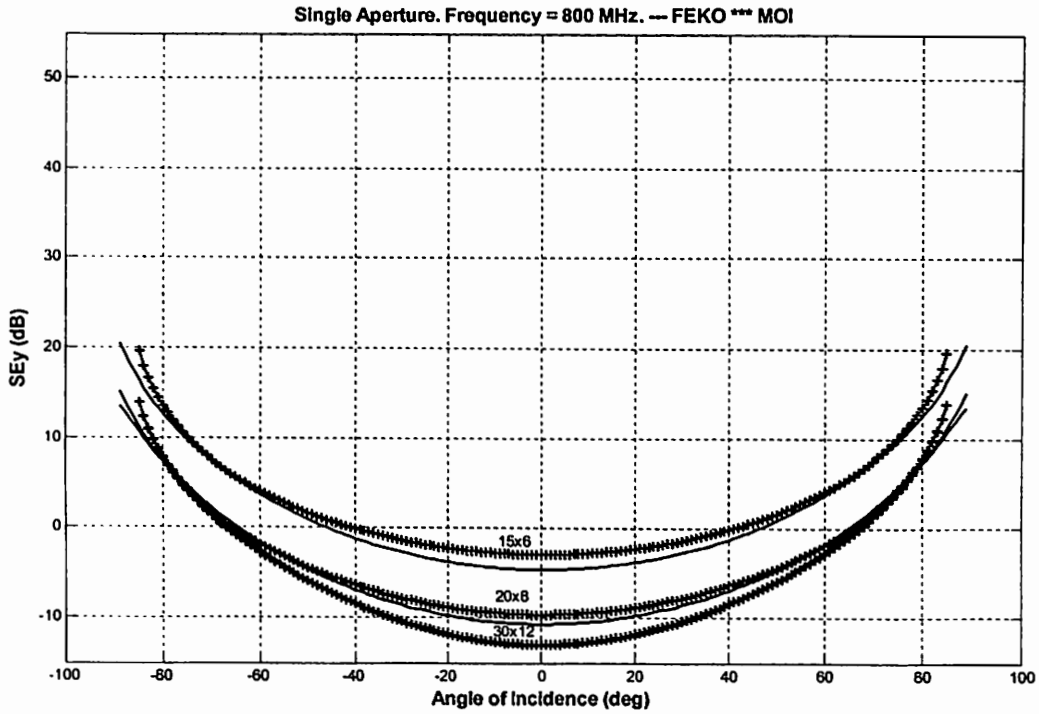

Figure 4.1.1.4 Comparison of SEy values from MOI and FEKO for multiple angles of incidence at a frequency of 800 MHz (Single Aperture-Large).

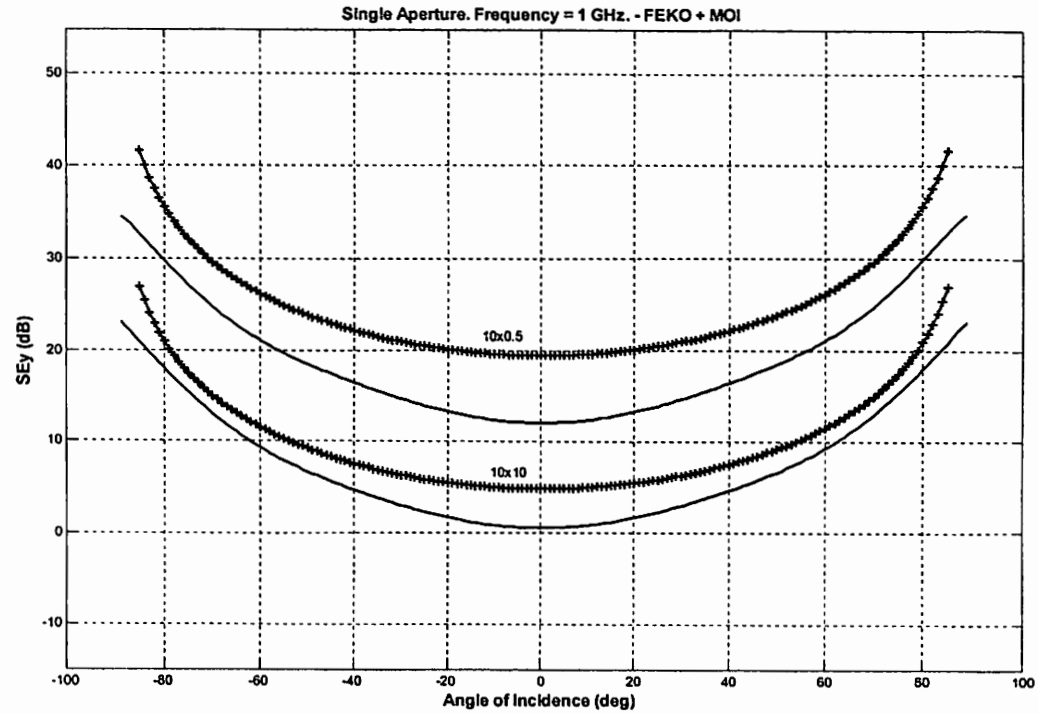

Figure 4.1.1.5 Comparison of SEy values from MOI and FEKO for multiple angles of incidence at a frequency of 1 GHz (Single Aperture-Thin).

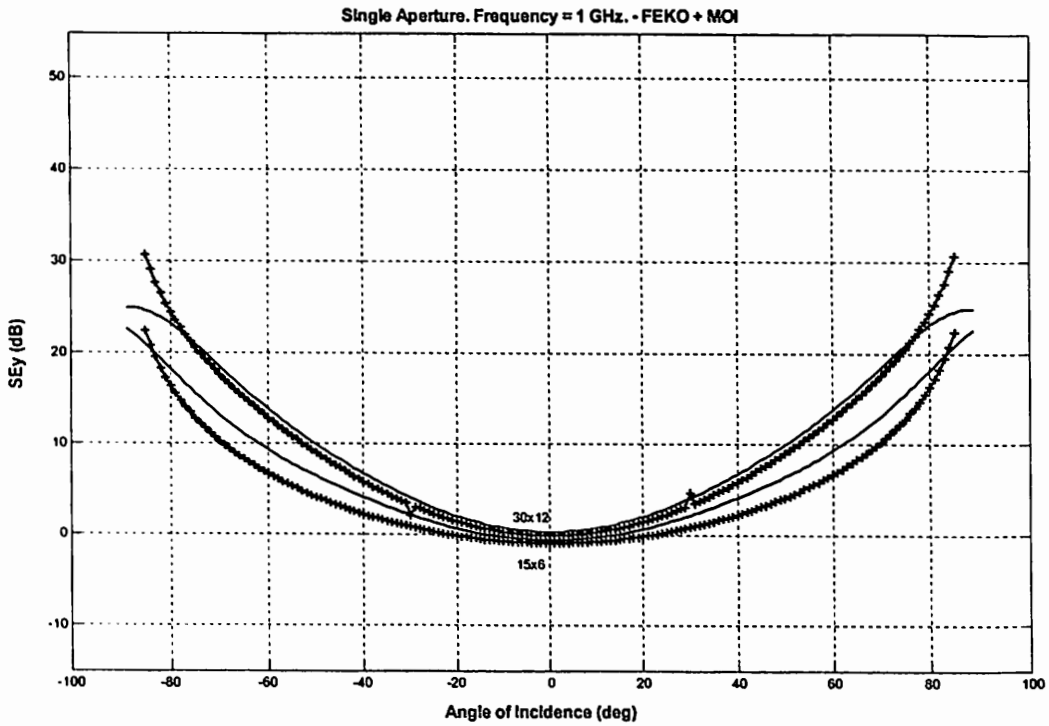

Figure 4.1.1.6 Comparison of SEy values from MOI and FEKO for multiple angles of incidence at a frequency of 1 GHz (Single Aperture-Large).

From the graphs it can be seen that MOI and FEKO values agree better when the aperture size is big. But there is a conflict in the values at -85 and 85 degrees angle of incidence. This is similar to the deviation that was addressed when the frequency is 500 MHz. Now the question that has to be answered here is which (MOI or FEKO) does a good job in predicting the shielding effectiveness when the plane wave is incident on the aperture from different angles. As there are no standards to compare, some of the measured results from ASU [48] for some special cases (Aperture 10 x 0.5 cms (Thin) and 20 x 3 cms (Large)) are used to compare the results. From the set of measured results, the measured values at 500 MHz, 800 MHz and 1 GHz has been taken and compared with the results from FEKO and MOI. As the graphs are symmetrical, the comparison is done only for one side (0 – 90 deg : Positive side). The graphs for aperture dimension 10 x 0.5 cms at three different frequencies are shown in the Figures 4.1.1.7, 4.1.1.8 and 4.1.1.9.

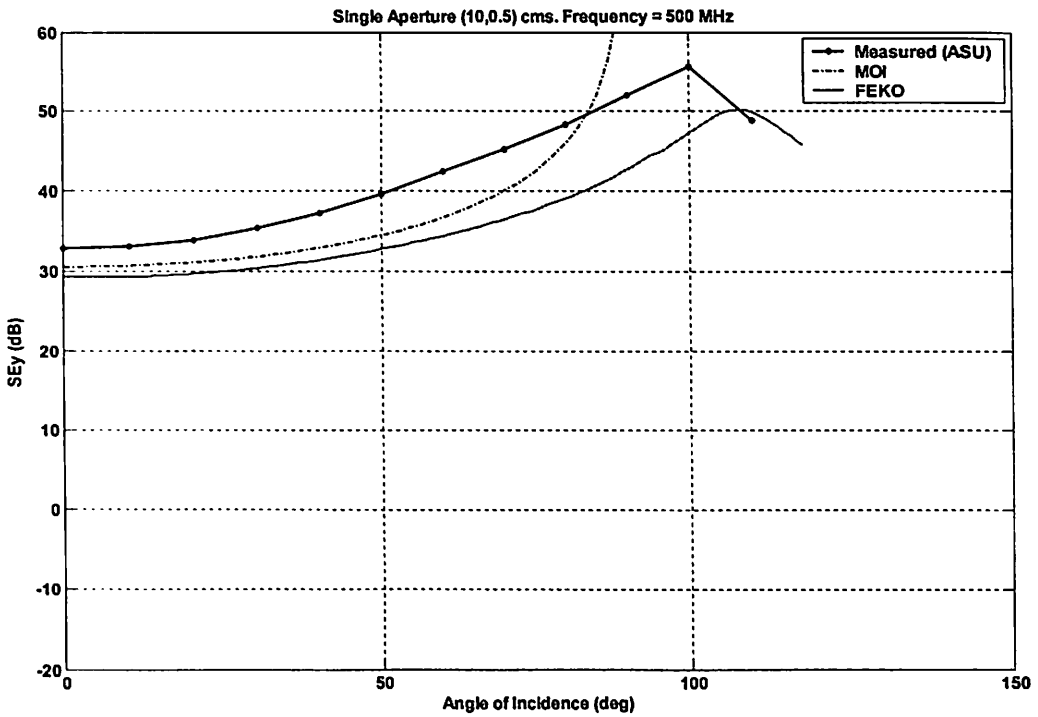

Figure 4.1.1.7 Comparison of SEy values from MOI, FEKO and Measured results for multiple angles of incidence at a frequency of 500 MHz.

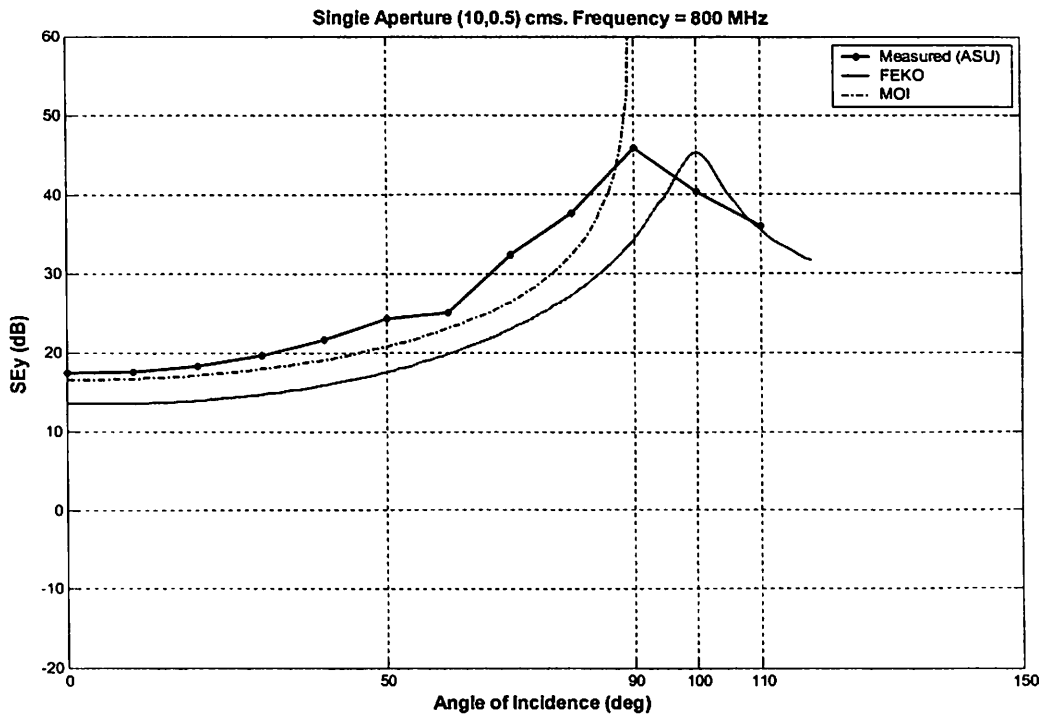

Figure 4.1.1.8 Comparison of SEy values from MOI, FEKO and Measured results for multiple angles of incidence at a frequency of 800 MHz.

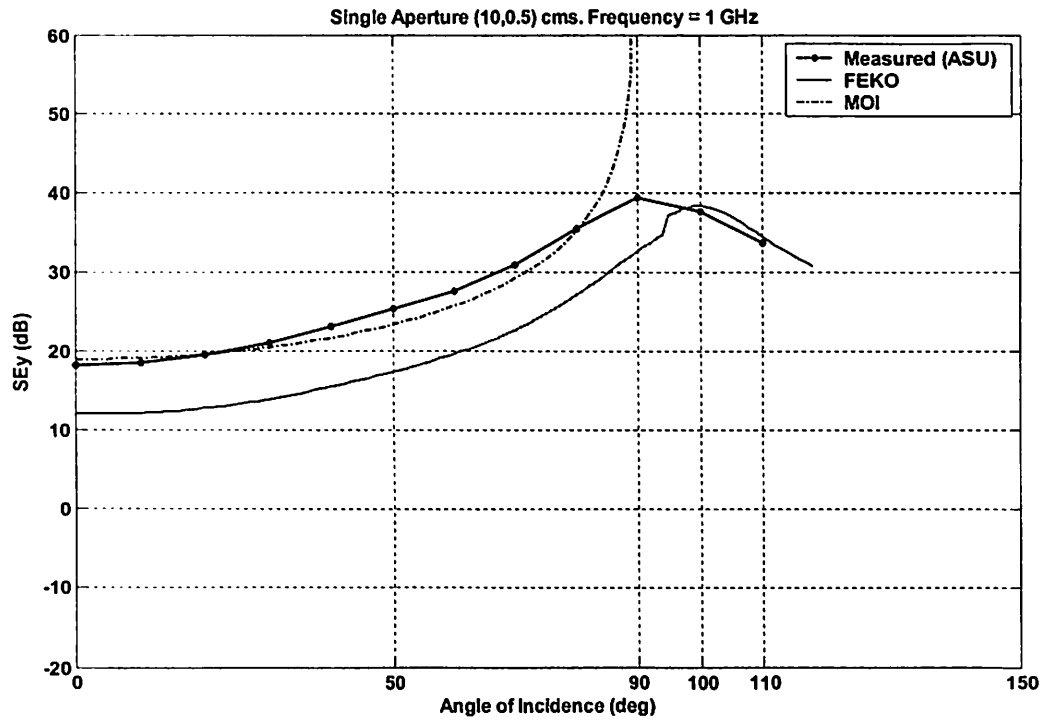

Figure 4.1.1.9 Comparison of SEy values from MOI, FEKO and Measured results for multiple angles of incidence at a frequency of 1 GHz.

From the graphs it can be seen that the values agree well but when the incidence angle increases, FEKO results are more close to the measured results. MOI cannot compute the shielding effectiveness values after 90 degrees. FEKO was used there to compare with the measured data. The disagreement between FEKO and measured results is because of the fact that during measurements, a probe was used to measure the field at the center of the box but during the simulation with FEKO a probe was not considered inside the box [PC 1] and [PC 3]. As this is for the smaller apertures, disagreement between the values of FEKO and MOI is expected due to the reasons explained before. MOI does not assume a probe inside the cavity but the variation between FEKO and MOI values might be due to the assumption of only the dominant mode at the aperture. The disagreement between FEKO and MOI is smaller for the large apertures and that can be seen in another set of

compared data for the aperture size of 20 x 3 cms. Refer to Figures 4.1.1.10, 4.1.1.11 4.1.1.12.

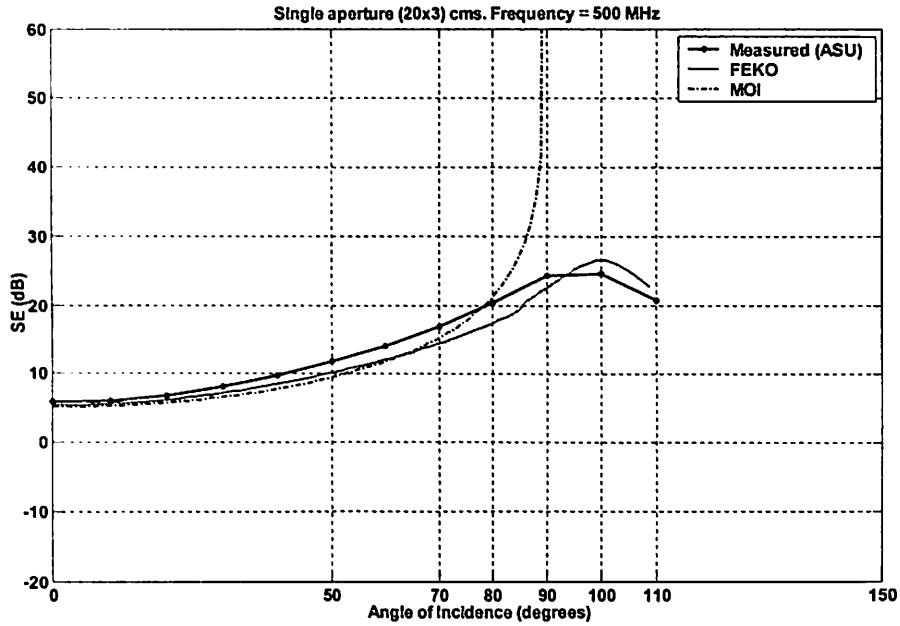

Figure 4.1.1.10 Comparison of SEy values from MOI, FEKO and Measured results for multiple angles of incidence at a frequency of 500 MHz.

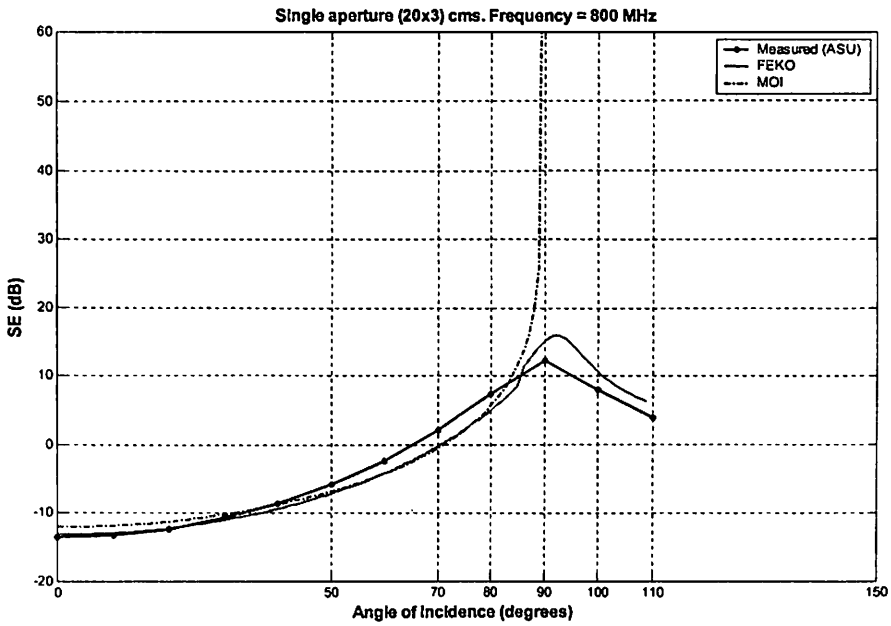

Figure 4.1.1.11 Comparison of SEy values from MOI, FEKO and Measured results for multiple angles of incidence at a frequency of 800 MHz.

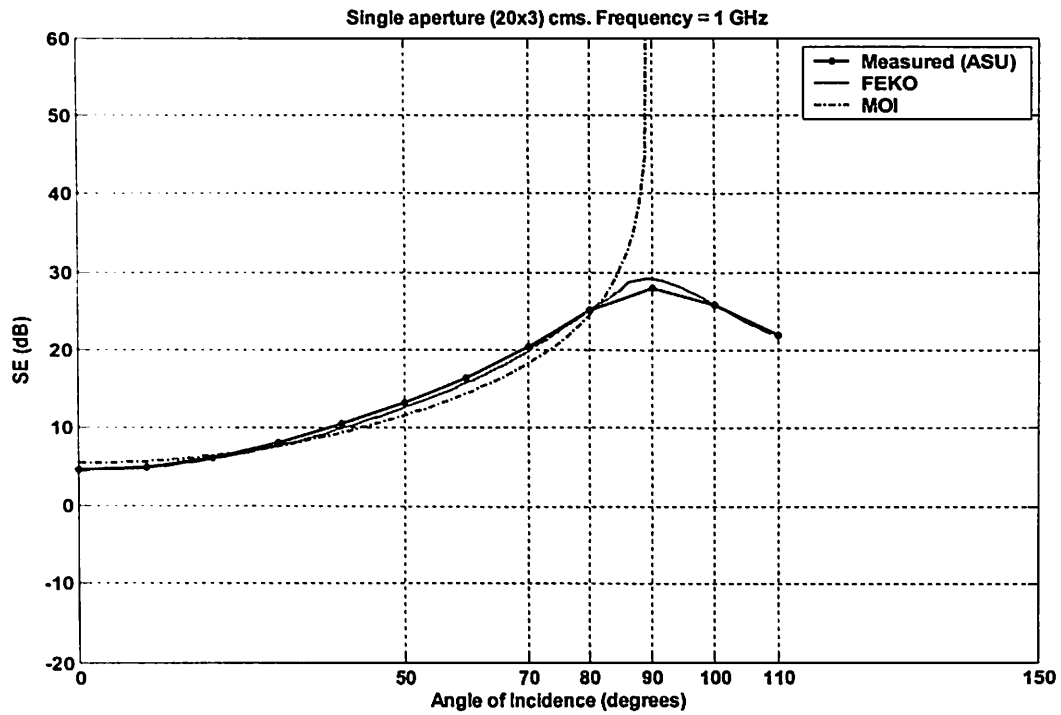

Figure 4.1.1.12 Comparison of SEy values from MOI, FEKO and Measured results for multiple angles of incidence at a frequency of 1 GHz.

From the graphs 4.1.1.10, 11 and 12, it has been noted that FEKO values are close to the measured results. Though MOI predicts the values correctly for lower angles of incidence at higher angles of incidence, the values predicted are not correct. This may be because, in MOI, the edges of the cavity are not taken into account. The edge effects can be neglected for normal angle of incidence but not for other angles of incidence. Thus there should be a bound set on the values of angles of angles of incidence over which MOI results may be considered valid. Comparing the graphs it can be seen that MOI, FEKO and measured values are close for the lower angles and as the angle of incidence is increased, MOI values exceed both measured and FEKO simulated results. It would appear as though MOI can be reasonably relied upon to provide accurate results up to about 75 degrees off normal incidence.

4.2 Two Aperture case

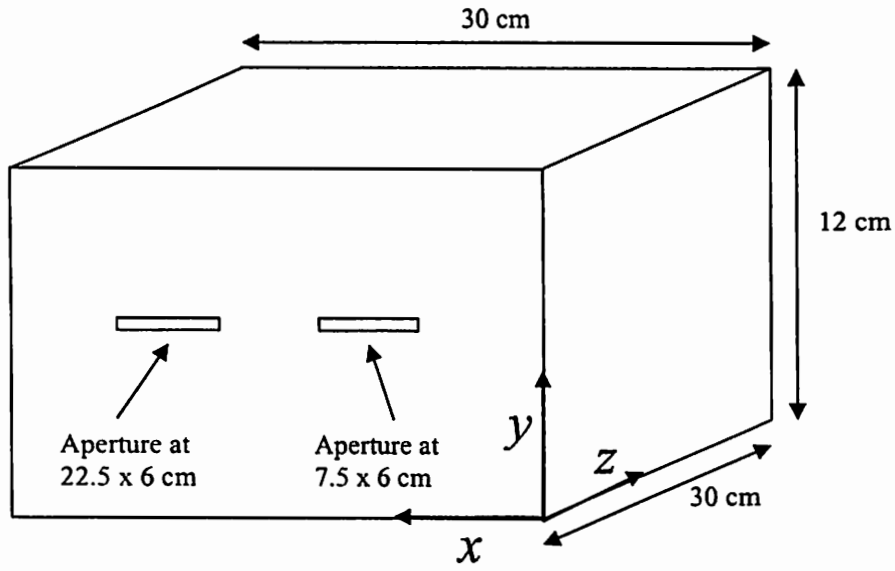

Figure 4.2.1 Geometry of the cavity with a two apertures at the front wall.

The geometrical configuration of the two-aperture case has been given in Figure 4.2.1. The apertures are located side by side in the front wall of the enclosure. The plane wave is incident on the front face of the box where the apertures are located. The field values at the center of the box are calculated for varying size of the apertures. At any point, the dimensions of both the apertures are the same. So when there is an increase in the aperture size, the increase is in both the apertures. The results obtained from MNI are shown in Figure 4.2.2.

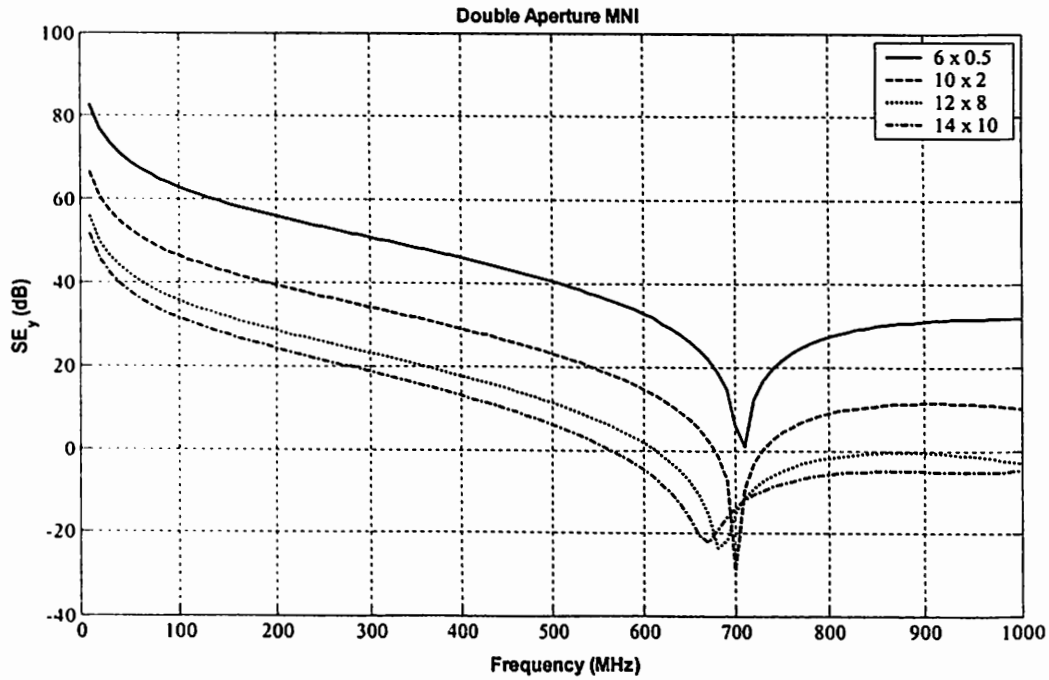

Figure 4.2.2 SEy results from MNI for varying aperture sizes (Two apertures).

From the figure it can be seen that the field penetration increases with increase with frequency and it is maximum at the resonant frequency and decreases with increase in frequency after that. The same pattern is also observed in the single aperture case. When the aperture size is made 14 x 10 (in cm) it is almost equal to opening one side of the box but for the thin walls of the aperture. So the results from MNI must again be verified for the same reason explained in the single aperture case. Hence FEKO was used to calculate SEy for the same case. The result obtained from FEKO for varying size of apertures is shown in Figure 4.2.3.

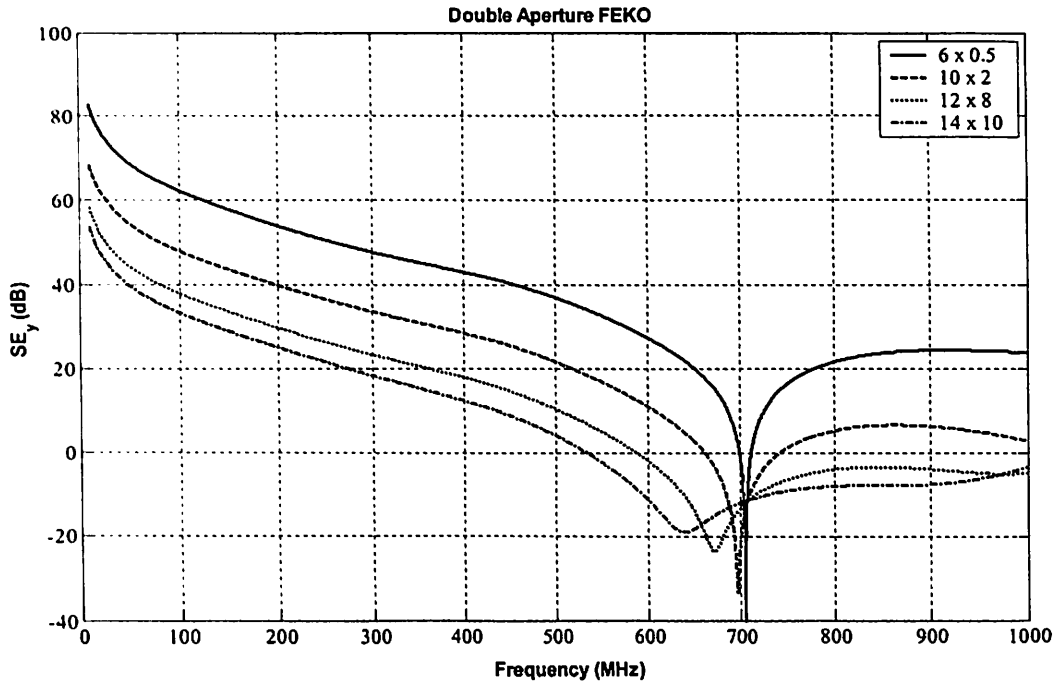

Figure 4.2.3 SEy results from FEKO for varying aperture sizes (Two apertures).

The graph shows that the pattern remains the same. There is a shift in the null with the increase in aperture size. The results from MNI and FEKO are compared and shown in the Figure 4.2.4.

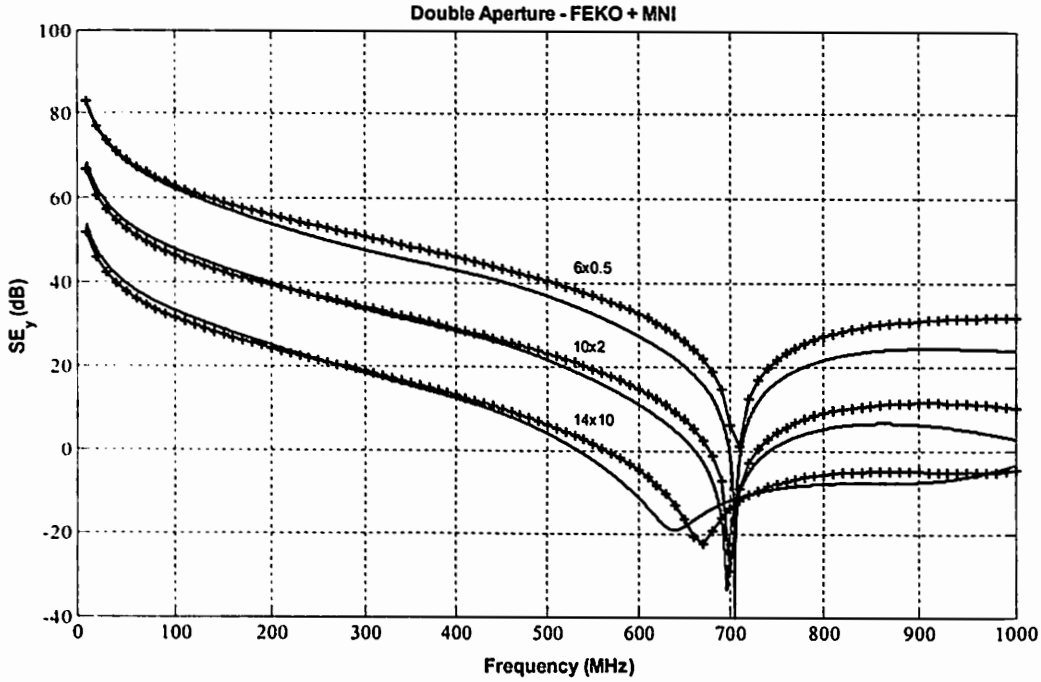

Figure 4.2.4 Compared SEy results from MNI and FEKO for varying aperture sizes (Two apertures).

From the comparison it is clear that the SEy values obtained from FEKO and MNI are close to each other for different aperture sizes. As seen in the single aperture case, even in the double aperture case, at the high frequency side there is a disagreement between MNI and FEKO for the aperture of smaller dimensions. When the aperture size is increased, the values agree well. In order to solve for the difference between FEKO and MNI for the smallest apertures, the same problem was carried out for different grid size and a convergence study was done. In FEKO the grid size was made smaller from $\lambda/15$ to $\lambda/25$ and the difference in SEy was about 0.2 dB. The other thing that has to be noted here is that in MNI only the dominant TE_{10} mode is considered at the apertures. Inclusion of higher order modes may decrease the value of SEy and the graphs might be close to each other for the smallest aperture case.

On the high frequency side, the number of variables that has to be solved using FEKO increases and due to certain limitations that many variables cannot be solved which also might be the reason for the low values. One other limitation with FEKO is that for a problem of finding the shielding effectiveness for a range of frequencies, it takes about 3 hours on a Xeon workstation with 4G RAM but MNI takes about 5-10 minutes. Comparing these, MNI is much faster than FEKO but the accuracy remains a question. Further research is required to ensure the accuracy. As in the single aperture case, the MNI values which were suspicious for the aperture of largest dimension, the double aperture values were also suspicious as depicted in Figure 4.2.5. From the comparison it is observed that the pattern of the graphs is not close to each other and there is a disagreement between the two. The null from MNI and FEKO are away from each other and the pattern of the graph that follows after the null is different from each other. This might be a limitation of MOI as suspected when the aperture size is big.

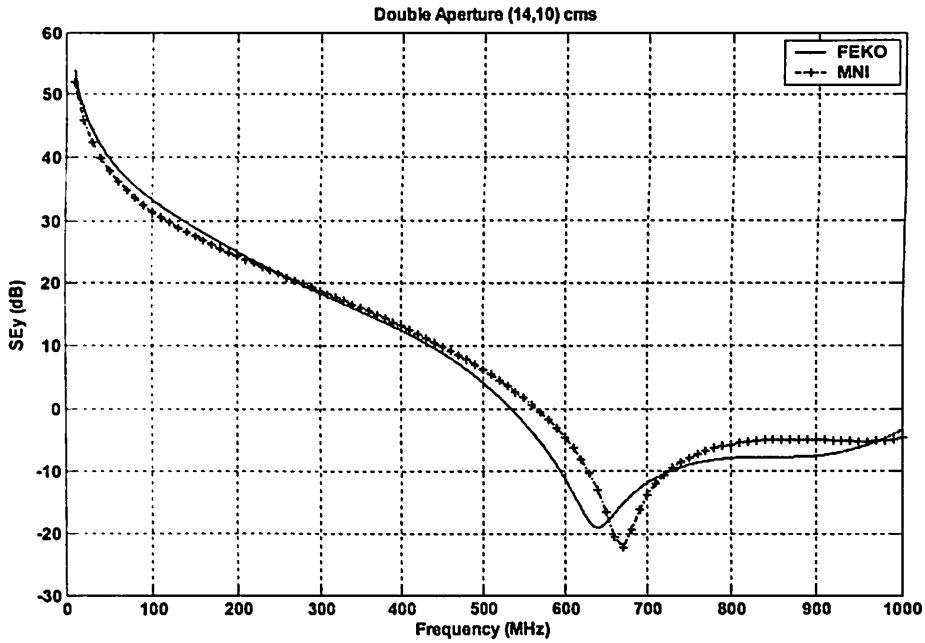

Figure 4.2.5 Comparison of SEy results from MNI and FEKO for aperture size (14 x 10) cms (Two Apertures).

4.2.1 Multiple angles of incidence for two apertures:

The MOI developed by Khan [10] to support multiple angle of incidence and different polarizations was used to compute the SEy values at the center of the box with two apertures and different aperture sizes and for certain frequencies like 500 MHz, 800 MHz and 1 GHz. The incidence angle was varied from -85 to 85 degrees (171 values) with one degree step. Note:- 0 degree is the normal angle of incidence. The same was developed in FEKO and the results from FEKO were compared with MOI results. The comparison of FEKO and MOI at 500 MHz for different aperture sizes is shown in Figure 4.2.1.1.

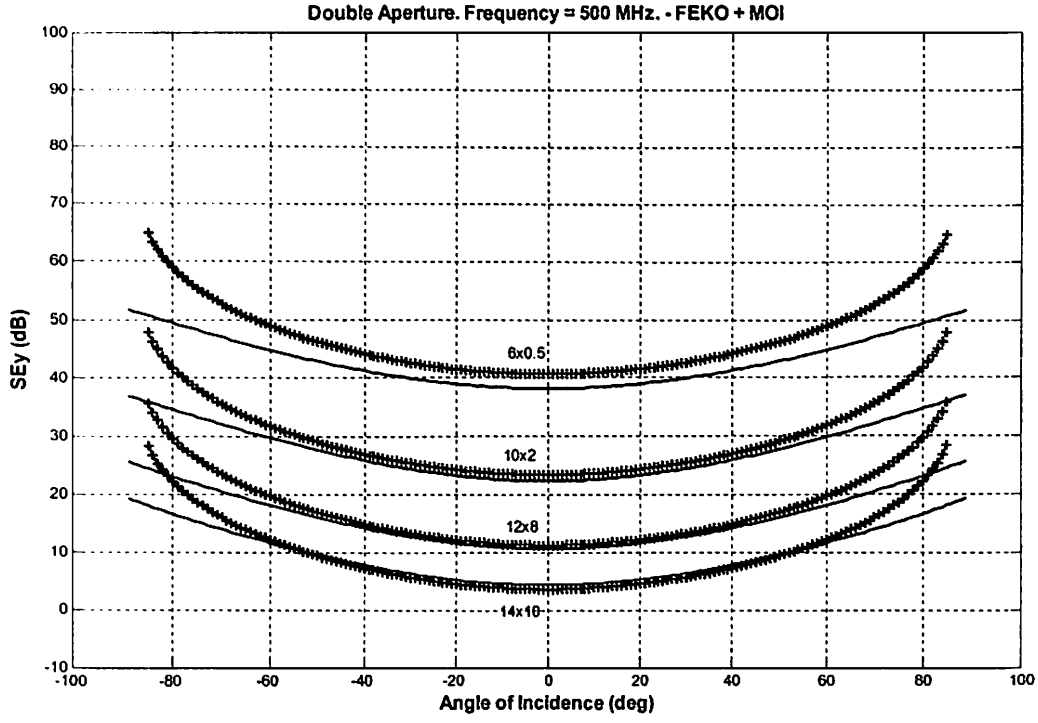

Figure 4.2.1.1 Comparison of SEy values from MOI and FEKO for multiple angles of incidence at a frequency of 500 MHz (Two apertures).

From the graph it can be seen that for apertures of small dimensions there is a disagreement between FEKO and MOI but when the size of the aperture increases the

values agree well. At larger angle of incidence like 85 and -85 degrees, the SEy values do not agree even for apertures with large dimension. Then the same simulation was done for higher frequencies like 800 MHz and 1 GHz. The comparison of FEKO and MOI at 800 MHz and 1GHz for different aperture sizes is shown in Figures 4.2.1.2 and 4.2.1.3.

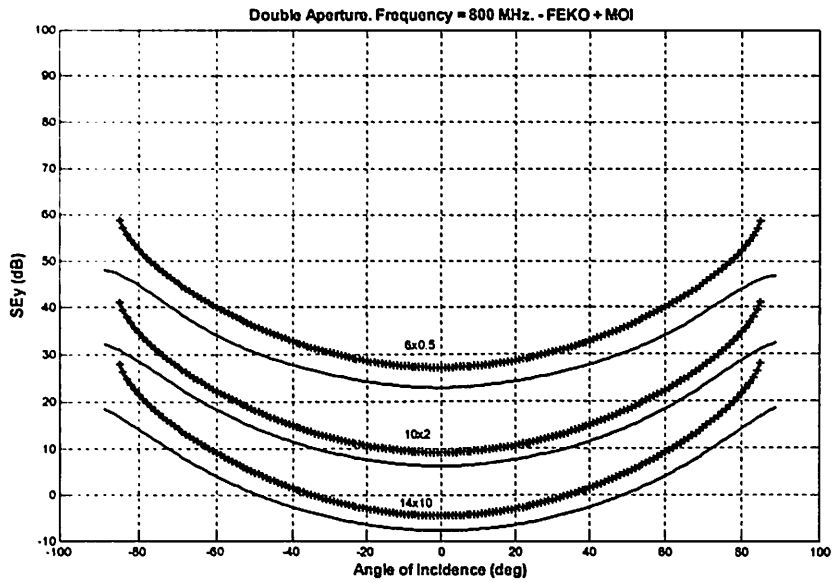

Figure 4.2.1.2 Comparison of SEy values from MOI and FEKO for multiple angles of incidence at a frequency of 800 MHz (Two apertures).

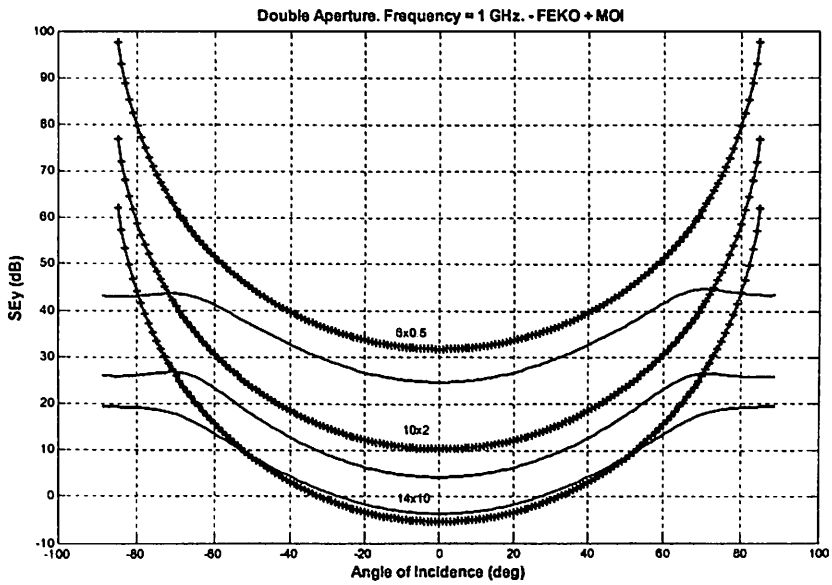

Figure 4.2.1.3. Comparison of SEy values from MOI and FEKO for multiple angles of incidence at a frequency of 1 GHz (Two apertures).

From the graphs 4.2.1.1, 2 and 3 it can be seen that as the frequency increases, the disagreement between the values at larger angle of incidence also increases. At 800 MHz even for the aperture with largest dimension, there is a disagreement between the values. Also the same trend of larger disagreement for the apertures of smaller size and better agreement for the large apertures is also maintained. In order to verify the results from MOI and FEKO, the computed values are compared with a set of measured data. But the measured data from ASU [48] is for the apertures on opposite walls. MOI that is used for multiple angles of incidence does not support apertures at opposite walls (Future work will be including apertures on both walls). Hence only FEKO values are available for comparison. Two apertures of (20x3) cms present on opposite walls of the cavity with the plane wave excitation at different incident angles, the field at the center of the cavity is calculated and compared with the measured results for frequencies like 500 MHz, 800 MHz and 1 GHz. Refer to Figures 4.2.1.4, 4.2.1.5 and 4.2.1.6.

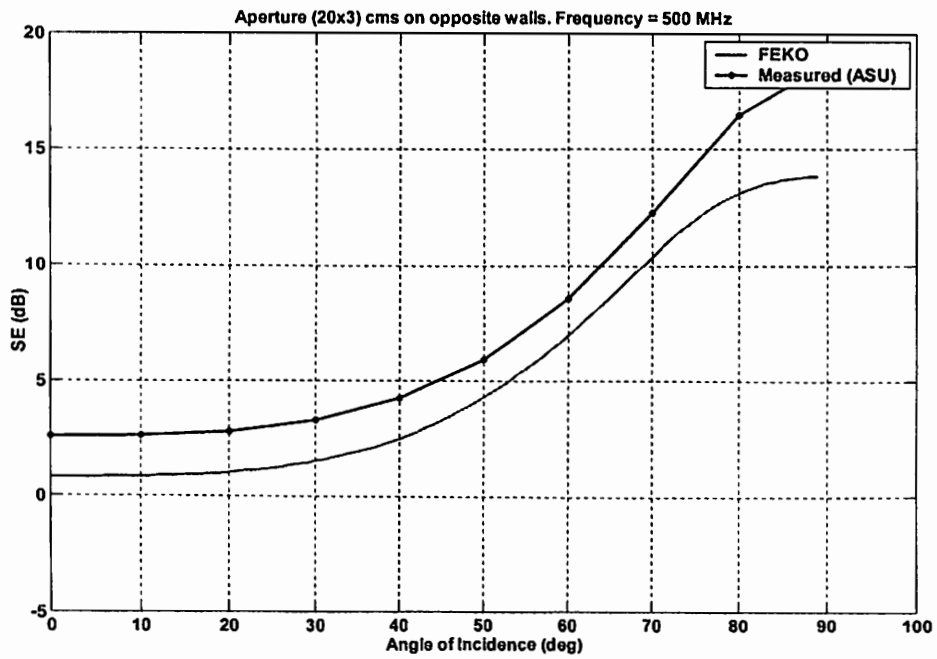

Figure 4.2.1.4 Comparison of SEy values from FEKO and Measured results for multiple angles of incidence at a frequency of 500 MHz. Two apertures (20x3) cms located on opposite walls.

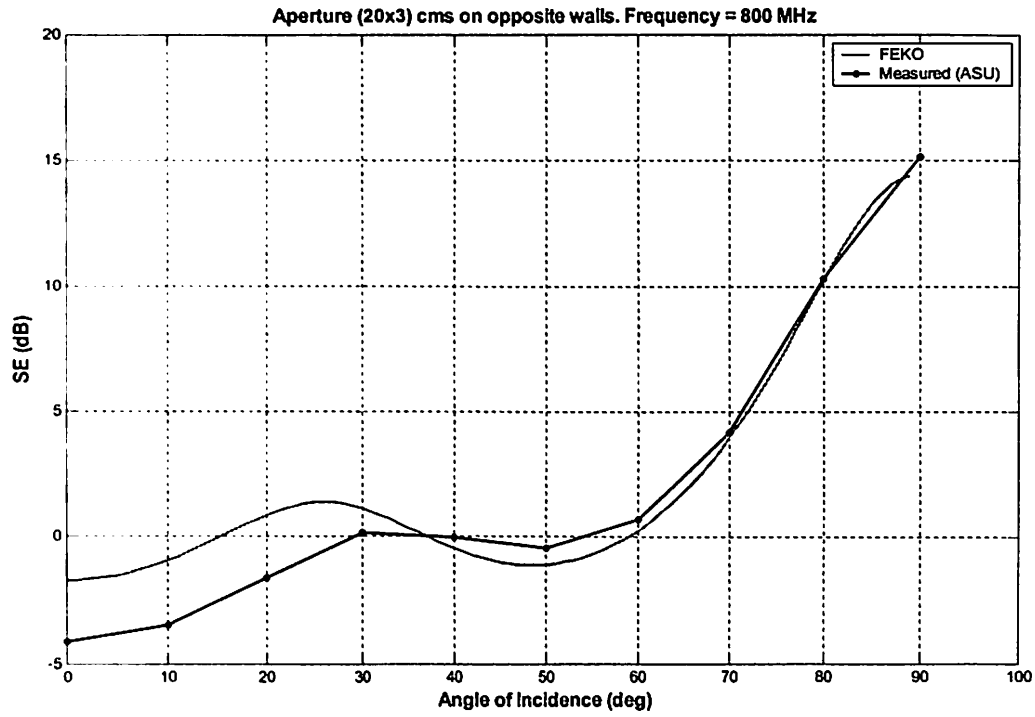

Figure 4.2.1.5. Comparison of SEy values from FEKO and Measured results for multiple angles of incidence at a frequency of 800 MHz. Two apertures (20x3) cms located on opposite walls.

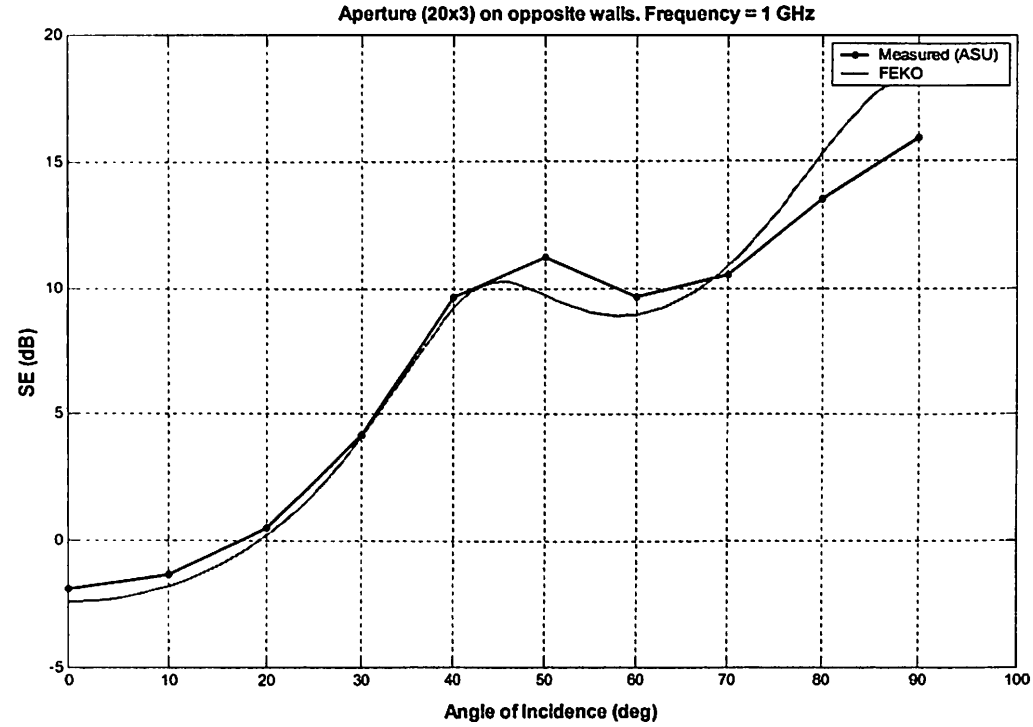

Figure 4.2.1.6 Comparison of SEy values from FEKO and Measured results for multiple angles of incidence at a frequency of 1 GHz. Two apertures (20x3) cms located on opposite walls.

From the graphs it can be seen that the computed values and the measured values agree well. To support the values predicted by FEKO for the shielding effectiveness for the multiple angles of incidence case, one more comparison between the measured and the computed data is made. This is for the two apertures on opposite walls one 10x0.5 cms and another 20x3 cms. The plane wave is incident on the aperture 20x3 cms wide and 10x0.5 cms aperture is present in the back wall. The incident wave then moves 180 degrees to hit the face of the back wall. For the same reason explained above, only FEKO and measured results are available for this problem. The compared graphs at three different frequencies are given below. Refer to Figures 4.2.1.7, 4.2.1.8 and 4.2.1.9.

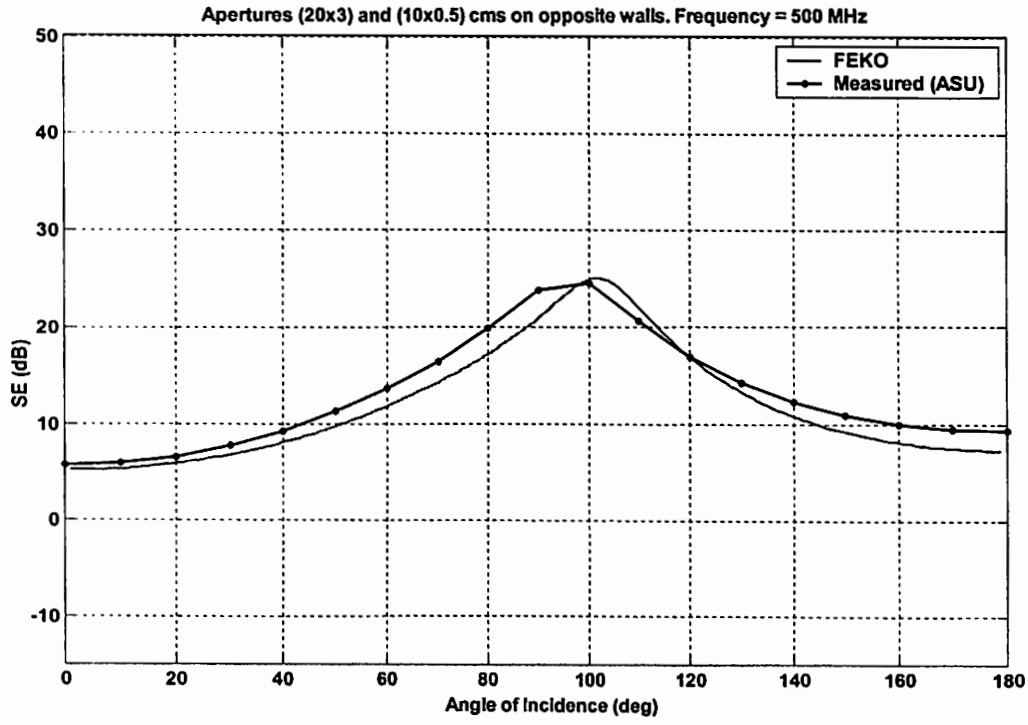

Figure 4.2.1.7 Comparison of SEy values from FEKO and Measured results for multiple angles of incidence at a frequency of 500 MHz. Aperture (20x3) cms located on Front wall and (10x0.5) cms in the back wall.

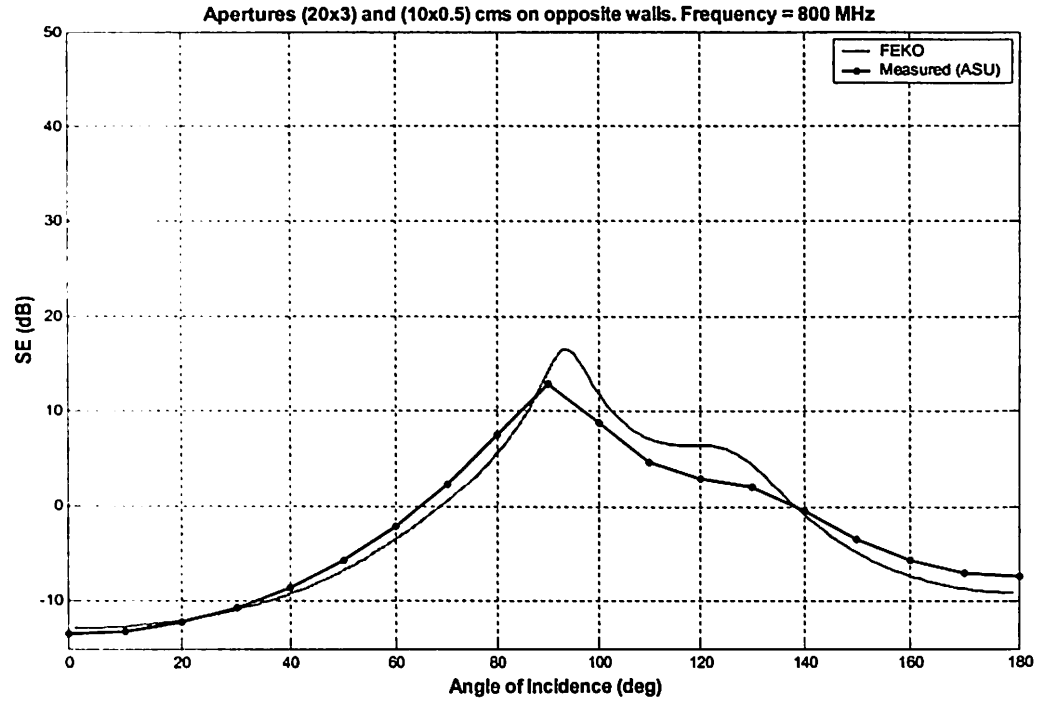

Figure 4.2.1.8 Comparison of SEy values from FEKO and Measured results for multiple angles of incidence at a frequency of 800 MHz. Aperture (20x3) cms located on Front wall and (10x0.5) cms in the back wall.

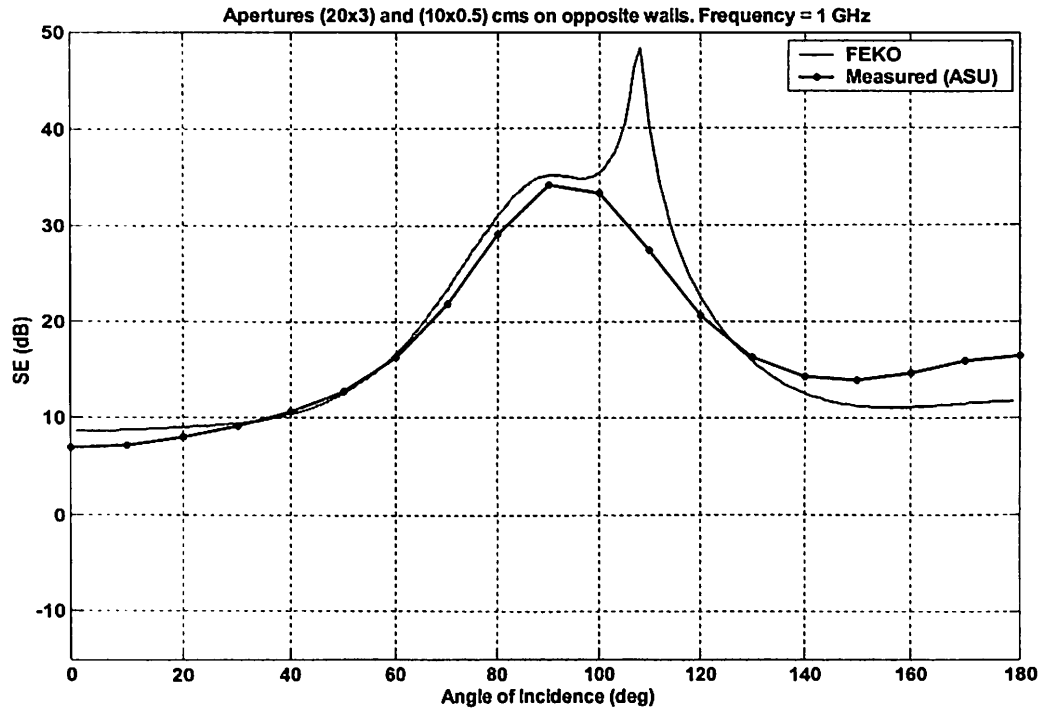

Figure 4.2.1.9 Comparison of SEy values from FEKO and Measured results for multiple angles of incidence at a frequency of 1 GHz. Aperture (20x3) cms located on Front wall and (10x0.5) cms in the back wall.

Note: The little disagreement between the measured values and the computed values by FEKO is because of the probe that is used to measure the field at the center of the cavity during the measurements but no such thing included during the simulation with FEKO [PC 2].

From the graphs comparing MOI, FEKO and measured results, it's been noted that FEKO values are close to the measured results. Though MOI predict the values right for lower angles of incidence, at higher angles of incidence the values predicted are not right. This is because, in MOI, the corners of the cavity are not taken into account which is very important for larger angles. The edge effects can be neglected for normal angle of incidence but not for other angles of incidence. Thus there has to be a bound set on the values of angles of angles of incidence until which MOI results can be valid. On the whole MOI results cannot be accurate after 80 degrees. Comparing the graphs it can be seen that FEKO and measured values are close. So on the whole MOI results appear to not be accurate after 70 degrees off normal for the double aperture case.

4.3 Investigation of the energy coupled to the probe

The third part of this thesis is dedicated to find the energy that can be coupled to a wire that is located inside the metallic enclosure. It must be understood that in this part the frequency at which the maximum energy can be coupled is alone analyzed and not the measure of energy. This problem can be approached in two ways; 1. A plane wave excitation can be used to couple energy from outside to the probe. By doing this the current that is induced on the probe and the field that is generated around the probe due to the current can be looked for the range of frequencies. It can be concluded that the frequency at which maximum current is induced on the probe which produces a maximum fields around the probe is the frequency at which maximum energy can be coupled. But when we have a plane wave excitation, the input impedance of the probe cannot be calculated. 2. In order to look at the impact of the probe, the input impedance of the probe is a primary thing that has to be looked at. To do this, the probe is excited using a voltage gap and the plane wave excitation is removed.

The input impedance of the probe that is attached to one of the cavity walls can be calculated now. From the pattern of the input impedance graph it can be said that the point of resonance is the point which determines maximum current or minimum current. In order to validate the results from MNI and FEKO, the cavity problem from [36] is considered. The dimension of the cavity is 2.29 x 1.02 x 4.19 (in cm) and a wire of length = 0.87 cm and diameter = 0.13 cm is located inside the cavity. The wire is fed at 1.145, 0.0, and 1.0 by a voltage gap. The input reactance graph with respect to a frequency sweep from 8.5 GHz to 12 GHz is plotted. The reference graph from Dr.Deshpande's

work [36] is given in Fig 4.3.1 and the results from MNI and FEKO are given in Fig 4.3.2.

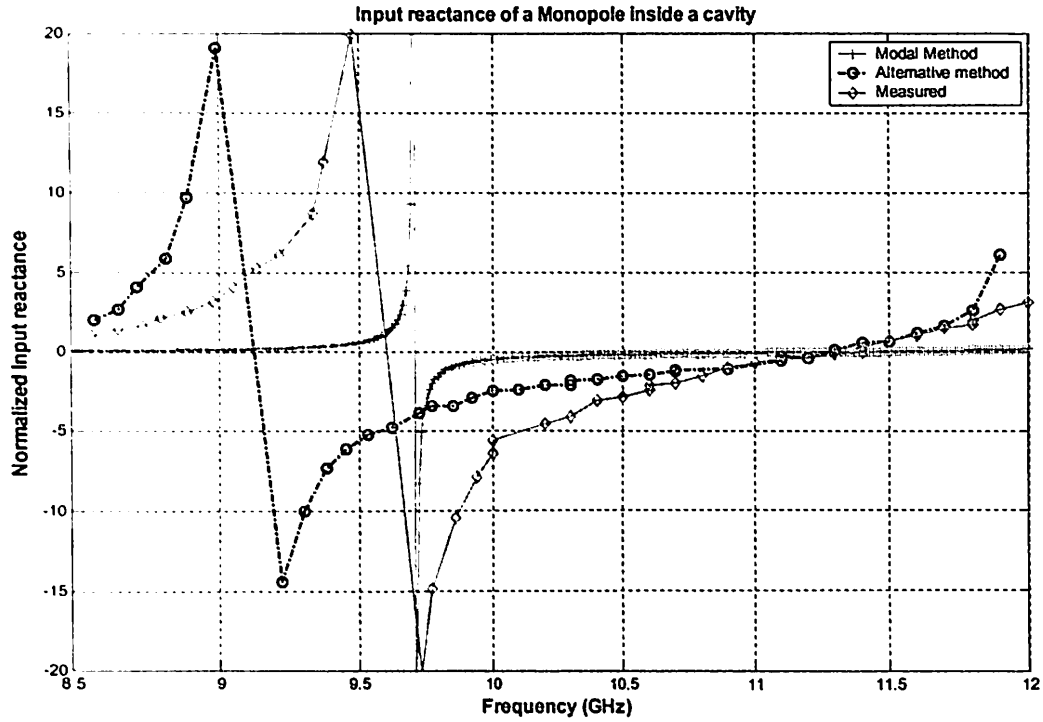

Figure 4.3.1 Input reactance of the monopole inside a closed cavity Ref: [32]

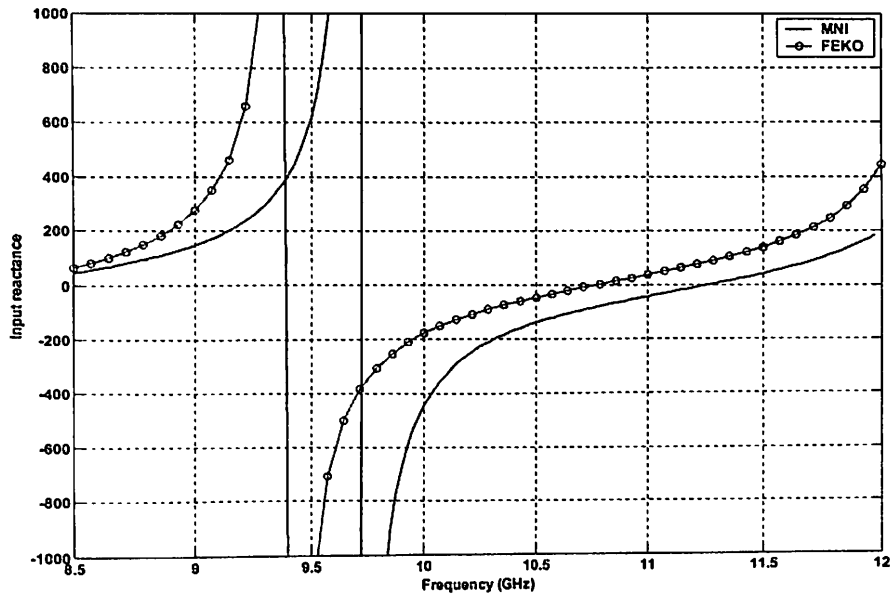

Figure 4.3.2 Input reactance of the monopole inside a closed cavity using MNI and FEKO

It can be seen from the graph that there is a clear disagreement between FEKO and MNI in computing the point of resonance (Zero crossing: 11.4 GHz (MNI) and 10.7 GHz (FEKO)). This might be because of the assumption in MNI that the monopole is not really touching the wall but located very close to the wall. When we consider resonance, there are two points of resonance, one where the reactive effects are maximum which is called the parallel resonance. As a normal behavior of parallel resonance, the current is minimum at the point of resonance. The point where the inductive and capacitive effects cancel each other (reactive effects = 0) is the point of series resonance. Current is maximized at the point of series resonance. The current behavior on the probe can be analyzed by computing the current on the probe and the input impedance using MNI and FEKO. MNI does not compute the current on the probe directly but it computes the maximum current on the probe. This current is substituted in equation (65) to obtain the current induced on the probe.

Fig 4.3.3 is the results from MNI and it can be seen that at the point where the reactive effects are maximum, is the point where the current is minimum. This is shown by a straight line connecting the two graphs. The point where the reactive effects are zero is the point where the current induced on the probe is maximum. The same trend can be found in Fig 4.3.4 which is the results computed from FEKO.

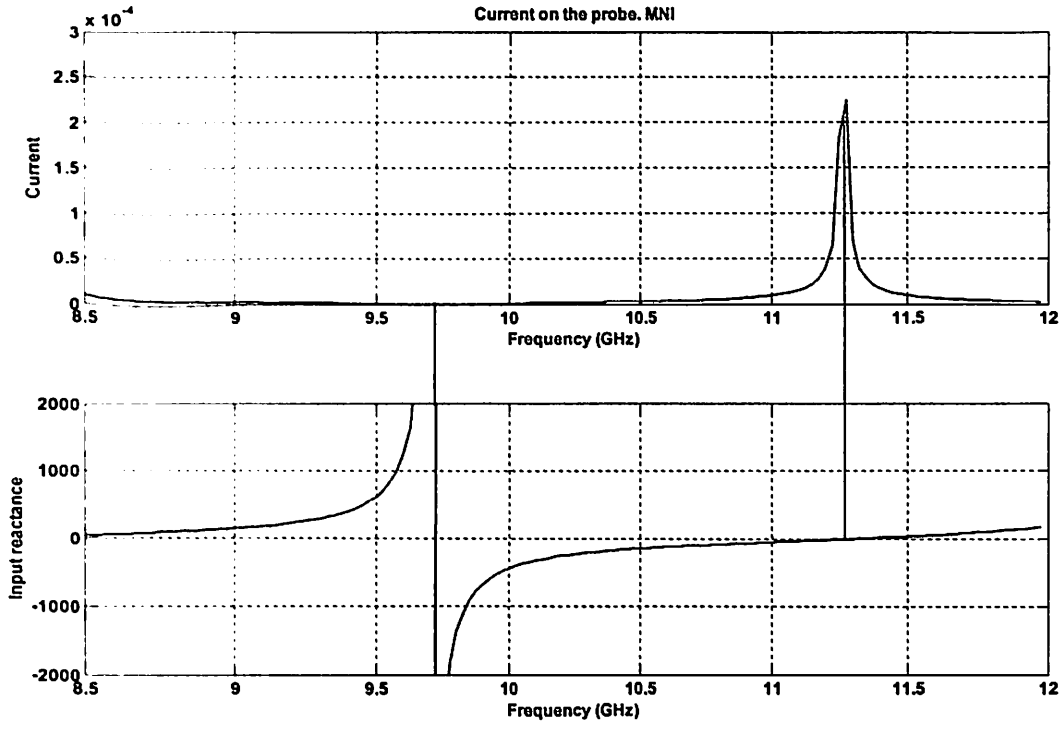

Figure 4.3.3 Current on the monopole (Top). Input reactance of the monopole (Bottom). MNI

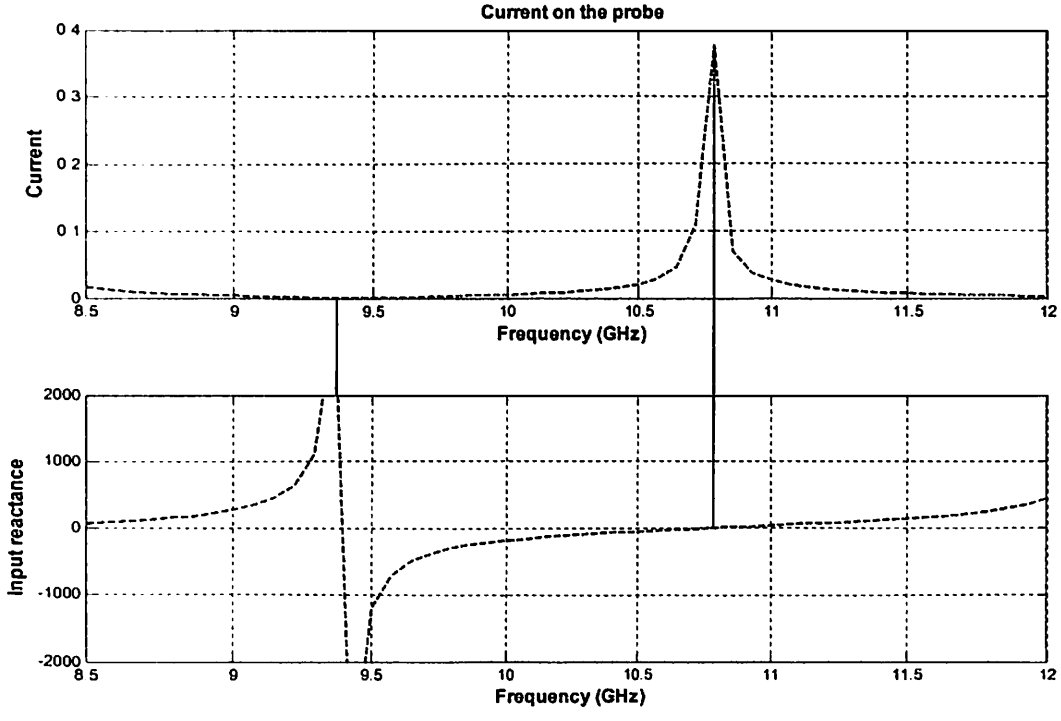

Figure 5.3.4 Current on the monopole (Top). Input reactance of the monopole (Bottom). FEKO

Thus it can be concluded that the maximum current is induced on the probe at the point of series resonance i.e... at the point where the reactance is zero.

The same analysis was extended to the problem of cavity size 30x12x30 (in cm) with a aperture 20x3 (in cm) located on the front wall. An infinitely thin monopole of length 4 cm is attached to one of the walls on the xz- plane so that the wire antenna is directed in the y- direction. The wire has to be assumed infinitely thin because of the assumption in Pocklington's integral equation which is used for solving the current on the wire. The wire antenna is excited using a voltage gap at the bottom and the current on the probe and the input impedance of the probe at the point where it is connected to the wall are calculated using MNI for a frequency sweep of 10 MHz to 1 GHz. The results are shown in Fig 4.3.5.

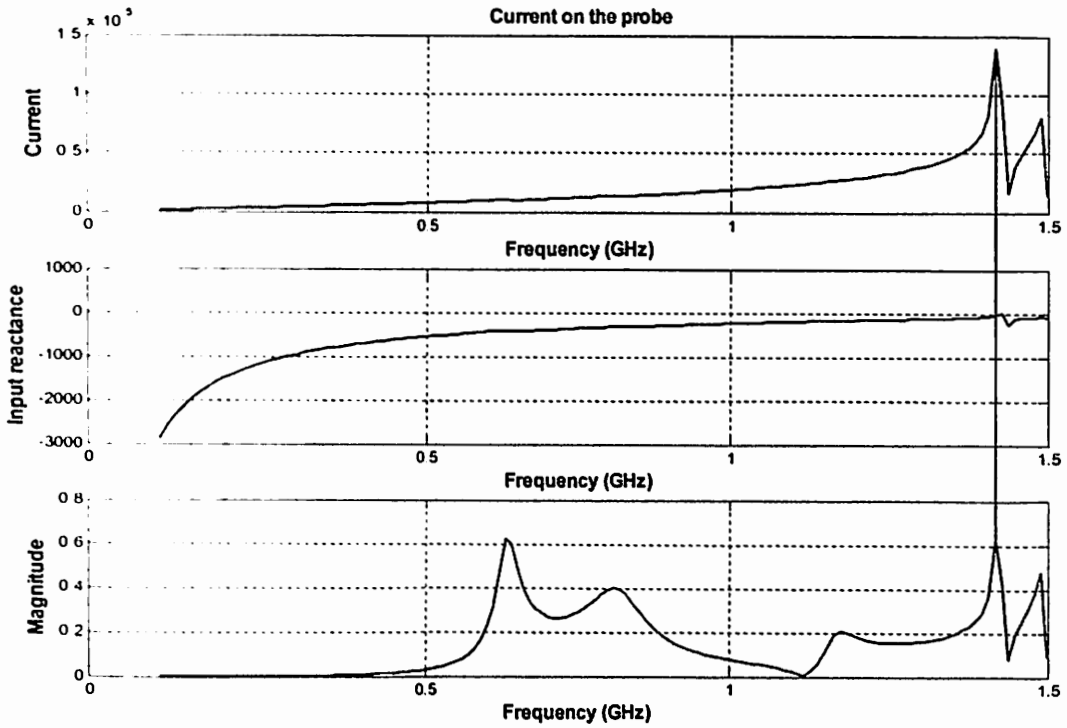

Figure 4.3.5 Current on the monopole (Top). Input reactance of the monopole (Middle). Field induced because of the current on the monopole (Lower). MNI

From the graphs it can be seen that the input reactance is zero at a frequency 1.42 GHz and that is the point where the current induced on the probe is maximum. Due to the current on the probe, the field that is induced because of the current is also maximum. The maximum current, maximum field and zero reactance are connected by a straight line in Fig 4.3.5 to show that all the three occur at the same frequency of 1.42 GHz. For a frequency sweep between 10 MHz and 1.5 GHz, 1.42 GHz is the frequency at which maximum energy can be coupled to the probe of this particular orientation.

This analysis is extended by varying the position of the monopole inside the cavity. This is done in order to sketch the energy coupled to the probe when the probe is located in four other positions in the same wall. The varying positions of the probe are shown in Fig 4.3.6.

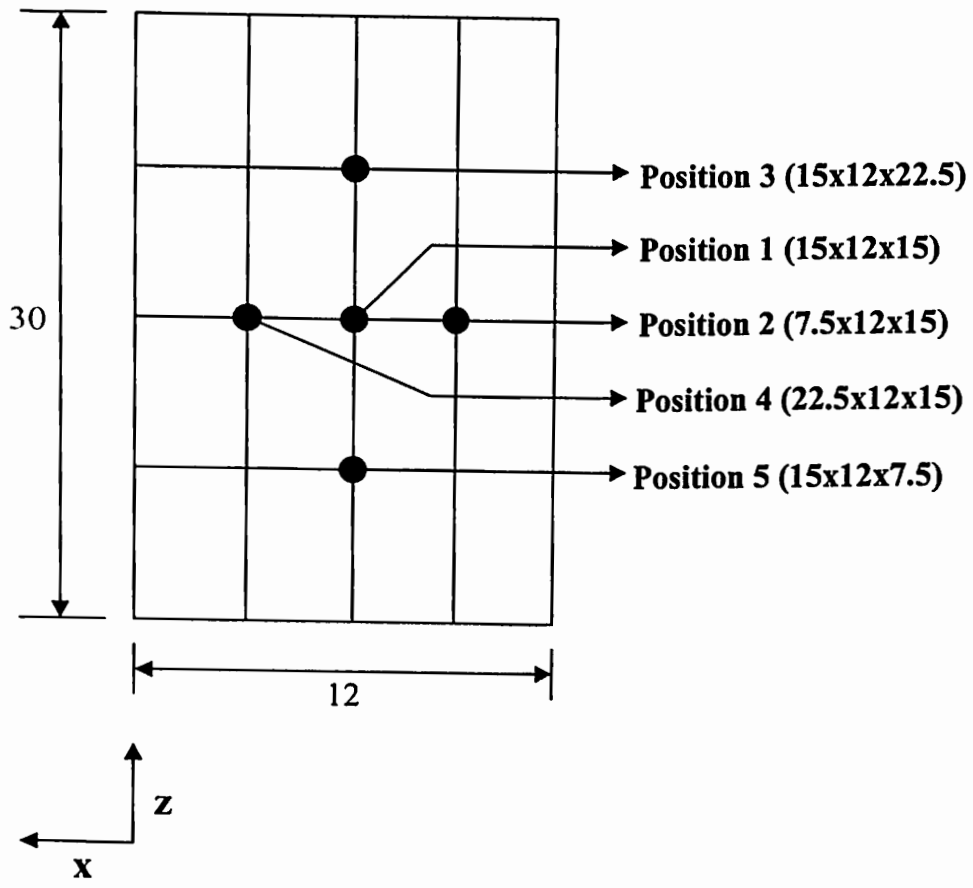

Figure 4.3.6 An illustration of the position of monopole on a wall of the cavity

For every position of the probe, the input impedance, the current induced on the probe and the fields induced due to the current are computed. The current computed in all the positions are compared and is shown in Fig 4.3.7.

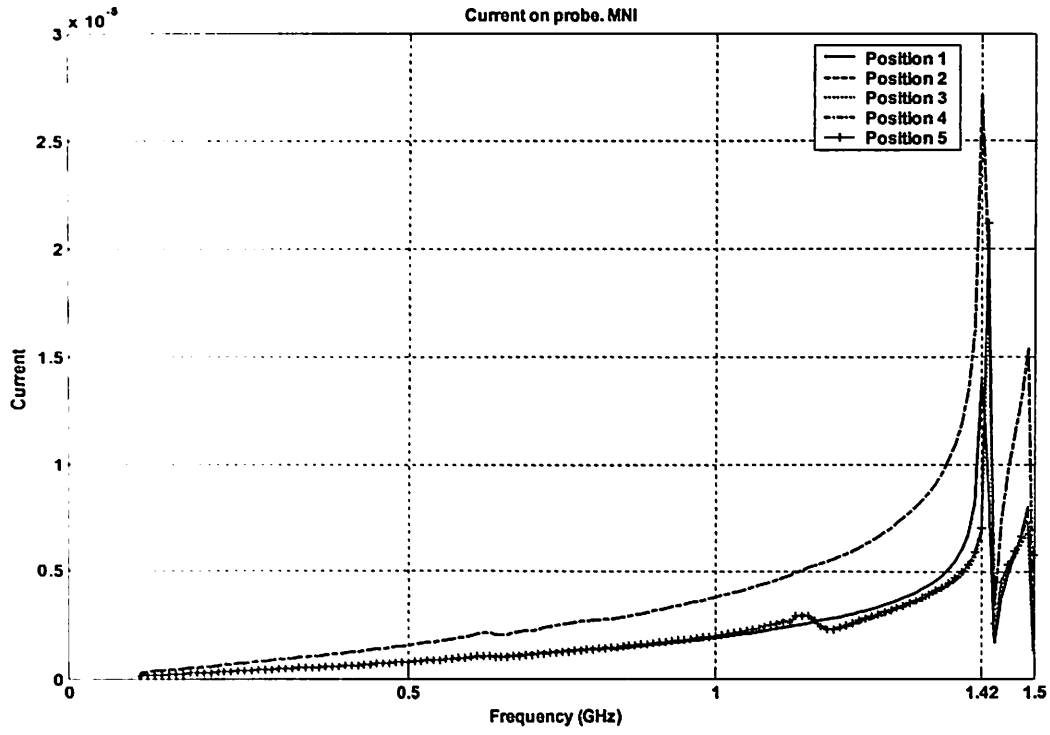

Figure 4.3.7 Current on the monopole. Frequency sweep – 10 MHz to 1.5 GHz

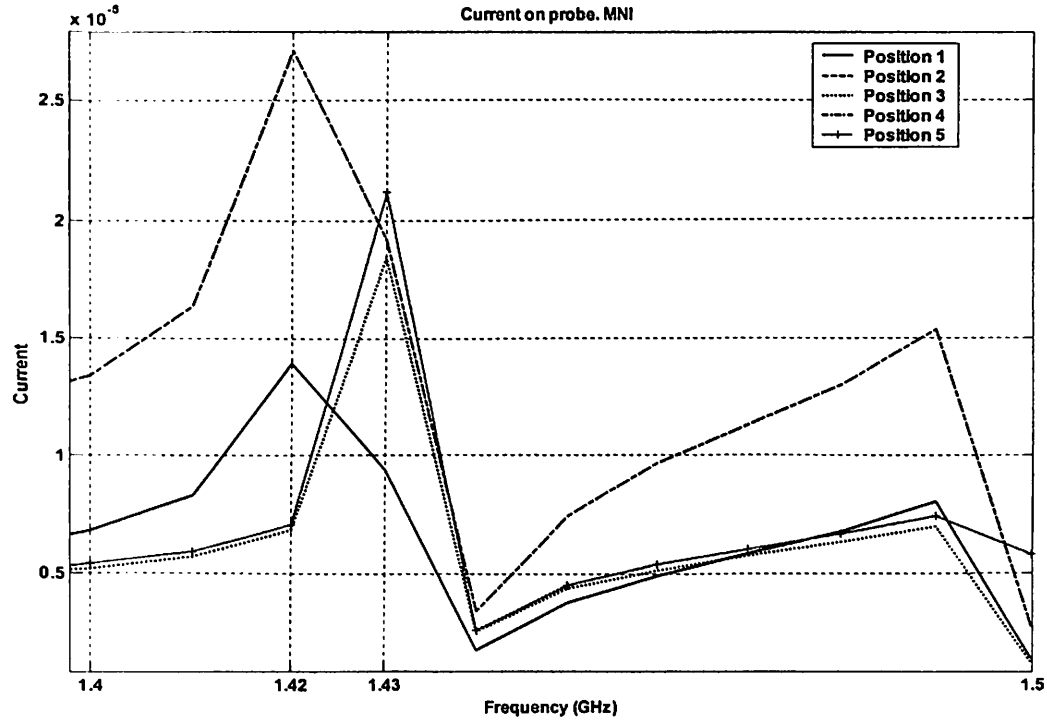

Figure 4.3.8 Current on the monopole. Frequency sweep – 1.2 GHz to 1.5 GHz

From the above graphs it can be seen that the current calculated on the probe during positions 1, 2 and 4 maximizes at 1.42 GHz. Comparing the magnitude of the current, the current in position 2 and 4 are equal and greater than the magnitude of the current calculated at position 1. For positions 3 and 5, the current maximum occurs at 1.43 GHz. The magnitude of current in both these positions is smaller when compared to the magnitude of the currents computed at position 2 and 4.

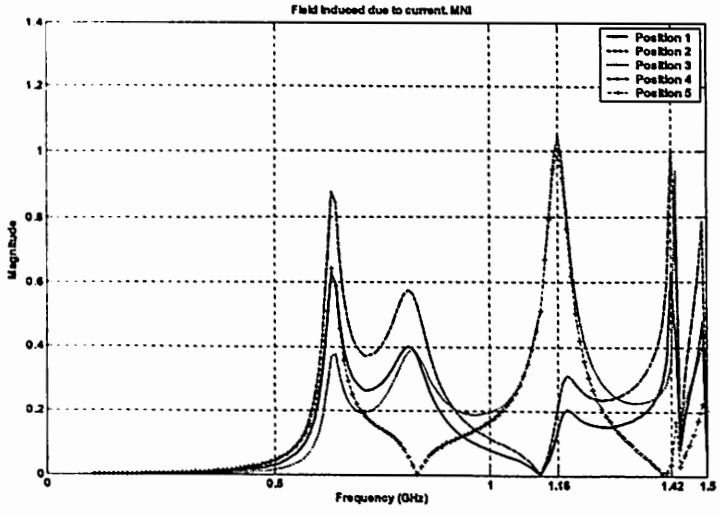

Figure 4.3.9 Field induced due to the current on the probe. Frequency sweep – 10 MHz to 1.5 GHz

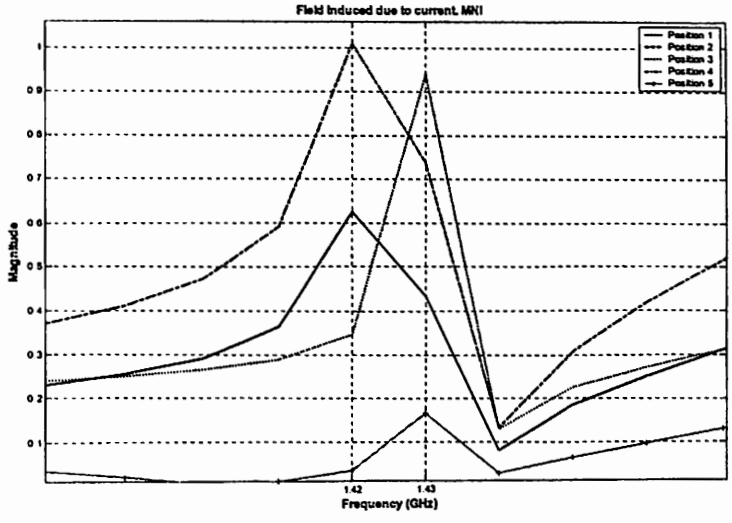

Figure 4.3.10 Field induced due to the current on the probe. Frequency sweep – 1.2 GHz to 1.5 GHz

Fig 4.3.9 and 4.3.10 represent the induced field due to the current on the probe. From the above graphs it can be seen that the magnitude of the fields induced due to the current on the probe for positions 1, 2 and 4 are maximized at 1.42 GHz. For positions 3 and 5 there is one peak at 1.16 GHz and another at 1.43 GHz. The magnitude of the field is comparatively higher at 1.16 GHz for positions 3 and 5. The field maximum should occur at the points where the current is maximized and that trend can be seen in all the positions.

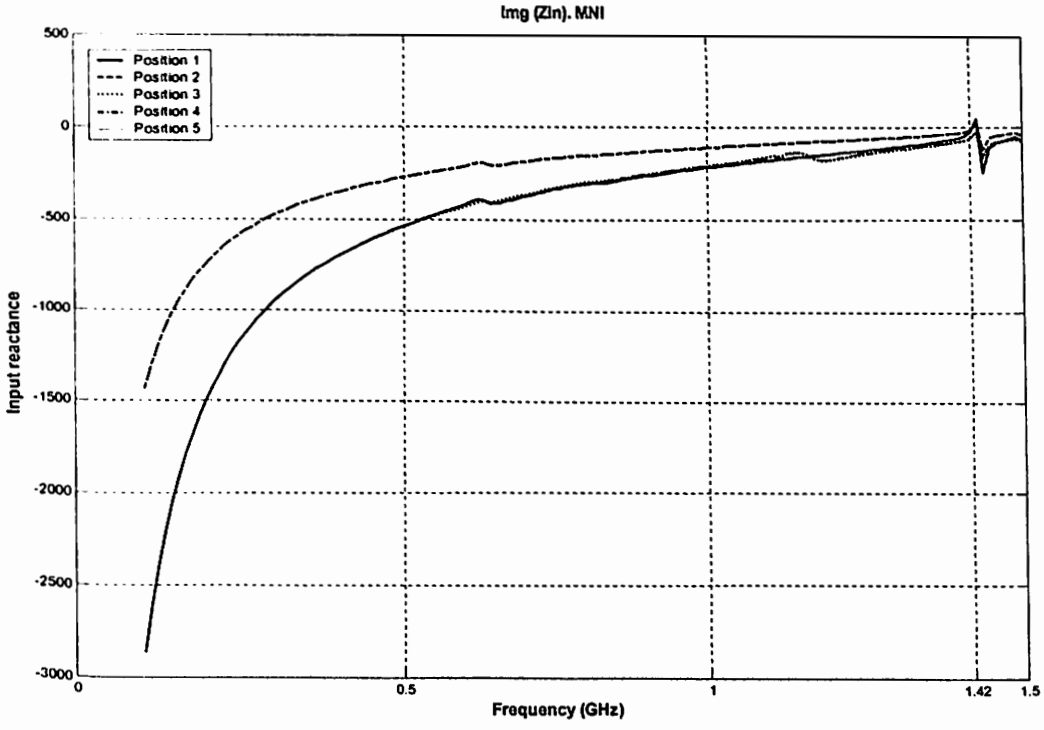

Figure 4.3.11 Input reactance of the monopole. Frequency sweep – 10 MHz to 1.5 GHz

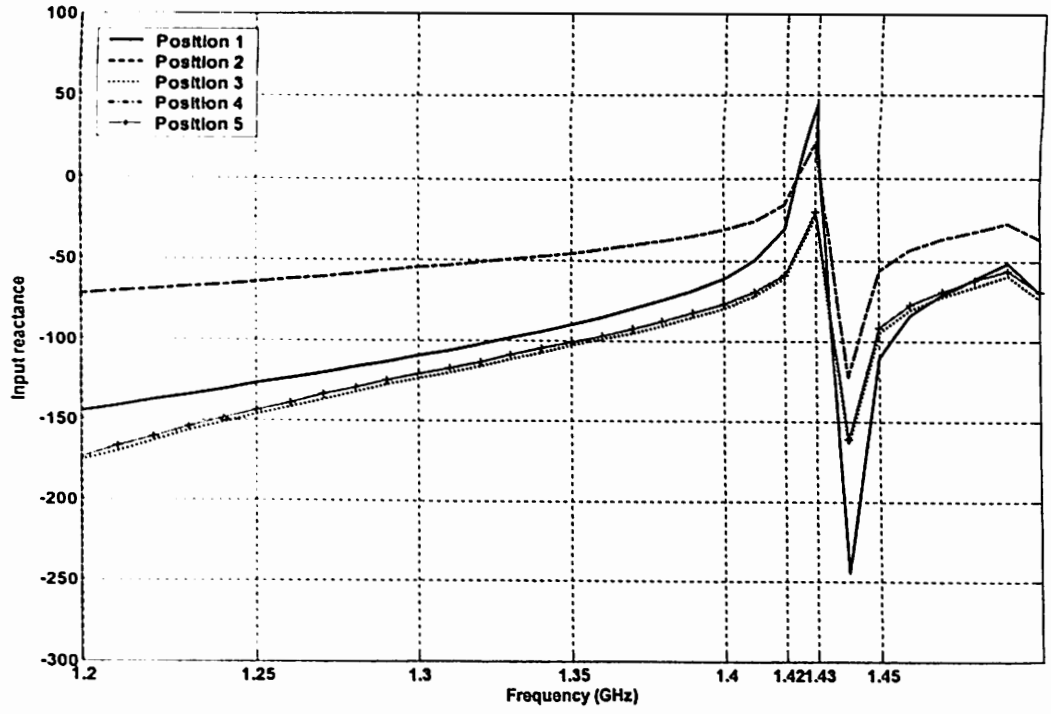

Figure 4.3.12 Input reactance of the monopole. Frequency sweep – 1.2 GHz to 1.5 GHz

Fig 4.3.11 and 4.3.12 represent the input reactance of the monopole computed using MNI. From the above graphs it can be seen that the input reactance goes to zero between 1.42 and 1.43 GHz for positions 1, 2 and 4. For positions 3 and 5 the reactance does not go to zero in the frequency range of 10 MHz to 1.5 GHz. The reactance graphs of positions 2 and 4 which are located symmetrically on either side of position 1, overlap each other.

As stated before, maximum current will be induced on the probe for at the frequency where the reactance goes to zero. The field will be maximum when there is a maximum current. This trend can be seen for positions 1, 2 and 4. Thus it can be concluded that the positional variation of the probe in the horizontal plane does not make much difference to

the energy coupled to the probe. The difference in the energy coupled due to the variation in the position of the probe in the vertical plane is not clear from this analysis.

Thus in this chapter all the results for validation of Modal MoM has been presented with the results from FEKO. The multiple angles of incidence problem which did not have any standard comparison has been validated using FEKO. Some of the results from FEKO and Modal MoM for the multiple angles of incidence case for both single and double apertures are also compared with a set of measured results from ASU [48]. Finally the energy that can be coupled to a probe that is located inside the enclosure has been analyzed. The positional dependence of the monopole inside the enclosure to couple maximum energy has been studied. In the next chapter, some of the conclusions drawn from this thesis and future work are discussed.

Chapter 5

5.0 CONCLUSIONS AND FUTURE WORK

Modal MoM is a computationally efficient tool that can predict the fields at any point inside the cavity and Khan's work (MOI) relaxed the limitations of MNI for multiple angles of incidence and polarizations. This particular contribution served as a motivation for this work as the validation of MNI and MOI always remained in question. MNI has been verified when the aperture size is made big. (Equal to opening up one of the walls). By comparing MOI data with the results produced from FEKO and measured results, a bound on the angle of incidence until which MOI can predict the results right has been thoroughly investigated.

In this work only single aperture and double apertures were considered. Also note, the apertures were present on the front wall. There were no apertures considered on the back wall especially with MOI. MNI can support apertures on both walls but cannot support two apertures on the front wall without any apertures on the back wall. Also MNI cannot support a cavity with no apertures on it. MOI can support any number of apertures on the front wall but cannot support any apertures on the back wall.

Using MNI for the cases like having one wall of the cavity opened completely, the shielding effectiveness values computed were not believed because of the limitation in

MNI that it can only support apertures of small dimension and also because the apertures are located in an infinite ground plane. When the aperture size is made big then the cutoff frequency is reduced so there exists more number of aperture modes. With the results from FEKO, now it has been proved that MNI computes the shielding effectiveness correctly even for the worst case of large single aperture.

For the multiple angles of incidence, MOI results have been believed to be right but the results were never compared to any other standard results. Here with help of FEKO, the angle up to which MOI results can predict the shielding effectiveness right has been verified. MOI predicts the values right until 75 degrees for single aperture and 70 degrees for double aperture and above that the results are not right. In MOI the corners are neglected due to the assumption of infinite ground planes and edge effects are much important for higher angles of incidence. This might be the reason MOI is not predicting the results correctly. By comparing a set of results with the measured results, the results from FEKO have been verified also. From the comparison with measured data FEKO results are much closer than MOI results.

In the final section, the frequency at which maximum energy can be coupled to a monopole present inside an enclosure has been studied. The theory has been supported with results from both MNI and FEKO. Though the actual amount of energy coupled has not been calculated, the frequency at which maximum coupling of energy can occur has been studied. By the positional variation of the monopole inside the enclosure, the

variations in coupling energy that can occur due to positional change of the monopole has been studied.

MNI computes the shielding effectiveness to close form accuracy. A convergence study in FEKO was done in computing the shielding effectiveness over a range of frequencies and for the variation from $\lambda/15$ to $\lambda/25$, the difference was about 0.2 dB. So more number of modes has to be included on the apertures for in MNI and same convergence study has to be made to predict the accuracy and convergence of the results.

Computationally Modal MoM (MNI and MOI) are much faster than FEKO for any case. For the same problem of computing the shielding effectiveness over a range of frequencies, MNI takes about 5-10 minutes while FEKO takes 3-4 hours. Inclusion of more number of modes in the apertures may increase the time of computation in MNI and MOI but still it can compute the results faster than FEKO.

Future work

There is a lot of work that can be done in future for improving MNI and MOI. MOI only accounts for the aperture on the front wall of the cavity. This can be expanded to include the apertures on the back wall also. Also by including a wire inside the cavity for MOI, the current induced on the wire, energy coupled on the wire can be looked when the plane wave is incident upon the face of the aperture in varying angles and polarizations. All over this work, the field is calculated only in the center of the cavity. This can be extended to calculating the fields at every point inside the cavity or over a specified set

of points inside the cavity and the statistical shielding effectiveness can be assessed with respect to change in frequency and change in the incidence angle. In this work MOI is validated for the multiple angle case without polarization effects. This can be improved to calculate the shielding effectiveness for varying polarizations.

Other aperture shapes like circular apertures, spherical apertures can be introduced on the walls replacing the rectangular apertures and the same study can be carried on that. Modal MoM formulation and also in FEKO we assume that the walls are lossless. This is a very narrow assumption because when the cavity is lossless it almost has an infinite Q. Practically speaking this is not possible and so loss must be introduced into the system. Loss can be introduced in different ways like the cavity walls can be made lossy, the space inside the cavity can be filled with lossy material and a dielectric sphere can be introduced into the space inside the cavity. Once loss is introduced into the system all the analysis done will find a new meaning and will be more applicable to the real world situation. When wire is introduced into the cavity, it can be excited using a voltage gap and the fields outside the cavity can be calculated. The size of the cavity can be increased and the scalability of shielding effectives using this approach can be checked.

In this analysis the position of the monopole is varied for 5 positions only. This can be improved by changing the position of the monopole over a set of points on the wall and the current induced and input impedance can be looked at to statistically sketch the energy coupled or the current induced on the wire for a wide range of frequency sweep.

More wires or wires and circuit boards can be introduced inside the enclosure and the shielding effectiveness of the cavity equipped with circuit components can be studied.

The shielding effectiveness calculation that is carried out here for a very small problem is not enough. To solve for the shielding effectiveness of an aircraft, a code that can compute the fields at every point inside the enclosure including all the apertures and circuit components is needed. The problem has to be solved in a reasonable amount of time with a reasonable accuracy. This is what is focused on the future work. The thesis validates and establishes bounds on the efficient and fast moment method code used for the statistical investigation of shielding effectiveness problem of metallic enclosures with apertures.

REFERENCES

[1] A. P. Duffy, T. M. Benson. and C. Christopoulous (1992). "*Application of Transmission Line Modeling (TLM) to Studying the Effectiveness of Screened Enclosures.*" IEE Colloquium on Screening of Connectors, Cables and Enclosures.

[2] B. Audone and M. Balma (1989). "*Shielding Effectiveness of Apertures in Rectangular Cavities.*" IEEE Transactions on Electromagnetic Compatibility **Vol. 31, No.1**.

[3] A. R. Attari and K. Barkshli (2002). "*Application of the Transmission Line Matrix Method to the Calculation of the Shielding Effectiveness for Metallic Enclosures.*" IEEE Antennas and Propagation Society International Symposium **Vol. 3**: 16-21.

[4] Bethe, H. A. (1944). "*Theory of Diffraction by Small holes.*" Phys. Rev. 2nd Series **Vol. 66**: 163-182.

[5] Bouwkamp, C. F. (1954). "*Field Theory of Guided waves.*" Reports and Progress in Physics **Vol. XVII**: 35-100.

[6] Bunting, C. F. (2000). "*Shielding Effectiveness, Statistical Characterization and the Simulation of a Two Dimensional Reverberation Chamber using Finite Element Techniques.*" The 19th Proceedings Digital Avionics Systems Conferences **1**: 7-13.

[7] Bunting, C. F. (2001). "*Shielding Effectiveness in a Reverberation Chamber using Finite Element Techniques.*" IEEE International Symposium on Electromagnetic Compatibility **2**: 13-17.

[8] Bunting, C. F. (2002). "*Statistical Characterization and the Simulation of a Reverberation Chamber using Finite Element Techniques.*" IEEE Transactions on Electromagnetic Compatibility **44 No.1**.

[9] Bunting, C. F., S. Yu (2002). "*Statistical Shielding Effectiveness - an Examination of the Field Penetration in a Rectangular Box Using Modal MoM.*" IEEE International Symposium on Electromagnetic Compatibility.

[10] Bunting, C. F. and Z. A. Khan. (2003). "*Shielding Effectiveness Studies of Rectangular Enclosures with Apertures against EM Fields with Arbitrary Angles of Incidence and Polarizations.*" IEEE International Symposium on Electromagnetic Compatibility.

[11] Bunting, C. F., S. Yu. and Z. A. Khan. (2003). "*Statistical Shielding Effectiveness - A Modal MoM method Approach to Characterize the Average Shielding Effectiveness*

over a wide Frequency Range Including Resonances." IEEE International Symposium on *Electromagnetic Compatibility*.

[12] Cohn, S. B. (1951). "*Determination of Aperture Parameters by Electrolytic - Tank Measurements*." Proc. IRE **Vol. 39**: 1416 - 1421.

[13] Cohn, S. B. (1952). "*The Electric Polarizability of Apertures of Arbitrary Shape*." Proc. IRE **Vol. 40**: 1069-1071.

[14] Cohn, S. B. (1952). "*Microwave Coupling by Large Apertures*." Proc. IRE **Vol.40**: 696-699.

[15] M. S. Tharf. and G. I. Costache (1994). "*A Hybrid Finite Element - Analytical Solutions for in-homogeneously Filled Shielding Enclosures*." IEEE International Symposium on Electromagnetic Compatibility **Vol.36, No.4**.

[16] D. Roisse, F. Toress and B. Jecko (1997). "*Electromagnetic Field Penetration through Small Apertures in a Room*." IEE 10th International Conference on Antennas and Propagation: 14-17.

[17] D. W. P. Thomas, Alan C. Denton, Tadeusz Konefal, T. M. Benson, C. Christopolous, J. F. Dawson, A. C. Marvin, S. J. Porter and Philip Sewell (2001). "*Model of the Electromagnetic Fields Inside a Cuboidal Enclosure Populated with Conducting*

Planes or Printed Circuit Boards." IEEE International Symposium on Electromagnetic Compatibility **Vol 43, No. 2**.

[18] D.A. Hill, M. T. Ma, A.R. Ondrejka, B.F. Riddle, M. L. Crawford and R. T. Johnk (1994). "*Aperture Excitation of Electrically Large, Lossy Cavities.*" IEEE International Symposium on Electromagnetic Compatibility **Vol. 36**.

[19] Deshpande, M. D. (2000). "*Electromagnetic Field Penetration Studies.*" NASA/CR-2000-210297.

[20] Florean, D. (2001). "*Computer Aided Predictio and Experimental Validation of Radiated Emission from a Shielding Box with Different Size Apertures.*" IEEE International Symposium on Electromagnetic Compatibility: 13-17.

[21] G. Cerri, R. De Leo and V. M. Primiani (1992). "*Theoritical and Experimental Evaluation of the Electromagnetic Radiation from the Apertures in Shielded Enclosures.*" IEEE International Symposium on Electromagnetic Compatibility **Vol 34, No.4**.

[22] G. Cerri, R. De Leo and V. M. Primiani (1994). "*Field Penetration into Metallic Enclosures through Slots excited by ESD.*" IEEE International Symposium on Electromagnetic Compatibility **Vol 36, No.2**.

[23] G. Fuwan, Z. Peibai and C. Wenzhen (1999). "*Analysis of Shielding Effectiveness using Finite- Difference Time- Domain Method.*" International Conference on Computational Electromagnetics and its Applications: 1-4.

[24] I. Belokour, J. Lo Vetri and S. Kashyap (2000). "*Shielding Effectiveness Estimation of Enclosures with Apertures.*" IEEE International Symposium on Electromagnetic Compatibility **Vol 2**: 21-25.

[25] J. De Moerloose, S. Criel and R. De Smedt "*Comparison of FDTD and MoM for Shielding Effectiveness Modelling of Test Enclosures.*"

[26] Jarem, J. M. (1987). "*A Multifilament Method-of_Moments Solution for the Input Impedance of a Probe-Excited Semi-Infinite Waveguide.*" IEEE Transactions on Microwave Theory and Techniques **MTT-35**.

[27] John M. Rollins and John M. Jarem (1989). "*The Input Impedance of a Hollow-Probe-Fed, Semi Infinite Rectangular Waveguide.*" IEEE Transactions on Microwave Theory and Techniques **Vol. 37, No.7**.

[28] Jay J. Ely, Truong X. Nguyen, Kenneth L. Dudley, Stephen A. Scearce, Fred B. Beck, Manohar D. Deshpande, C. R. Cockrell "*An Investigation of EME As A Potential Cause of Fuel Tank Ignition.*"

[29] Jay J. Ely, Truong X. Nguyen, Kenneth L. Dudley, Stephen A. Scearce, Fred B. Beck, Manohar D. Deshpande, C. R. Cockrell (2000). "*Investigation of Electromagnetic Field Threat to Fuel Tank Wiring of a Transport Aircraft.*" NASA/TP-2000-209867.

[30] John. N. Bombart, Jr. "*Magnetic Field Shielding Degradation due to Circular Apertures in Long Hollow Cylinders.*"

[31] Joo G. Lee, Hyo J. Eom, Byung W. Kim and Hyun H. Park (2001). "*Shielding Effectiveness of Enclosures With Thick Multiple Apertures.*" Microwave And Optical Technology Letters **29. No. 3**.

[32] K. P. Ma, J. L. Drewniak, T. H. Hubing and T. P. Van Doren (1996). "*A Comparison of an FDTD Thin Slot Algorithm and Method of Moments for Modeling Slots near Corners.*" IEEE International Symposium on Electromagnetic Compatibility: 19-23.

[33] Kaden, H. (1959). "*Wirbelstrome und Schirmung in der Nachrichtentechnik.*" Springer - Verlag.

[34] Kraft, C. H. (1994). "*Modeling Leakage through Finite Apertures with TLM.*" IEEE International Symposium on Electromagnetic Compatibility: 22-26.

[35] M. D. Deshpande, C. R. Cockrell and F.B. Beck "*Estimation of Electromagnetic Energy Coupling to a Wire Residing Inside a Transport Aircraft Due to External Radiating Sources.*"

[36] M. Li, J. L. Drewniak, T. H. Hubing and R. E. Dubroff and T. P. Van Doren (1999). "*Slot and Aperture Coupling for Airflow Aperture Arrays in Shielding Enclosure Designs.*" IEEE International Symposium on Electromagnetic Compatibility **Vol. 1**: 2-6.

[37] M. P. Robinson, J. D. Turner C. Christopolous, J. F. Dawson, M. D. Ganley, A. C. Marvin, S. J. Porter and D. W. P. Thomas (1996). "*Shielding Effectiveness of a Rectangular Enclosure with a Rectangular Aperture.*" Electronic Letters **Vol 32, No. 17**.

[38] M. P. Robinson, T. M. Benson, C. Christopolous, J. F. Dawson, M. D. Ganley, A. C. Marvin, S. J. Porter and D. W. P. Thomas (1998). "*Analytical Formulation for the Shielding Effectiveness of Enclosures with Apertures.*" IEEE International Symposium on Electromagnetic Compatibility **Vol 40, No. 3**.

[39] Mendez, H. A. (1970). "*On the Theory of Low Frequency Excitation of Cavity Resonators.*" IEEE transactions on Microwave Theory and Techniques **MTT 18, No. 8**.

[40] Mendez, H. A. (1978). "*Shielding Theory of Enclosures With Apertures.*" IEEE International Symposium on Electromagnetic Compatibility **EMC-20 No.1**: 296-305.

[41] P. Argus, P. Fisher, A. Konrad, A. J. Schwab (2000). "*Efficient Modeling of Apertures in Thin Conducting Screens by TLM method.*" IEEE International Symposium on Electromagnetic Compatibility: 21-25.

[42] R. Azaro, S. Caorsi, M. Donelli and G.L. Gragnani (2002). "*A Circuitial Approach to Evaluating the Electromagnetic Field on Rectangular Apertures Backed by Rectangular Cavities.*" IEEE transactions on Microwave Theory and Techniques **Vol. 50, No.10**.

[43] R. Jabova, R. Zaridze, P. Shubitidze, N. Adzinba, D. Pommerenke and D. Karkashadze (1997). "*Investigation of Aperture Penetration of Transient Fields into a Cylindrical Cavity.*" Direct and Inverse Problems of Electromagnetic and Acoustic Wave Theory: 15-17.

[44] R.E.Collin (1960). "*Field Theory of Guided Waves.*"

[45] B. Archambeault and O. Ramahi (1998). "*Evaluating Tools which predict the Shielding Effectiveness of Metal Enclosures using a Set of Proposed Standard EMI Modeling Problems.*" IEEE International Symposium on Electromagnetic Compatibility **Vol. 1**: 24-28.

[46] S M Booker, A P Lambert and P D Smith "*A Numerical Calculation Of Transient Antenna Impedance.*"

[47] S. Benhassine, L. Pinchion and W. Tabbara (2002). "*An Efficient Finite Element Time Domain Method for the Analysis of the Coupling between Wave and Shielded Enclosure.*" IEEE Transactions on Magnetics **Vol.38, No.2**.

[48] S. V. Georgakapoulos, C. R. Birtcher and C. A. Balanis (2001). "HIRF Penetration through Apertures: FDTD versus Measurements." IEEE Transactions on Electromagnetic Compatibility **Vol 43, No.3**.

[49] S. Tanabe, N. Nagano, T. Itoh, Y. Murata and S. Mizukawa (1996). "*3D - FEM Analysis for Shielding Effects of a Metallic Enclosure with Apertures.*" IEEE International Symposium on Electromagnetic Compatibility: 19-23.

[50] Taylor, C. D. (1973). "*Electromagnetic Pulse Penetration through Small Apertures.*" IEEE Transactions on Electromagnetic Compatibility **Vol. EMC 15, No.1**.

[51] R. De Smedt, J. D. M., S. Criel, D. De Zutter, F. Olyslager, E. Laermans, W. Wallyn and N. Lieteart (1998). "*Approximate Simulation of the Shielding Effectiveness of a Rectangular Enclosure with a Grid Wall.*" IEEE International Symposium on Electromagnetic Compatibility **Vol. 2**: 24-28.

[52] M. Kimmel and H. Singer (1995). "*A Modular Formulation of Electromagnetic Transmission through Shields of Arbitrary Shape using the Method of Moments.*" IEEE International Symposium on Electromagnetic Compatibility: 14-18.

[53] Zutter, W. W. a. D. D. (2001). "*Modeling the Shielding Effectiveness and Resonances of Metallic Shielding Enclosures Loaded with PCB's.*" IEEE International Symposium on Electromagnetic Compatibility: 13-7.

[54] Z. A. Khan, Bunting, C. F., M. D. Deshpande "*Shielding Effectiveness of Metallic Enclosures At Oblique And Arbitrary Polarizations*" To appear: IEEE International Symposium on Electromagnetic Compatibilty.

[55] http://www.advancemag.com/shieldin.htm

[56] Robert Grover Brown, Robert A. Sharpe, William Lewis Hughes and Rober. E. Post, (1973)." *Lines, Waves and Antennas*", The Ronald Press Company.

[PC 1] Personal Communication: Dr. C. J. Reddy. *EMSSUSA*. 24 Research Drive Hampton, VA 23666. cjreddy@emssusa.com

[PC 2] Personal Communication: Dr. Deshpande. *NASA Langley Research Center, Hampton VA*. m.d.deshpande@larc.nasa.gov

[PC 3] Personal Communication: C. R. Birtcher. craig.birtcher@asu.edu

VITA

Vignesh Rajamani

Candidate for the Degree of

Master of Science

Thesis: VALIDATION AND EXTENSION OF MODAL / *MOM IN SHIELDING* EFFECTIVENESS STUDIES OF METALLIC ENCLOSURES WITH APERTURES

Major Field: Electrical Engineering

Personal Data: Born in Vellore, Tamilnadu, India on 3rd December 1981.

Education: Higher secondary education from the Vani Vidhyalaya Matriculation Higher Secondary School, Vellore, India in May 1998. Bachelor of Engineering (First class with distinction) from University of Madras in May 2002. Completed the requirements for the Master of Science degree in Electrical Engineering at Oklahoma State University in December 2004.

Experience: Graduate Teaching Assistant, School of Electrical and Computer Engineering, Oklahoma State University, Fall 2003. Graduate Research Assistant, School of Electrical and Computer Engineering, Oklahoma State University, 2004.

Professional Memberships: IEEE, IEEE APS, IEEE EMC, IEEE MTT.